Titre: Title:	New Materials and Processing Routes for Organic Electrochemical Transistors
Auteur: Author:	Zhihui Yi
Date:	2016
Type:	Mémoire ou thèse / Dissertation or Thesis
Référence: Citation:	Yi, Z. (2016). New Materials and Processing Routes for Organic Electrochemical Transistors [Ph.D. thesis, École Polytechnique de Montréal]. PolyPublie. https://publications.polymtl.ca/2198/

UNIVERSITÉ DE MONTRÉAL

NEW MATERIALS AND PROCESSING ROUTES FOR ORGANIC ELECTROCHEMICAL TRANSISTORS

ZHIHUI YI

DÉPARTEMENT DE GÉNIE CHIMIQUE

ÉCOLE POLYTECHNIQUE DE MONTRÉAL

THÉSE PRÉSENTÉE EN VUE DE L'OBTENTION

DU DIPLÔME DE PHILOSOPHIAE DOCTOR

(GÉNIE CHIMIQUE)

AOÛT 2016

UNIVERSITÉ DE MONTRÉAL

ÉCOLE POLYTECHNIQUE DE MONTRÉAL

Cette thèse intitulée:

NEW MATERIALS AND PROCESSING ROUTES FOR ORGANIC ELECTROCHEMICAL TRANSISTORS

présentée : YI Zhihui

en vue de l'obtention du diplôme de : Philosophiae Doctor

a été dûment acceptée par le jury d'examen constitué de :

M. AJJI Abdellah, Ph. D., président

M. CICOIRA Fabio, Ph. D., membre et directeur de recherche

M. PATIENCE Gregory S., Ph. D., membre

M. MARCACCIO Massimo, Ph. D., membre externe

ACKNOWLEDGMENTS

I would like to express my sincere gratitude for all the support that I have received over the past four years at Polytechnique Montréal.

First and foremost, I would like to thank my research director, Prof. Fabio Cicoira, for supporting, guiding, and encouraging me. His scientific rigorous and work ethics have left an enormous and positive impact on me. I would also like to thank Prof. Clara Santato for her professional advices and insight during my Ph.D. studies, not only within the field of organic electronics, but also from the perspective of a successful career. Moreover, I would like to thank Prof. Francesca Soavi for sharing her invaluable expertise in electrochemistry via many fruitful discussions. In addition, I am grateful for the time and interest invested by the jury members, Prof. Abdellah Ajji, Prof. Gregory Patience, Prof. Massimo Marcaccio and Prof. Oussama Moutanabbir into my work.

I am grateful for the time Prof. James D. Wuest spent on encouraging, advising and helping me during the past years. This thesis would not have been possible without the support of Christophe Clément and Alireza H. Mesgar in microfabrication; Patricia Moraille, Josianne and Samir Elouatik in materials characterization. Furthermore, I would like to thank my collaborators Giovanniantonio Natale for rheology experiments and Luca Bettini for preparation of nanostructured carbon electrodes.

I would like to acknowledge the Canadian government for providing me a Vanier Canada Graduate Scholarship through NSERC, through which I was able to pursue my work, as well to Prof. Gilles Brassard for establishing the Gilles Brassard Doctoral Prize for Interdisciplinary Research. Thanks to this prize, I have been able to meet top Canadian scientists at the award ceremony at Rideau Hall in Ottawa. In addition, I would like to acknowledge Fonds de recherche du Québec–Nature et technologies (FRQNT) for awarding me the “Lauréate du concours Étudiants-chercheurs étoiles” prize and the Merit fellowship; the Schlumberger Foundation for providing a scholarship and additional research funds through the “Faculty for the Future” program and CMC Microsystems for covering part of my cleanroom expenses.

I would like to thank my friends and colleagues, past and present, for the countless fruitful discussions and wonderful times over the past four years. In particular, I would like to thank my

dear colleagues and friends Irina Valitova, Fanny Boubée de Gramont, Alexander Dieplam, Jonathan Sayago, Tian Lan, Ri Xu, Ruili Wang, Prajwal Kumar, Eduardo Di Mauro, Gaia Tomasello, Francis Quenneville and Guido Soliveri for all the fruitful discussion during my stay at Polytechnique.

Last but not least, I would like to wholeheartedly thank my parents and my brother for their unconditional love and unlimited support. To you, I would simply like to say: “I love you”, for no other words are able to capture my feelings.

ABSTRACT

Organic electronics, which use thin films or single crystals of organic π-conjugated materials as semiconductors, enable technologies for large-area, mechanically flexible and low-cost electronics.

Intense research in organic electronics started in the 90s, with the demonstration of the first light-emitting diodes, transistors and solar cells based on organic materials. Today, such devices are becoming ubiquitous in our society as they can be found in displays based on organic light-emitting diodes in mobile phones, televisions and many other consumer devices. Other organic electronic devices, such as transistors for radio frequency identification tags, are expected to enter the market in the near future. Organic electronic materials present several advantages over inorganic ones, which make them more viable for targeted applications. One the most significant advantages of organic materials is their ability to transport both ionic and electronic charges, which can be exploited in bioelectronics, a multidisciplinary field that deals with the coupling of electronic devices with biological systems.

The primary goal of bioelectronics is to exploit electronic devices for biological applications, such as implants, drug delivery systems, artificial skin, and sensors for in vivo or in vitro environments. Interfaces between biological systems and electronics require devices that are mechanically flexible and stretchable, chemically inert and in some cases biodegradable. Bioelectronics based on organic materials, known as organic bioelectronics, especially promising because promise to yield devices that are able to combine ionic and electronic transport and to offer improved mechanical interfaces with living tissues, due to the soft nature of the polymer surface.

An example of a bioelectronic device is the organic electrochemical transistor (OECT), which has found applications in biosensors and implantable devices. OECTs are attractive because of their ability to operate at low voltages (< 1 V) in aqueous solutions, where biological processes take place. OECTs can be composed solely of conducting polymers and consist of source and drain electrodes and a channel in ionic contact with a gate electrode *via* an electrolyte solution.

The gate voltage modulates the current flowing in the channel. In most OECTs, the application of a positive gate bias induces a reversible redistribution of positive ions within the conducting polymer channel and the electrolyte. This, together with charge injection from source and drain, results in electrochemical dedoping of the conducting channel, accompanied by a decrease of the source-drain current.

In this thesis, we have fabricated rigid, flexible and degradable OECTs on glass, plastics and degradable shellac substrates. Unconventional techniques such as parylene patterning and orthogonal photolithography have been used for device fabrication. These processing techniques let us avoid placing organic materials in contact with other materials (such as photoresists, solvents and strippers) typically used in photolithography, which can result in the degradation of the electrical properties of the organics. To understand how OECTs work and to optimize their performance, we have investigated the role of their main components (electrolyte, gate electrode and substrate). Moreover, we have realized a flexible device integrating a transistor and a supercapacitor, for applications in energy micro-storage.

Ionic liquids (ILs) are interesting candidates as gating media in OECTs. However, ILs can exhibit excessively high viscosity that prevents their straightforward use. We report two ways to employ the highly viscous ionic liquid triisobutyl(methyl)phosphonium tosylate (Cyphos® IL 106) in OECTs based on poly(3,4-ethylenedioxythiophene) polystyrenesulfonate (PEDOT:PSS), namely IL–H_2O binary mixtures and ion gels. The use of these formulations as gating media increases the OECT modulation with respect to experiments where pure ionic liquids are used. Using high surface area activated carbon gates, we achieved ON/OFF ratios as high as 5000 with Cyphos® IL 106–H_2O mixtures at 5 and 10% H_2O v/v.

Planar OECTs using PEDOT:PSS as the channel material, nanostructured carbon as the gate electrode material and poly(sodium 4-styrenesulfonate (PSSNa) gel as the electrolyte were fabricated on flexible polyethylene terephthalate (Mylar®) substrates. Nanostructured carbon was deposited at room temperature by supersonic cluster beam deposition (SCBD). Interestingly, the OECT acts as a hybrid supercapacitor to give a device that we called *transcap*. The energy storage ability of transcaps has been studied with two configurations: one features PEDOT:PSS

as the positive electrode and nanostructured carbon as the negative electrode; the other has a reversed electrode polarity. Potentiostatic charge/discharge studies show that both supercapacitors show good performance in terms of voltage retention, particularly when PEDOT:PSS is used as the positive electrode. Galvanostatic charge-discharge characteristics show typical symmetric triangular shape, indicating a nearly ideal capacitive behaviour with a columbic efficiency close to 100%.

Finally, we developed “green” OECTs, which employ degradable substrates and water as the gating medium. OECTs were patterned onto degradable shellac substrates by transfer printing. To explore the gate effect in presence of water as the gating medium, we have employed AC gate electrodes and PEDOT:PSS gate electrodes. Results indicate that OECTs with AC gates have slower current response and higher current modulation than those with PEDOT:PSS gates. The shellac substrate can be degraded in 1 M KOH solution.

Our study of various electrolytes, high specific surface area gates and diverse substrates has significantly advanced the knowledge in the field of OECTs, thereby paving the way to applications in vivo and in vitro. Interestingly, OECTs can be used as energy storage devices. The concept of a transcap integrating an organic electrochemical transistor and a supercapacitor can be further optimized to achieve faster time responses, decreased self-discharge and optimized electrical and energy storage properties.

RÉSUMÉ

La bioélectronique est un domaine pluridisciplinaire dont l'objectif est le couplage des dispositifs électroniques avec les systèmes biologiques. La bioélectronique vise l'exploitation des dispositifs électroniques pour des applications biologiques, comme les systèmes de livraison de médicament implantables, la peau artificielle, ou encore les capteurs capables d'opérer *in vivo* ou *in vitro*. Les interfaces entre la biologie et l'électronique nécessitent des dispositifs qui soient à la fois mécaniquement flexibles et étirables, chimiquement inertes, ainsi que, dans certains cas, biodégradables. La bioélectronique basée sur des matériaux organiques, ou bioélectronique organique, donne les moyens technologiques de produire des dispositifs électroniques mécaniquement flexibles ou dégradables, le tout à faible coût sur de larges surfaces.

Les recherches intensives dans le domaine de l'électronique organique ont commencé dans les années '90, avec les premières diodes électroluminescentes, transistors ainsi que cellules photovoltaïques basés sur des matériaux organiques. Les dispositifs électroniques organiques deviennent omniprésents dans notre société moderne avec l'introduction sur le marché d'écrans basés sur l'utilisation de diodes électroluminescentes pour les téléphones cellulaires, les télévisions et d'autres produits commerciaux. D'autres dispositifs électroniques organiques, tels que les transistors organiques pour les *tags* d'identification radiofréquence, devraient faire à leur tour une entrée sur le marché dans un futur proche. Les matériaux organiques électroniques présentent plusieurs avantages sur leurs homologues inorganiques, ce qui les rend plus adaptés à certaines applications spécifiques. L'un des avantages les plus importants réside sans doute dans la capacité des matériaux organiques électroniques à transporter les porteurs de charge ioniques et électroniques, pour pouvoir développer de nouveaux dispositifs faisant l'interface avec les systèmes biologiques. Le transistor organique électrochimique (OECT), qui a trouvé de nombreuses applications dans les biocapteurs ou dans les dispositifs implantables, en est un bon exemple. Les OECTs offrent la capacité prometteuse à opérer à de faibles voltages (<1 V) en solutions aqueuses, où les procédés biologiques ont lieu. Les OECTs peuvent être réalisés entièrement à l'aide de polymères conducteurs et sont composés d'électrodes appelées *source* et *drain*, ainsi que d'un canal en contact ionique avec une électrode appelée grille *via* une solution électrolytique. Le potentiel appliqué à la grille module le courant qui circule dans le canal. Dans

la plupart des OECTs, l'application d'une différence de potentiel positive à la grille induit une redistribution réversible des ions positifs à l'intérieur du polymère conducteur composant le canal, ainsi qu'à l'intérieur de l'électrolyte. Ceci, couplé avec l'injection de charges par la source et le drain, résulte en un dédopage électrochimique du canal conducteur, qui s'accompagne d'une diminution du courant source-drain.

Dans cette thèse, nous décrivons la fabrication de différents types d'OECTs, rigides, flexibles ou encore dégradables, sur des substrats de verre, de plastique ou de shellac dégradable. Des techniques non-conventionnelles comme la gravure sur parylène et la photolithographie orthogonale ont été utilisées pour la fabrication des dispositifs. Ces méthodes permettent d'éviter le contact direct entre les matériaux organiques et d'autres matériaux (i.e. les photorésines, les solvants et les décapants) typiquement utilisés en photolithographie, évitant ainsi une dégradation des propriétés électriques. Afin de mieux comprendre le mécanisme de fonctionnement des OECTs, qui est toujours largement méconnu, ainsi que d'optimiser leurs performances, nous avons étudié le rôle de leurs composants clé, i.e. l'électrolyte, l'électrode de grille et le substrat. Nous avons aussi exploré la possibilité de fabriquer un dispositif flexible intégrant un transistor et un supercondensateur, qui pourrait être intéressant pour des applications dans le domaine du micro-stockage d'énergie.

Les liquides ioniques (ILs) sont des candidats intéressants pour servir de milieu de grille (*gating medium*) dans les OECTs. Néanmoins, les ILs présentent une viscosité excessivement élevée qui empêche de les utiliser directement dans les OECTs. Nous rapportons ici deux approches permettant d'utiliser le liquide ionique hautement visqueux triisobutyl(méthyl)phosphonium tosylate (Cyphos® IL 106) dans des OECTs basés sur le poly(3,4-éthylènedioxythiophène) polystyrènesulfonate (PEDOT:PSS). Ces deux approches sont l'utilisation d'un mélange binaire IL-H_2O et l'utilisation de gels ioniques. Ces formulations du milieu de grille mènent à une augmentation de la modulation de l'OECT, comparativement aux résultats obtenus avec le liquide ionique pur. En utilisant des grilles en carbone activé de grande surface, des ratios ON/OFF allant jusqu'à 5000 ont été obtenus avec les mélanges Cyphos® IL 106–H_2O à 5% et 10% de H_2O, v/v.

Des OECTs planaires utilisant du PEDOT:PSS comme matériau pour le canal, du carbone nanostructuré comme matériau pour l'électrode de grille et du gel poly(sodium 4-styrènesulfonate)

(PSSNa) comme électrolyte ont été fabriqués sur des substrats flexibles de poly(téréphtalate d'éthylène) (Mylar®). Le carbone nanostructuré a été déposé à température ambiante par déposition supersonique de faisceaux en agrégats (SCBD). L'OECT résultant se comporte comme un supercondensateur hybride (ce qui donne un dispositif que nous avons appelé *transcap*). La capacité à stocker l'énergie des transcaps a été étudiée dans deux configurations : l'une utilise le PEDOT:PSS comme électrode positive et le carbone nanostructuré comme électrode negative, tandis que la deuxième configuration inverse la polarité des électrodes. Les études de la charge/décharge potentiostatique révèlent que les deux supercondensateurs montrent de bonnes performances en termes de rétention de voltage. Ceci est particulièrement vrai quand du PEDOT:PSS est utilisé comme électrode positive. Les caractéristiques de la charge/décharge galvanostatique présentent une forme triangulaire symétrique typique, ce qui indique un comportement capacitif quasiment idéal, avec une haute efficacité coulombienne (proche de 100%).

Enfin, nous avons développé des OECTs "verts", qui emploient des substrats dégradables et de l'eau comme milieu de grille. Des OECTs fabriqués sur du PET (polytéréphtalate d'éthylène) ont été transférés sur un substrat de shellac par *transfer printing*. Afin d'étudier l'effet de grille en présence d'eau comme milieu de grille, nous avons utilisé une électrode de grille en carbone activé ainsi qu'une électrode de grille en PEDOT:PSS. Les résultats ont montré que les OECTs utilisant des grilles en carbone activé présentent une réponse en courant plus lente et une modulation de courant plus élevée que les grilles en PEDOT:PSS. Le substrat en shellac peut être dégradé en utilisant une solution de KOH à une concentration 1 M.

Nos études sur différents électrolytes, grilles de grande surface spécifique et substrats ont permis des avancées significatives dans le domaine des OECTs, qui vont mener vers de nouvelles applications in vivo et in vitro. De plus, les OECTs peuvent être utilisés comme des dispositifs de stockage d'énergie. Le concept de transcap intégrant un transistor organique électrochimique et un supercondensateur peut être davantage optimisé pour obtenir des temps de réponse plus rapides et une autodécharge plus faible, ainsi que des propriétés électriques et de stockage d'énergie optimisées.

TABLE OF CONTENTS

LIST OF TABLES

LIST OF FIGURES

LIST OF SYMBOLS

A_{ch}	Channel area
A_g	Gate area
c_{ch}	Channel capacitance per unit area
c_g	Gate capacitance per unit area
C	Capacitance
d	Thickness
dQ	Dissipated charge
e^-	Electron
E	Stored energy
G	Conductance of the channel
G'	Dynamic storage modulus
G''	Loss modulus
I	Drain-source current at $V_g \neq 0$ V
I_0	Drain-source current at $V_g = 0$ V
I_d	Source-drain current
I_{on}	ON-state current
I_{off}	OFF-state current
I_g	Gate-source current
l	Drift length
L	Length
M^+	Cations
P	Power
ΔQ	Stored charge
t	Time
u	Drift velocity
V_{cell}	Cell voltage
V_d	Drain-source voltage
V_g	Gate-source voltage

V_p	Pinch-off voltage
V_{sol}	Solution voltage
W	Width
η	Newtonian viscosity
η^*	Complex viscosity

LIST OF ABBREVIATIONS

AC	Activated carbons
ADH	Alcohol dehydrogenase
Al	Aluminum
Ag	Silver
AgCl	Silver chloride
Ar	Argon
Au	Gold
[BMIM][PF6]	1-butyl-3-methylimidazolium hexafluorophosphate
[bmim][Tf_2N]	1-butyl-3-methylimidazolium bis(trifluoromethanesulfonimide)
[C2mIm][$EtSO_4$]	1-ethyl-3-methylimidazolium ethylsulfate
CE	Counter electrode
CMC	Critical micellar concentration
Cyphos® IL 106	Triisobutyl(methyl)phosphonium tosylate
CTAB	cetyltrimethylammonium bromide
D	Drain
DBSA	Dodecyl benzene sulfonic acid
DMPA	(Dimethoxyphenyl)acetophenone
EG	Electrolyte-gated
[EMIM][TFSI]	1-ethyl-3-methylimidazolium bis(trifluoromethylsulfonyl)imide
EIS	Electrochemical Impedance Spectroscopy
Et_2O	Ethyl acetate
Fc	Ferrocene [bis(η-5-cyclopentadienyl)iron
FET	Field-effect transistor
G	Gate
GO_x	Glucose oxidase
H_2O_2	Hydrogen peroxide

IL	Ionic liquid
KCl	Potassium chloride
MBAAm	*N*,*N*'-methylenebis(acrylamide)
MEH PPV	Poly[2-methoxy-5-(20-ethylhexyloxy)-1,4-phenyl-enevinylene
NaCl	Sodium chloride
NAD	Nicotinamide adenine dinucleotide
NIPAAm	*N*-isopropylacrylamide
nsC	Nanostructure carbon
OECTs	Organic electrochemical transistors
OFETs	Organic field-effect transistors
OLEDs	Organic light-emitting diodes
OTFTs	Organic thin-film transistors
$[P_{1,4,4,4}][Tos]$	Triisobutyl-(methyl)phosphonium tosylate
P3HT	Poly(3-hexylthiophene)
PBS	Phosphate-buffered saline
PDMS	Poly(dimethylsiloxane)
PEDOT:PSS	Poly(3,4-ethylenedioxythiophene):polystyrenesulfonate
PEDOT-S	Poly(4-(2,3-dihydrothieno[3,4-*b*]-[1,4]dioxin-2-yl-methoxy)-1-butanesulfonic acid)
PET	Polyethylene terephthalate
PLGA	Poly(L-lactide-co-glycolide)
PMATFSI	Polymethacrylate trifluoromethylsulfonyl)sulfonylimide
poly[ViEtIm][Tf_2N]	Poly(1-vinyl-3-methylimidazolium) bis(trifluoromethanesulfonimide)
PPV	Poly(*p*-phenylene vinylene)
PQT-12	Poly(3,3‴-didodecylquaterthiophene
PSPEO-PS	Poly(styrene-b-ethylene oxide-b-styrene)
PS-PMMA-PS	Poly(styrene-b-methylmethacrylateb-styrene)
PSS	Polystyrenesulfonate
PSSNa	Poly(sodium 4-styrenesulfonate)

PSTFSI	Polystyrene (trifluoromethylsulfonyl)sulfonylimide
Pt	Platinum
PTHS	Poly(6-(thiophene-3-yl)hexane-1-sulfonate) tetrabutylammonium
RE	Reference electrode
RFID	Radio-frequency identification
RIE	Reactive ion etching
S	Source
SCBD	Supersonic cluster beam deposition
SMMAS	Polystyrene-b-poly(methyl methacrylate)-b-polystyrene
SWNT	Single-walled nanotube
transcap	Transistor-capacitor
WE	Working electrode

LIST OF APPENDICES

CHAPTER 1 INTRODUCTION

1.1 Overview

Organic electronics, based on π-conjugated organic molecules and polymers, is attracting enormous interest for applications that complement and extend silicon based electronics, such as colorful displays and large-area mechanically flexible devices [1]. Organic semiconductors have captured the interest of the research community because of their intriguing properties, such as i) solubility in organic solvents, ii) ease of processing by several techniques (e.g. evaporation, spin coating, printing) and iii) compatibility with a variety of substrates including mechanically flexible ones. Research on organic electronics dates back to the 1960s, when the first studies of the properties of organic single crystals were carried out [2]. At the end of the 1970s, A. J. Heeger, A. G. MacDiarmid and H. Shirakawa demonstrated that the conjugated polymer polyacetylene could become highly conducting when doped with iodine [3]. In 2000 they were awarded the Nobel Prize in chemistry for contributing to the discovery of conducting polymers.

Much progress has been made in the optimization of electrical, structural, chemical, mechanical and optical properties of various organic materials for electronic device applications [4]. Organic semiconductor materials including conjugated polymers and small molecules exhibit excellent performance in many electronic devices, including organic light-emitting diodes (OLEDs), organic solar cells, and organic thin-film transistors (OTFTs) [5-13].

In 1990, Burroughes et al. reported the first example of electroluminescence from conjugated polymers, which used a poly(*p*-phenylene vinylene) (PPV) film coated by two metallic electrodes in a vertical geometry to construct a single-layer OLED (Figure 1.1) [5]. A transparent indium-tin oxide (ITO) electrode was used, which allowed the generated light to leave the device. The electrode on the top consisted of thermally evaporated aluminum, magnesium or calcium. In the OLEDs, electrons and holes are injected by the cathode and the anode, and bound excitons are formed from electron-hole capture within the semiconductor film. The decay of this excited state results in radiative emission [6]. Nowadays, OLEDs use a much more complex multilayer structure to enhance the efficiency and improve the lifetime [12].

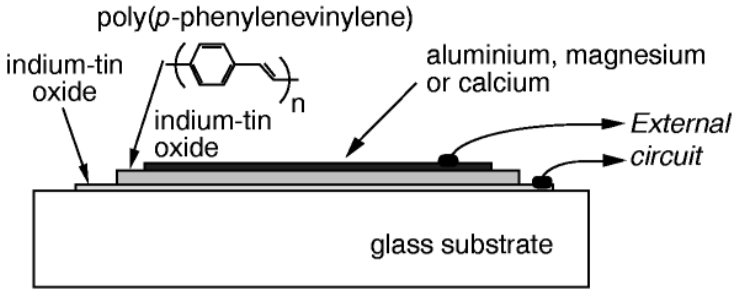

Figure 1. 1. Device structure of a single-layer polymer electroluminescent diode (ITO/PPV/Al) [6]. Adapted with permission. Copyright © 1999, Rights Managed by Nature Publishing Group.

After the discovery of the photoelectric effect by E. Becquerel, a great deal of attention has been dedicated to the conversion of solar light into electric power [7]. Investigation of organic solar cells can be considered to have originated in 1959, when Kallmann and Pope observed a photovoltaic effect in a single crystal of anthracene [9]. The structure of organic solar cells involves a sandwich geometry (Figure 1.2), which is similar to that of OLEDs. The active layer, which consists of electron donors and acceptors mixed together, is typically a polymer blend sandwiched between the electrode and the hole-transport layer (typically made of poly(3,4-ethylenedioxythiophene):polystyrenesulfonate, PEDOT:PSS, a *p*-type conducting polymer). The working mechanism of an organic solar cell for converting light into electricity consists of the following steps: i) capture of photons, which leads to the formation of an excited state in the form of an electron-hole pair, ii) exciton dissociation into electrons and holes, and iii) charge (electrons and holes) transport in the organic semiconductor layer to the respective electrodes [10].

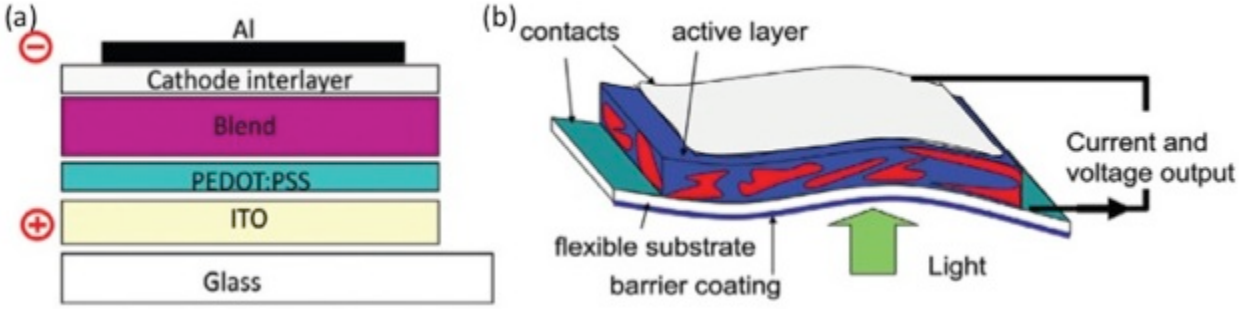

Figure 1. 2. Layer structure of an organic solar cell (a) and (b) schematic of the layers in an OPV module on a flexible substrate [10]. Adapted with permission. Copyright © 2011 Elsevier Ltd.

OTFTs are attracting a great deal of interest due to their potential for applications in flexible active matrix displays, radio-frequency identification (RFID) tags, sensors and flexible/stretchable electronics [14-17]. An OTFT is composed of source and drain electrodes in contact with an organic semiconductor channel and a gate electrode, which acts as an *ON/OFF* switch of the channel and modulates the magnitude of the source-drain current. Current modulation in OTFTs can be induced either by field-effect doping or by electrochemical doping, depending on the materials used for the various device components. According to the type of organic film and gate electrode, OTFTs can be roughly divided into two classes: organic field-effect transistors (OFETs) and organic electrochemical transistors (OECTs).

The field-effect transistor (FET), which was introduced in 1925 by Lilienfeld [11], uses an electrostatic field to modulate the current in the channel. Shockley, Bardeen and Brattain were awarded the Nobel Prize in Physics in 1956 "for their research on semiconductors and their discovery of the transistor effect" [18]. In a FET, a dielectric layer is employed to separate the semiconducting layer from the gate electrode (Figure 1.3a). Application of a gate-source potential increases the density of charge carriers in the semiconductor channel and consequently increases channel conductance. The operating voltage of a FET depends on the capacitance at the channel/dielectric interface. The higher the capacitance, the lower the operating voltage. A high gate operating voltage (tens of volts) is usually needed in OFETs making use of conventional dielectrics, due to their low capacitance (usually less than 20 nF/cm^2) [19].

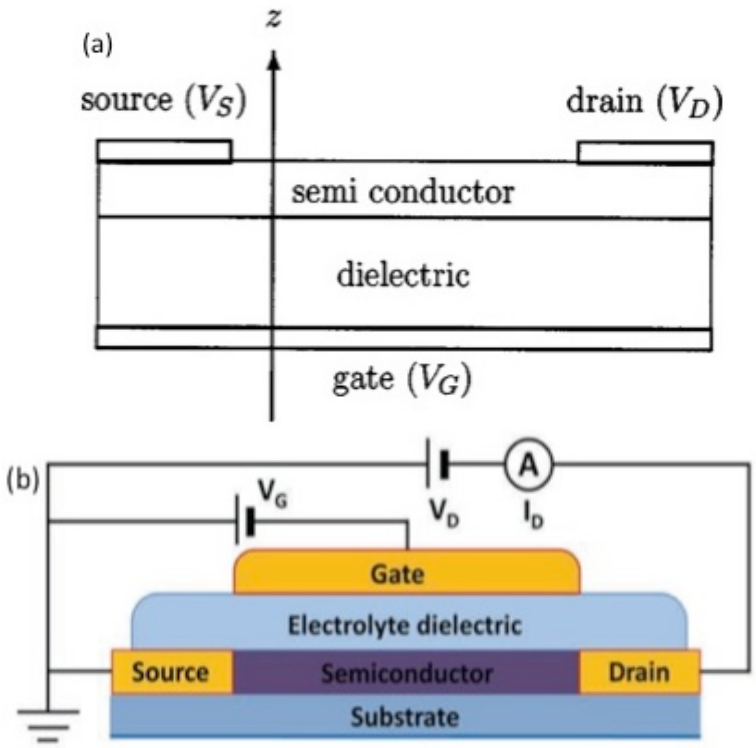

Figure 1. 3. (a) Schematic plot of a bottom-gate, top contact FET [19]. (b) Device schematic in cross section of an electrolyte gated top-gate FET (not to scale) [20]. Adapted with permission. (a) Copyright © 2002 American Physical Society. (b) Copyright © 2013 WILEY-VCH Verlag GmbH & Co. KGaA, Weinheim.

In an alternative device structure, an electronically insulating but ionically conducting electrolyte replaces the gate dielectric (Figure 1.3b) [20]. This device is known as electrolyte-gated transistor [21]. Electrolyte-gated (EG) transistors were first proposed in the 1950s. In EG transistors the application of a gate bias leads to the formation of an electrical double layer at the electrolyte/semiconductor interface. The low thickness of the electrical double layer leads to a high capacitance (in the μF/cm^2 range); therefore, these transistors can be operated at low voltage (<2 V).

Although EG transistors could work at low voltage compared to conventional transistors, their applications are rather limited, due to the presence of the liquid electrolyte [22]. Nevertheless, in the last couple of decades there has been a resurgence of the research on EG transistors and several devices based on organic and inorganic materials, such as organic semiconductors [20, 23,

24, 25], conducting polymers [26, 27], metal oxides [28, 29] and carbon nanomaterials [30, 31] have been reported.

Frisbie et al. [23] have utilized polymer semiconductors as the channel and ion gels as the gate dielectric to fabricate EG transistors (Figure 1.4a). The semiconductors employed as channel materials were poly(3,3‴-didodecylquaterthiophene) (PQT-12) and poly(3-hexylthiophene) (P3HT), in which the hole densities are in the order of 10^{14} charge carriers/cm^2. Ion gels are mixtures of ionic liquids and block copolymers (Figure 1.4b), which can provide specific capacitances of ~30 μF/cm^2 at 10 Hz. The details of ion gels will be given in Chapter 2. The working mechanism of EG transistors includes both electrochemical and electrostatic contributions. The electrochemical doping process happens in time scales greater than 1 ms, while the electrostatic process occurs in time scales shorter than 1 ms.

a

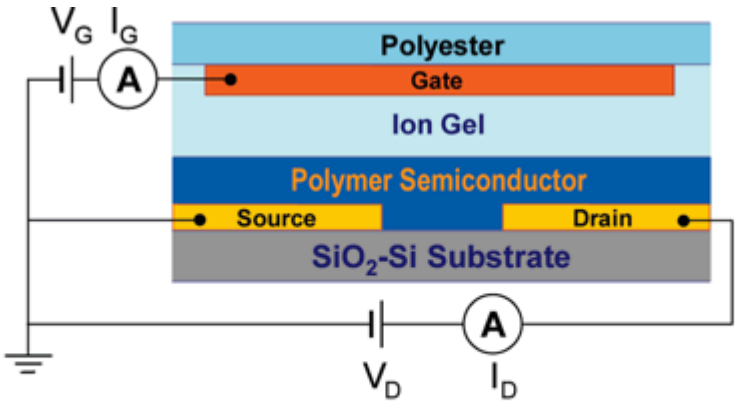

b

Polymer Semiconductors	Ion Gel Dielectrics	
	Triblock Copolymers	Ionic Liquids
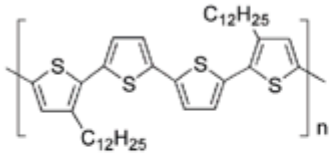 PQT-12	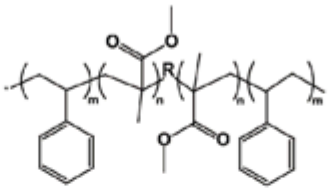 PS-PMMA-PS	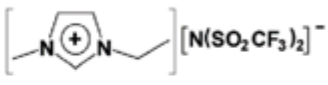 [EMIM][TFSI]
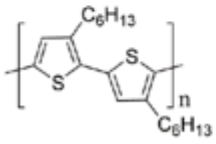 P3HT	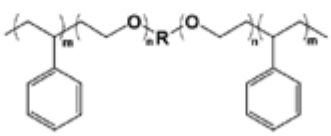 PS-PEO-PS	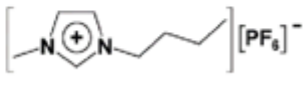 [BMIM][PF_6]

Figure 1. 4. (a) Cross-sectional scheme of an ion gel-gated organic thin-film transistor (GEL-OTFT). The devices have channel lengths of 20 μm and channel widths of 400 μm. (Not drawn to scale: the gate is several times larger than the channel length). Typical gel thicknesses in this work are on the order of 100 μm; the polymer semiconductor thickness is ~20 nm. Source (I_s), drain (I_d), and gate (I_g) currents were measured simultaneously while applying the source-gate (V_g) and source-drain (V_d) voltages. (b) Molecular structures of the polymer semiconductors (left) and ion gel dielectrics (right) [23]. Reprinted with permission. Copyright © 2009, American Chemical Society.

The electrostatic and the electrochemical working mechanism can be understood with the scheme in Figure 1.5 [20]. For a transistor working under an electrostatic regime, with an applied gate bias, an electric double layer (EDL) forms at the interface between the electrolyte and the channel. In an electrochemical process, the ions permeate into the channel and dope/dedope the channel, which lead to electrochemical doping/dedoping (by oxidation or reduction of the channel material). For EG transistors with semiconductors or conducting polymers channels impermeable to ions, the working mechanism is electrostatic. By application of a gate bias (V_g), EDL form at the interfaces between the gate and the electrolyte and also between the electrolyte and the channel (Fig. 1.5a, left). For EG transistors employing ion-permeable channels, one EDL forms at the interface between the gate and the electrolyte, the other EDL vanishes due to the ions permeating into the channel, causing an electrochemical doping/dedoping process (Figs. 1.5a and b, right).

Considering the effect of the gate bias on the density of the charge carriers, EG transistors can be divided into accumulation and depletion mode transistors (not related with the permeability of the channel material, Fig. 1.5).

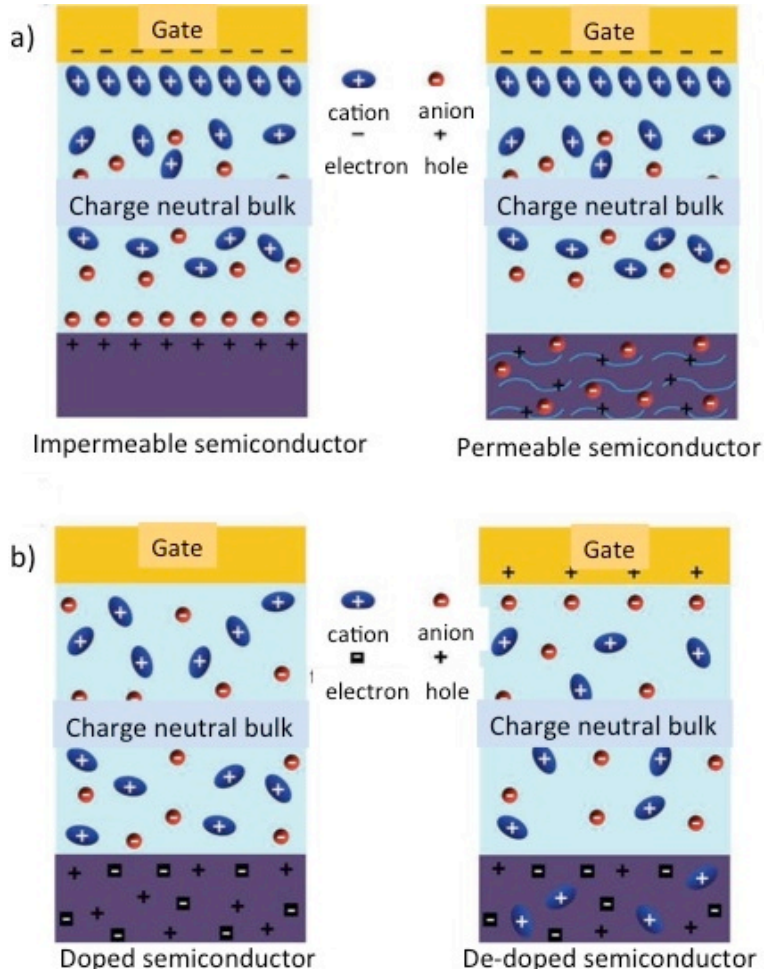

Figure 1. 5. (a) Carrier accumulation-mode operation of an EGT for un-doped ion-impermeable (left) and permeable semiconductors (right) and (b) depletion-mode operation for degenerately doped semiconductors without (left) and with (right) a gate voltage [20]. Reprinted with permission. Copyright © 2013 WILEY-VCH Verlag GmbH & Co. KGaA, Weinheim.

First reported by Wrighton and coworkers in the 1980s [32], OECTs are nowadays intensively investigated for applications in bioelectronics, owing to their ability to operate at low voltages (< 1 V) in aqueous solutions, where biological processes take place [33]. As OECTs are relatively new devices, intense investigations of the effect of device components on the electrical characteristics, including the polymer channel, the electrolyte and the gate, are carried out by several groups worldwide [34-40].

OECTs can work under accumulation mode or depletion mode depending on the pristine property of the conjugated polymer channel. Malliaras group has contributed to investigate conjugated polymers that can be used in OECTs working both on accumulation and depletion mode (Figure 1.6) [25-27].

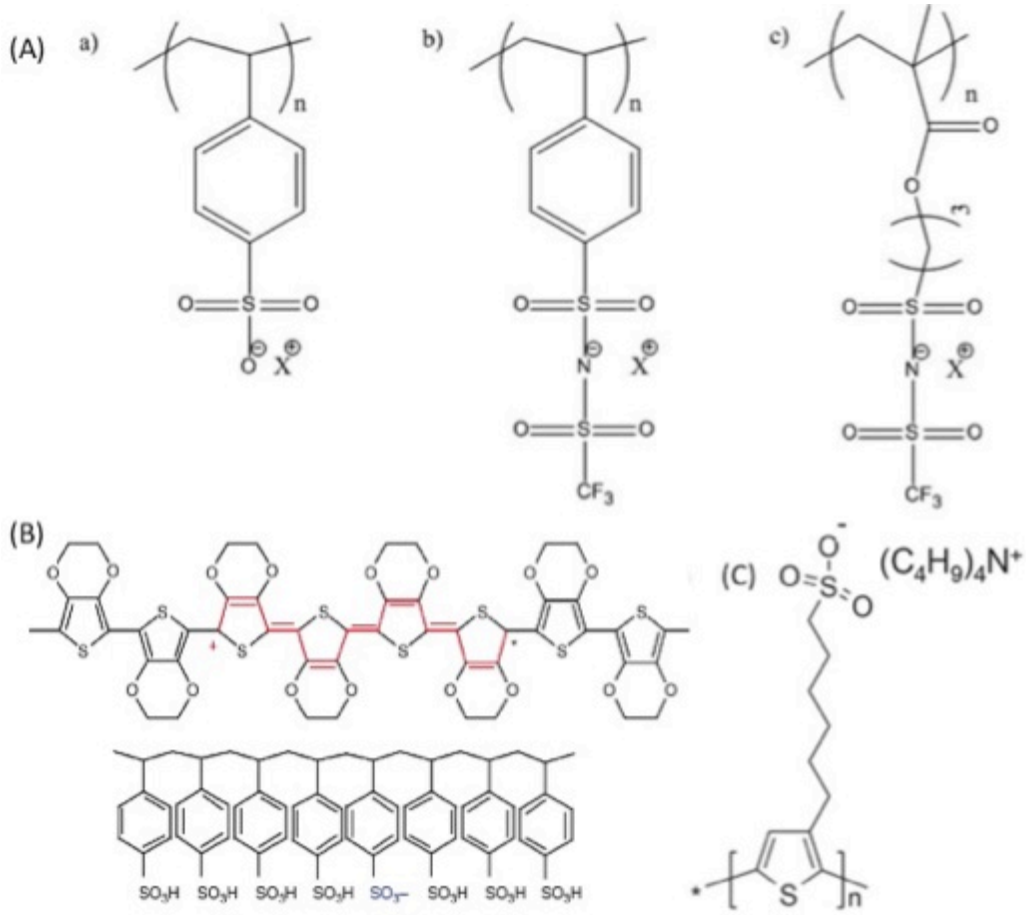

Figure 1. 6. (A) Chemical structures of the anionic polyelectrolytes: (a) PSS, (b) PSTFSIX (styrenic backbone, counter ion X = K^+/Li^+), and (c) PMATFSIX (methacrylic backbone, counter ion X = K^+/Li^+). For PSTFSIK20 (styrene backbone, M_n = 20 kDa, X = K^+): n = 60; for PSTFSIK250 (styrene backbone, Mn = 250 kDa, X = K^+): n = 700–800; for PSTFSILi100 (styrene backbone, Mn = 100 kDa, X = Li^+): n = 60; for PMATFSILi80 (methacrylic backbone, Mn = 80 kDa, X = Li^+): n = 220 [26]. (B) Chemical structure of PEDOT:PSS. A hole is indicated on the PEDOT chain in red in the form of a positive polaron. The acceptor on the PSS chain is indicated in blue [41]. (C) The chemical structure of PTHS [25]. Adapted with permission. (A) with copyright © 2015 Wiley Periodicals, Inc. (B) Copyright © Materials Research Society 2010. (C) © 2014 WILEY‐VCH Verlag GmbH & Co. KGaA, Weinheim.

We have recently investigated the role of the gate electrode materials, the electrolytes and the conductivity enhancers on the performance of PEDOT:PSS OECTs [165] on rigid and flexible substrates [168]. In particular, we have demonstrated that high current modulations are achieved using high surface area activated carbon gate electrodes, regardless of the channel materials [135, 75, 165, 166, 169]. We have also investigated the effects of the electrolyte ions, including ionic liquids, CTAB, PSSNa and NaCl.

1.2 Research problems

Despite the impressive improvements achieved in recent years in the field of OECTs, a number of challenges are open. The main issues that need to be addressed are: i) the effect of the type of electrolyte ions on OECT characteristics, ii) the role of the electrolyte/channel and electrolyte/gate interfaces, iii) the influence of the gate materials on the performance of OECTs, and iv) the fabrication of OECTs on unconventional substrates (rigid, flexible, stretchable or degradable) in OECTs.

In an OECT, the electrolyte serves as the ionic conductor and thereby connects ionically the gate electrode with a conducting polymer film (channel). By application of a potential difference between the gate and the source, which constitutes the common ground, (V_g), a reversible redistribution of ions within the electrolyte occurs, which results in electrochemical doping/dedoping, hence in the modulation of the current. Although the operating mechanism of OECTs has been thoroughly investigated, the effect of the type of electrolyte on the device performance is not yet very well understood.

The electrical characteristics of OECTs also depend on the effective electrochemical potential of the gate electrode, affecting the doping/dedoping of the conducting polymer channel. The application of a gate vbias has a direct influence on OECT modulation. For example, a gate electrode with a high surface area would supply more opportunities for ion accumulation, thus resulting in high modulation of OECTs.

The substrate is another important key component of the OECT device. Properties such as flexibility, stretchability and degradability partially establish the device performance and the applications of OECTs.

1.3 Motivation

Studying the organic electrochemical transistor requires a multidisciplinary approach, including chemistry, physics, engineering and biology. The area has great potential for original high-impact research. The main motivation of our work is to advance the state-of-the-art of OECTs and to develop novel organic bioelectronic devices. The general objective of this thesis is to provide a understanding of the working mechanism of OECTs, considering the effect on device performance of different kinds of substrates, different electrolyte ions and gate electrode materials as well as possible electrochemical reactions taking place within the OECT channel.

The specific objectives of this Ph. D. work are the following:

1) *Development of the working mechanism of unconventional electrolytes based on water/ionic liquids mixtures.*

The role played by electrolyte ions on OECT operation is still not completely understood, although several electrolytes have been investigated in OECTs. Most OECTs use electrolytes, such as sodium chloride (NaCl) and aqueous buffer solutions. Unconventional electrolytes that are still under investigation include ionic liquids and charged micellar systems, which are interesting for potential applications in drug loading and release. However, the complex chemical structures of these unconventional electrolytes is expected to lead to more complex mechanisms of dedoping/doping in OECTs.

2) *Development of gate electrode materials*

The type of material and structure of the gate strongly affects the behavior of OECTs. Gate electrodes with high surface areas enable high conductivity modulation in channel materials prone to bulk electrochemical doping and/or electrostatic doping. Carbon materials with high surface area and high conductivity are among the most interesting candidates. Such materials are expected to lead to a high double-layer capacitance at the electrolyte-gate interface, which is expected to translate into a higher OECT modulation. Commercial porous carbon paper, which is made of conductive carbon, is a good candidate for gate electrodes in OECTs. However, the surface area is not large enough to produce high modulation: to increase the gate surface area, a carbon ink made from activated carbon mixed with suitable liquids (such as water, isopropanol

and ionic liquids), can be drop-cast on the carbon paper to be used as the gate electrode. Activated carbon (AC) electrodes on carbon paper lead to high current modulation and good operational stability in OECTs. However, of these electrodes are not bendable and mechanically fragile. Flexible and bendable gate electrodes, can be assembled into planar devices, are required to integrate with flexible circuits or textiles. Herein, we will contribute to develop high surface area and flexible gate electrodes, which can be integrated with the flexible OECTs.

3) *Development of new substrates used for OECTs*

In devices based on thin films the substrate is by far the most bulky part. Therefore, there is a great interest to move towards lightweight and thin substrates. In case of OECTs, various substrates, such as paper, poly(L-lactide-co-glycolide) (PLGA) and shellac, are considered based on requirements about use in implantation, drug delivery, artificial skin, sensing or monitoring the behaviour of cells in vivo or in vitro (see *2.2.4.2 Degradable substrates*). Herein, we will develop OECTs with the natural resin shellac. Considering the low glass transition temperature of shellac, we will concentrate on developing patterning methods to obtain shellac-based OECTs.

A current trend in organic electronics is to move towards disposable, low-cost and low power devices. Rigid (glass or silicon), flexible, degradable and stretchable substrates are currently used. Plastics and papers are the most intriguing candidates for flexible electronics applications. PDMS is the most popular candidate for stretchable devices. Paper, silk, leather, cellulose-based polymers, gelatine and shellac are interesting for biodegradable devices. In this thesis, we focused mainly on flexible and biodegradable OECTs.

1.4 Organization of the work

This thesis starts with a literature review of organic electrochemical transistors (Chapter 2). Chapter 2 introduces the general working mechanism of an OECT and describes the components of an OECT, i.e. the channel, the gate, the conducting polymer and the substrate. Chapters 3 to 5 are reprints of three articles.

Article 1: Ionic liquid–water mixtures and ion gels as electrolytes for organic electrochemical transistors (Published in the Journal of Materials Chemistry C). This article has been recognized by Fonds de recherché du Québec–Nature et technologies (FRQNT) and a prize of “Lauréate du concours étudiants-chercheurs étoiles” has been granted.

Article 2: Flexible conducting polymer transistors with supercapacitor function (submitted to the Journal of Polymer Science B: Polymer Physics).

Article 3: Water gated organic electrochemical transistors on flexible/degradable shellac substrate (submitted to the Journal of Materials Research)

The following paragraphs describe how these articles contribute to the objectives of the thesis.

In article 1, we identified two approaches to use the highly viscous, hydrophilic, phosphonium-based ionic liquid triisobutyl(methyl)phosphonium tosylate (Cyphos® IL 106) as the electrolyte in OECTs. With PEDOT:PSS OECTs, the use of Cyphos® IL 106–H_2O binary mixtures and ion gels as gating media determines an increase of the OECT modulation, with respect to the pure ionic liquid. Similar modulations were obtained for ion gels based on the same ionic liquid, when using PEDOT:PSS gates. Experiments with activated carbon gates point to the weak dependence of the OECT performance on the ionic conductivity and viscosity of the electrolyte, for values >1 mS/cm and <500 mPa s, respectively. By making use of high surface area activated carbon gates, ON/OFF ratios as high as 5000 were reached in OECTs making use of binary mixtures at 10% H_2O v/v.

In article 2, we designed planar OECTs including PEDOT:PSS channel and planar porous carbon gate deposited by SCBD on flexible Mylar substrates. OECTs with channel length as low as 5 μm were patterned by orthogonal lithography. OECTs with PSSNa gel electrolyte exhibit much higher OECT modulation than OECTs making use of aqueous NaCl electrolytes. These OECTs can be used as supercapacitors, it is a continued work about the concept of transcap. The two electrodes of the supercapacitor consist of a PEDOT:PSS transistor channel included between the source and the drain electrodes and the carbon gate. This planar and flexible transcap can be easily cut and paste onto different substrates. By using this OECT as the transcap, we observed efficient charge retention and a satisfying energy storage mechanism to keep the ON status of the OECT, without a power supply.

In article 3, we developed “green” OECTs, which employ degradable substrates and water as the gating medium. OECTs patterned on PET were transferred onto degradable shellac substrate in order to explore the gate effect in presence of water as the gating medium, we employed AC and PEDOT:PSS gate electrodes. OECTs with AC gates present slower current response and higher current modulation than those using PEDOT:PSS gates.

Following these three articles, supplementary methods and results that have been obtained during the work for this thesis are presented in Chapter 6. Finally, conclusions are drawn and perspectives on future work are given (Chapter 7).

CHAPTER 2 LITERATURE REVIEW

The primary goal of organic bioelectronics is to find biological applications for electronic devices based on organic materials [41]. The interfacing of organic electronics with biology has recently attracted attention from the research community as a way to create novel biosensors and tools for nanomedicine [42, 43]. There are multiple advantages of integrating organic electronics with biology. For example, organic electronic materials are compatible with mechanically flexible substrates, a property that is highly demanded for certain types of implants. In addition, organic electronic materials can serve as vehicles for transporting both electronic and ionic charge carriers, thereby creating a communication channel with biological systems, where ion fluxes are important. Finally, the formation of interfaces with electrolytes without dangling bonds or oxides of the type frequently encountered in inorganic materials, which prevent the entry of ions in the semiconductor.

A particularly interesting device for applications of bioelectronics is the organic electrochemical transistor (OECT). OECTs have been utilized to exploit the ability of organic electroactive materials to transport both ionic and electronic charge carriers [44-48]. OECTs have been used as transducers between ionic currents in the electrolyte and electronic currents in the organic channel [49], and as sensors to monitor the attachment of cancer cells and fibroblasts cultured directly on the channel [35]. OECTs have also been employed as sensors for hydrogen peroxide [36], glucose [37-39], dopamine [36], chloride ions [50] and bacteria [40]. OECTs with single-strand DNA probes immobilized on Au gate electrodes have been used to detect complementary DNA targets [40].

2.1 The working principle of an organic electrochemical transistor

OECTs consist of source and drain electrodes and a channel in ionic contact with a gate electrode via an electrolyte solution. The gate voltage modulates the current flowing in the channel. In most OECTs based on conducting polymers, the application of a positive gate bias induces a reversible redistribution of positive ions within the *p*-type conducting polymer channel. This, together with charge injection from source and drain, results in electrochemical dedoping of the conducting channel, accompanied by a decrease of the source-drain current (I_d) [50].

Poly(3,4-ethylenedioxythiophene):poly(styrenesulfonate) (PEDOT:PSS) is commercially available as an aqueous suspension and can be processed with easy methods, such as spin coating and drop casting. PEDOT:PSS films can reach conductivities as high as ~1000 S/cm and are stable in water at neutral pH. A PEDOT:PSS-based OECT can be used as a model to explain the working mechanism of a representative device (Figure 2.1).

The OECT shown in Figure 2.1 consists of a PEDOT:PSS conducting polymer channel in contact with the gate electrode through the electrolyte (Figure 2.1a) [50]. PEDOT:PSS is a p-type material, it conducts holes upon application of a drain-source voltage (V_d). When no gate voltage is applied, holes drift from source to drain in the channel to generate a drain-source current (V_g = 0) (I_d) (Figure 2.1b). When a positive gate-source voltage (V_g) is applied, anions from the electrolyte move towards the gate electrode, and cations (M^+) from the electrolyte permeate into the channel (Figure 2.1c). $PEDOT^+$ accepts electrons (e^-) and is reduced to the non-conductive $PEDOT^0$, while M^+ cations neutralize the PSS^- dopant to form M^+PSS^-. The overall result of the process is a decrease of the source/drain current I_d ($V_g \neq 0$). The process can be reversed (1) [51].

$$PEDOT^+:PSS + M^+ + e^- \leftrightarrow PEDOT^0 + M^+:PSS^- \quad (1)$$

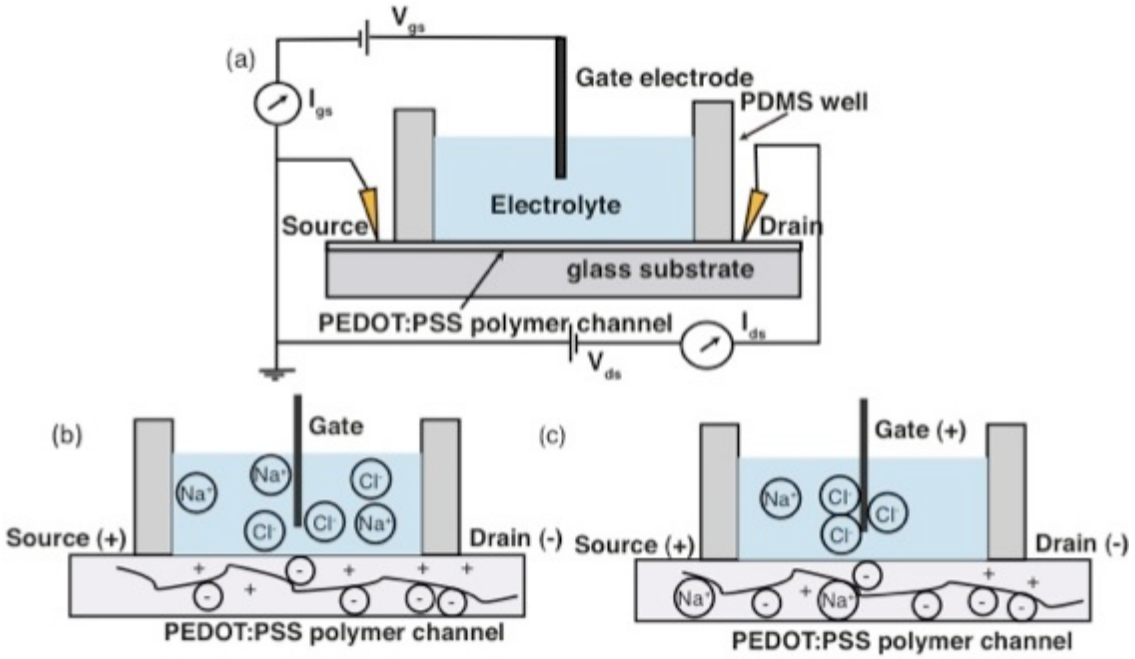

Figure 2. 1. (a) Device structure and electrical circuit of a PEDOT:PSS OECT; [(b) and (c)] OECT working principle. Circles filled with indicate PSS^- ions and + indicate mobile holes. (b) Being PEDOT:PSS a hole conductor, the application of a negative V_d bias generates a drain-source hole current (I_d). (c) Upon application of a positive V_g, the electrolyte ions redistribute in solution. Part of these ions enter the PEDOT:PSS channel, thus affecting I_d (de-doping process) [50]. Reprinted with permission. Rights managed by AIP Publishing LLC.

OECTs can work in non-Faradaic (capacitive) regime and Faradaic regime at the gate/electrolyte interface. In the non-Faradaic regime, the application of V_g induces a transient current in the electrolyte and determines exclusively a capacitive current at the gate electrode; the OECT acts as an *ion-to-electron converter*. In the Faradaic regime, the application of V_g determines a steady-state current at the gate electrode due to reduction/oxidation (redox) reactions. The redox reaction alters the potential within the electrolyte and results in a change of the drain-source current (I_d). In both regimes, two interfaces in OECTs, which are the electrolyte/channel interface and the electrolyte/gate interface, are involved. As reported in the literature, device geometry is an important parameter to establish the performance of OECTs operated both as ion-to-electron converters and electrochemical sensors.

2.2 Key components of OECTs

2.2.1 Channel

PEDOT:PSS (Figure 1.6b) is the most used and commercially available conductive polymer in OECTs. PEDOT:PSS is a degenerately doped *p*-type conducting polymer, in which hole transport takes place in the PEDOT phase while the PSS phase supports the sulfonate acceptors.

2.2.1.1 The effect of the channel size with respect to a gate electrode

For operation as an ion-to-electron converter, the gate electrode needs to be larger than the channel [52]. For an OECT composed of a polarizable electrode, such as platinum (Pt), as a gate and PEDOT:PSS as a channel, the electrolyte potential V_{sol} is calculated by equation (2) [52]:

$$V_{\mathrm{sol}} = \frac{V_{\mathrm{g}}}{1 + \dfrac{c_{\mathrm{ch}} \cdot A_{\mathrm{ch}}}{c_{\mathrm{g}} \cdot A_{\mathrm{g}}}} \qquad (2)$$

where A_{ch} and A_g are the areas of the channel and the gate, c_{ch} and c_g are the channel and gate capacitance per unit area, respectively, with the assumption that $c_{ch} = c_g$ for better understanding of the influence of device geometry. As shown in Figure 2.2a, in a device having a small channel and a big gate ($A_{ch}/A_g < 1$), the potentials of the electrolyte and the gate are similar, which results in a large potential drop between the electrolyte and the channel, leading to a high modulation of the drain current. In the case of Figure 2.2b, which illustrates a big-channel and a small-gate ($A_{ch}/A_g > 1$) device, the large potential drop at the interface between the gate and the electrolyte results in a weak modulation of the drain current.

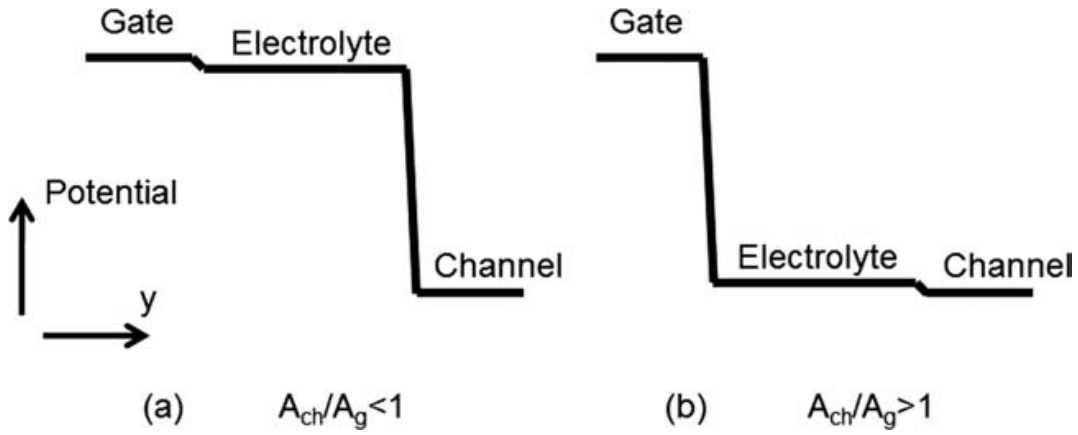

Figure 2.2. Potential distribution between the gate electrode and the channel for two device geometries [52]. Reprinted with permission. Copyright © 2010 Wiley Periodicals, Inc.

For a nonpolarizable gate electrode (such as Ag/AgCl) [50], there will be no potential drop at the gate/electrolyte interface. The potential distribution will be similar to the one sketched in Figure 2.2a.

In addition, in order to optimize the conductance of the channel, a geometry that maximizes channel width and minimizes channel length is necessary [53]. The response of an OECT with a large gate depends on the conductance of the channel. The conductance depends on the

conductivity of the polymer and the geometrical factor W d/L (W: channel width; L: channel length; d: thickness of the polymer film).

For operation as an electrochemical sensor, OECTs with a gate electrode smaller than the channel show higher sensitivity and lower background [36]. The sensitivity can be increased by improving the material parameters of the conducting polymer, such as hole mobility and capacitance per unit area, and the ability of ions from the electrolyte to enter the polymer film. A geometry that maximizes channel width and minimizes channel length can also improve sensitivity, and a faster response time of OECTs was observed when the length of the source-drain line was decreased [54].

Cicoira et al. investigated the effects of the gate area (A_g) and channel area (A_{ch}) on the ability of OECTs to detect hydrogen peroxide (H_2O_2) via an electrochemical reaction at the Pt gate electrode [36]. Working under the non-Faradaic regime (i.e. without H_2O_2 in the electrolyte), there are no charge transfer reactions at the gate electrode. When H_2O_2 is added to the electrolyte, the current modulation is greatly enhanced due to the Faradaic contribution (Figure 2.3).

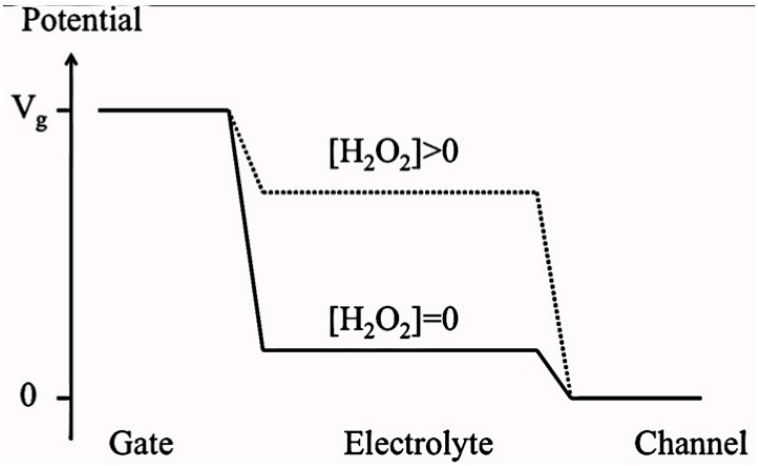

Figure 2.3. Sketch of potential profiles in the electrolyte in the absence and presence of H_2O_2 [36]. Adapted with permission. Copyright © 2010 WILEY-VCH Verlag GmbH & Co. KGaA, Weinheim.

2.2.1.2 Ion transport in the channel

Ions transport is of primary important to understand OECT working mechanism. Malliaras et al. also designed a new OECT device structure (Figure 2.4) and reported the direct measurement of ion mobility in a conducting polymer [55]. In this device structure, PEDOT:PSS was sandwiched between an ion barrier (Su-8: negative photoresist) and a glass substrate. The electrolyte (0.1 M aqueous NaCl), located on the left side, was confined in a PDMS well. Ag/AgCl was used as the gate electrode. Upon application of a positive gate voltage, cations of the electrolyte began to move into the PEDOT:PSS channel and reduction occurred. The typical color switching from light blue (oxidized PEDOT) to dark blue (reduced PEDOT) can be observed during this process.

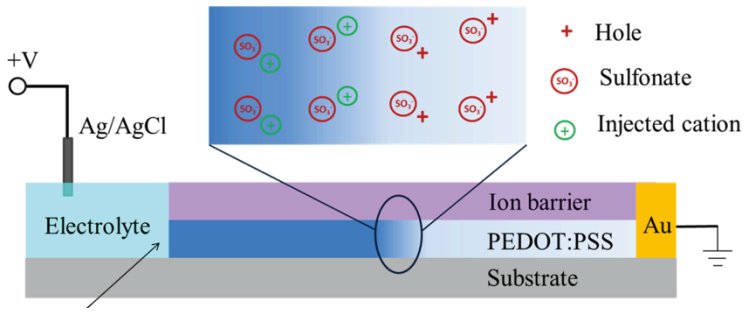

Figure 2. 2. Schematic of the device indicating the charge distribution around the dedoping front according to the model (not to scale) of the electrolyte/conducting polymer junction [55]. Adopted with permission. Copyright © 2013 WILEY‐VCH Verlag GmbH & Co. KGaA, Weinheim.

OECTs working in the non-Faradaic regime (at the interface between gate and electrolyte) are the main subject of the project. In the process of ion-to-electron conversion, ions from an electrolyte enter a polymer film and change its electronic conductivity. This results in ionic-to-electronic signal transconduction. Mixed electronic/ionic conductivity is of particular importance for devices that interface electronics with biology.

2.2.2 Electrolyte

The electrolyte plays an important role in supplying an environment for connecting the gate and the channel ionically in an OECT. Aqueous solutions of salts, such as NaCl and potassium chloride (KCl) and aqueous buffer solutions, such as phosphate-buffered saline (PBS), are commonly used for studying the working mechanism of an OECT. Investigations of the role of the electrolyte in device performance are of primary importance for various applications of OECTs

Micelles

Micelles are of primary interest for drug delivery systems, and a compact sensor that detects micelle formation would constitute a technological breakthrough. Cicoira et al. exploited OECTs to monitor the formation of micelles [56]. As shown in Figure 2.5, the modulation of an OECT increased with the increase of the concentration of CTAB (cetyltrimethylammonium bromide). I is the *OFF* current ($V_g \neq 0$) and the I_0 is the *ON* current ($V_g = 0$). There was no major difference for concentrations above 10^{-3} M, the critical micellar concentration (CMC). Furthermore, investigation of NaCl proved that modulation of the OECT with conventional electrolytes does not depend on concentration.

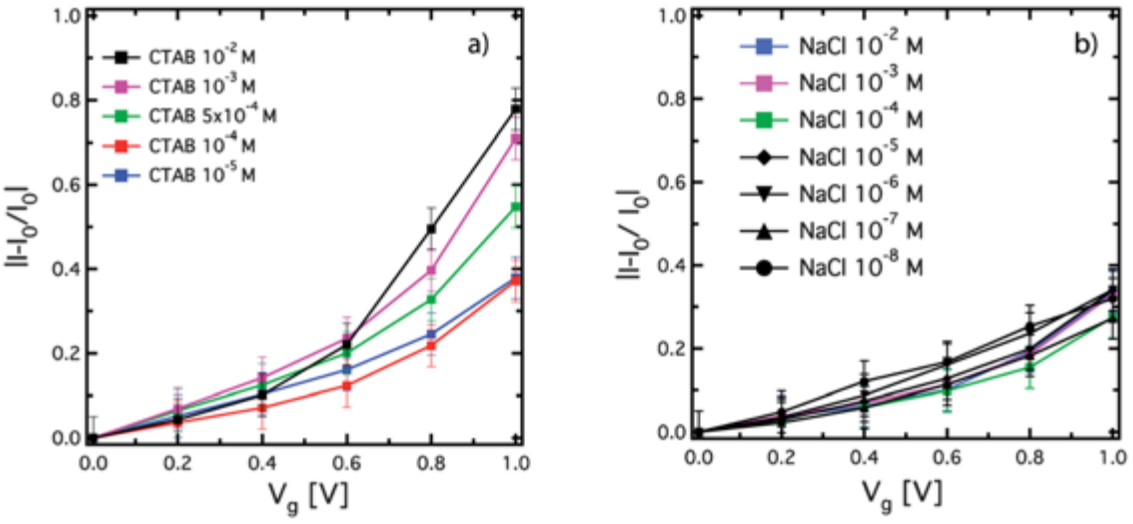

Figure 2. 3. OECT response $|(I-I_0)/I_0|$ as a function of V_g, with V_d = -0.4 V, for different concentrations of (a) CTAB and (b) NaCl [56]. Reprinted with permission. Copyright © 2012, Royal Society of Chemistry.

Further study of the modulation of OECTs with different concentrations of CTAB and NaCl as electrolytes shows that the CTAB electrolyte-based OECT clearly differs from that of an analogous OECT employing an aqueous solution of NaCl as the electrolyte, which does not form micelles (Figure 2.6). Obviously, positively charged CTA^+ micelles modulate PEDOT:PSS OECTs more efficiently than CTA^+ dissociated ions. The results reveal that PEDOT:PSS OECTs can be used for monitoring the formation of micelles.

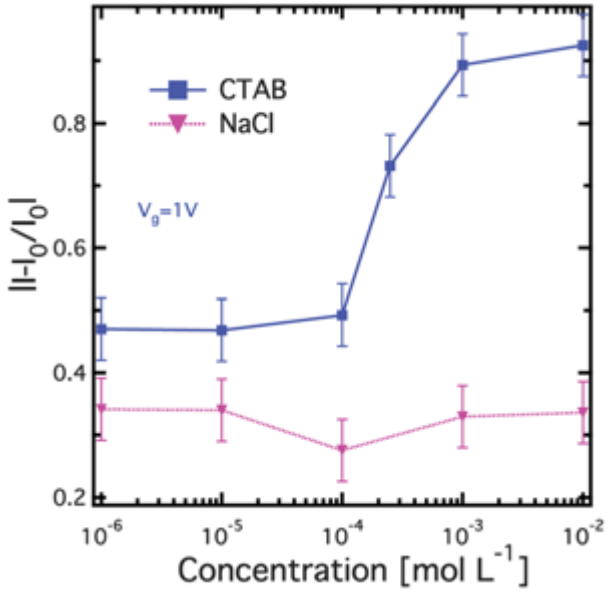

Figure 2. 4. OECT modulation ($|(I - I_0)/I_0|$, where I is the *OFF* current ($V_g \neq 0$) and the I_0 is the *ON* current ($V_g = 0$)) versus molar concentration of CTAB and NaCl aqueous solutions at $V_g = 1$ V, with the drain-source voltage (V_d) kept constant at -0.4 V. The error bars correspond to the maximum spread between the minimum and maximum value of the modulation obtained on 5 repeated measurements. The lines are guides to the eye [56]. Reprinted with permission. Copyright © 2012, Royal Society of Chemistry.

Ionic liquids

Ionic liquids are molten salts at relatively low temperature (typically below 100 °C) that possess high thermal and chemical stability, optical transparency, low volatility and wide electrochemical

stability windows [57-61]. In particular, phosphonium ionic liquids are interesting for their thermal stability and wide window of electrochemical stability [62].

Usually, the glucose concentration is around 0.008-0.21 mM in human saliva and 2-30 mM in blood. Monitoring glucose concentrations is important in healthcare. The ionic liquid can be used as an immobilization medium for the enzyme and the mediator in a glucose sensor [38]. The phosphornium ionic liquid triisobutyl-(methyl)phosphonium tosylate (Cyphos® IL106) has been selected due to its hydrophilicity. The experiments were carried out by placing the enzyme glucose oxidase (GO_x, 500 units per mL) and the mediator ferrocene [bis(η-5-cyclopentadienyl)iron] (Fc, 10 mM) into 1.43 mL of Cyphos® IL106 followed by mixing with 50 mL of glucose-PBS solution as an electrolyte.

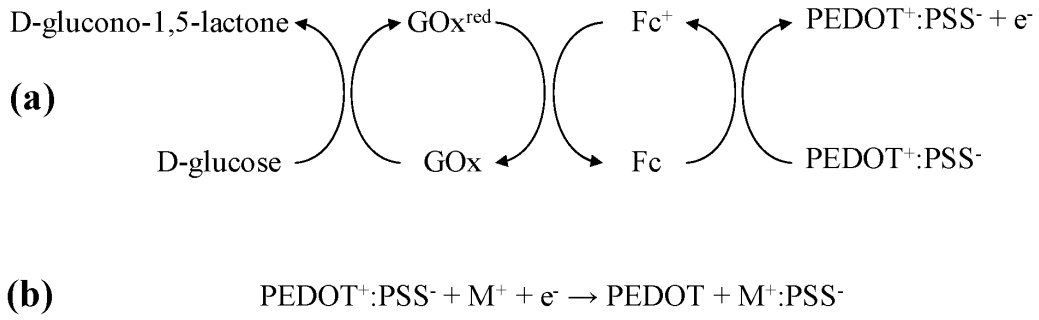

Figure 2. 5. Reactions at (a) the gate electrode and (b) the channel of the OECT [38]. Reprinted with permission. Copyright © 2010, Royal Society of Chemistry.

The glucose is oxidized by application of a gate voltage, while the enzyme (GO_x) is reduced. In the back cycle, oxidation of GO_x is coupled with conversion of Fc to ferricenium ion (Fc^+), and formation of Fc^+ shuttles electrons to the gate electrode (Figure 2.7a). Meantime, the PEDOT:PSS channel was dedoped by cations from solution (M^+) (Figure 2.7b), which decreases the drain current to a certain degree depending on the glucose concentration. The sensitivity is in the range of 10^{-7} to 10^{-2} M (Figure 2.8) [38].

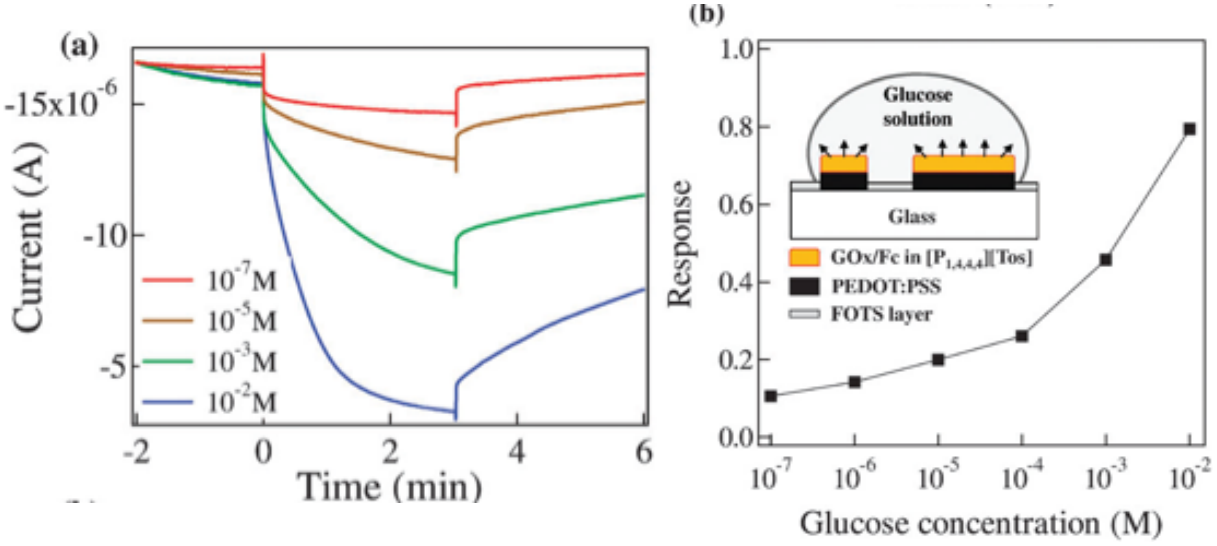

Figure 2. 6. (a) Transient response of the drain current of an OECT upon application of a gate voltage of 0.4 V and duration of 3 min. The drain voltage was 0.2 V. (b) Current modulation (represented as the dimensionless quantity $\Delta I/I$) of the OECT as a function of glucose concentration. Inset shows the concept of device operation, and the arrows indicate the dissolution of the RTIL carrying the enzyme and the mediator into the analyte solution [38]. Reprinted with permission. Copyright © 2010, Royal Society of Chemistry.

Ion gels

Ion gels are solid or gel-like materials, formed from the room temperature ionic liquids (RTILs) crosslinked by polymers to realize structural and dimensional stability. Ion gels have recently found application in bioelectronics, such as for DNA sensing [35]. Owens et al. reported a lactate sensor with an ionogel-based electrolyte [63]. The ionogel was prepared by dissolving a ferrocene mediator Fc (10 mM) in the hydrophilic ionic liquid 1-ethyl-3-methylimidazolium ethylsulfate [C2mIm][$EtSO_4$], followed by mixing with the monomer *N*-isopropylacrylamide (NIPAAm), the cross-linker *N*,*N*'-methylenebis(acrylamide) (MBAAm) and the photo-initiator (dimethoxyphenyl)acetophenone DMPA (Figure 2.9). When the mixture was heated at 45° C for 10 min, a clear and monophasic solution was obtained.

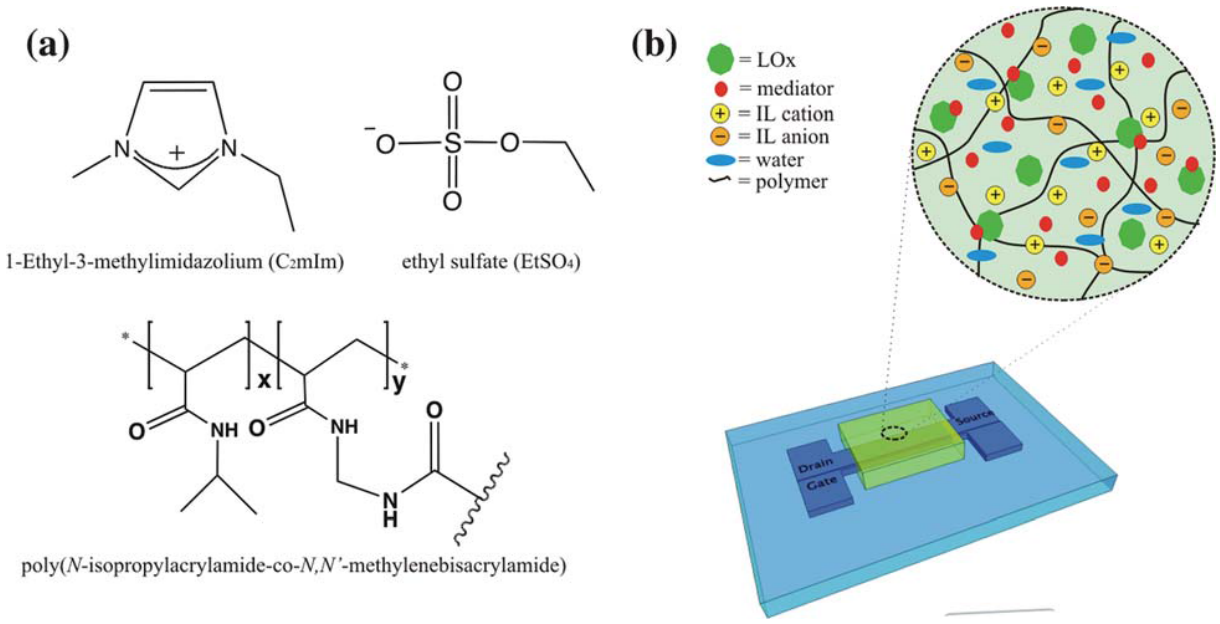

Figure 2. 7. (a) Ionogel components and (b) a schematic representation of the OECT device with ionogel/enzyme mixture [63]. Reprinted with permission. Copyright © 2012, Royal Society of Chemistry.

The working mechanism of the lactate sensor is similar to the one described for the glucose sensor. Lactic acid is oxidized to pyruvate by application of a gate voltage, and Fc is converted into ferricenium ion (Fc^+). The creation of Fc^+ shuttles electrons to the gate electrode (Figure 2.10a). Meantime, the PEDOT:PSS channel was dedoped by cations from the solution, leading to a decrease of the drain current (Figure 2.10b). This is the first flexible transistor-based biosensor with solid electrolyte, which suggests potential applications in wearable sensors.

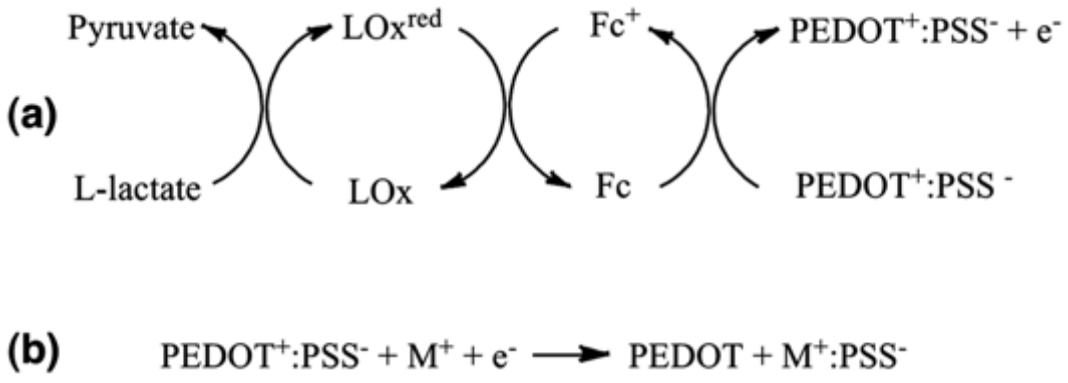

Figure 2. 8. Reactions at (a) the gate electrode and (b) the channel of the OECT [63]. Reprinted with permission. Copyright © 2012, Royal Society of Chemistry.

2.2.3 Gate

Several materials have been explored for OECT gate electrodes, namely PEDOT:PSS, Ag, Pt and carbon materials [50, 64–66]. Cicoira et al. [50] reported that in a halide-based electrolyte (such as NaCl solution), a large steady-state gate-source current (I_g) is found if a non-polarizable Ag gate is employed, which indicates the presence of Faradaic processes at the gate electrode. On the other hand, if a polarizable Pt gate electrode is used, a small I_g is found, consistent with the nature of a Pt electrode. A Faradaic process takes place on the Ag electrode, which results in a large potential drop at the channel/electrolyte interface. As shown in Figure 2.11, an Ag OECT leads to high current modulation compared to a Pt OECT. This was attributed to a redox reaction between ions in the electrolyte and the Ag gate electrode. This could be explained by the fact that an EDL forms at the Pt/NaCl interface ($V_{sol} < V_g$), but no EDL forms at the Ag/NaCl interface ($V_{sol} = V_g$).

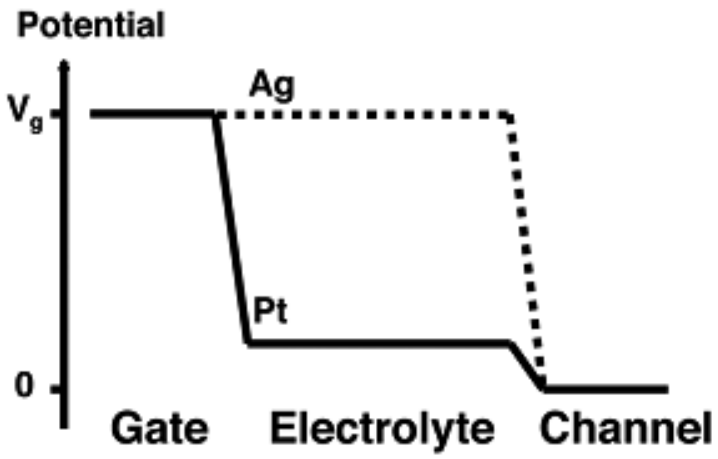

Figure 2. 9. Potential distribution between the gate electrode and the channel for Ag and Pt gate electrodes [50]. Reprinted with permission. Rights managed by AIP Publishing LLC.

It should be noted that OECTs with a Pt gate can also be made to operate in a Faradaic regime, and as such they have been used in enzymatic glucose sensors [35, 64, 67]. OECTs with Pt gate

electrodes modified with enzyme glucose oxidase (GO_x), carbon-based nanomaterials (single-walled nanotube (SWNT), graphene flakes and biocompatible polymer (Nafion) show high sensitivity to epinephrine (Figure 2.12) [68]. The sensitivity of the device was ensured by adding Nafion, a material that can attract epinephrine molecules to the gate electrode. Furthermore, the sensitivity has been improved by introducing a gate electrode modified by SWNTs and graphene flakes, which enhanced electrocatalytic activity of the gate electrode, hence a decrease in the detection limit of the device. The detection limit is around 0.1 nM with a modified gate electrode incorporating Nafion and SWNTs. This level of sensitivity is adequate for some practical applications.

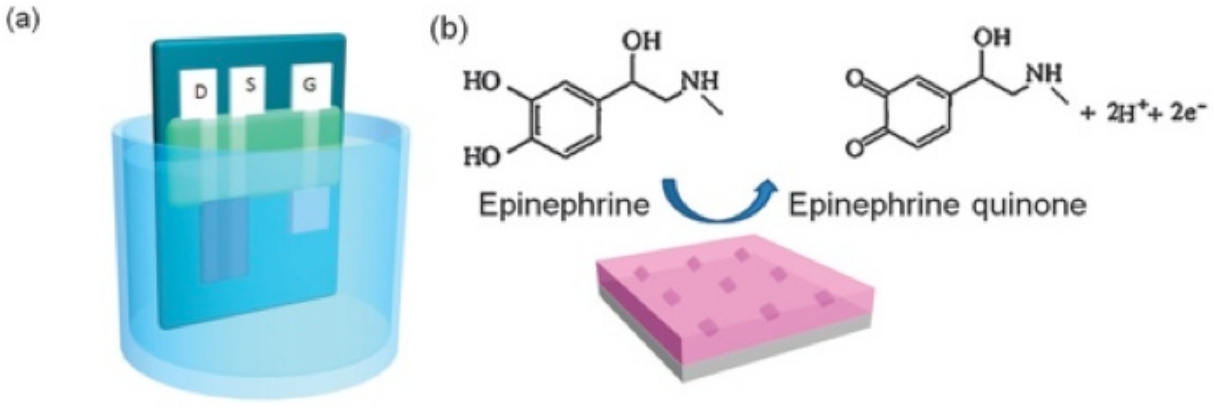

Figure 2. 10. (a) Schematic diagram of an OECT-based epinephrine sensor with a nanomaterial-modified gate electrode including Nafion (b) Oxidation of epinephrine at the gate electrode modified with Nafion and carbon-based nanomaterials [68]. Reprinted with permission. Copyright © 2015, Royal Society of Chemistry.

Carbon electrodes have been intensively investigated for electrochemical sensors, owing to their low cost, good chemical stability, biocompatibility and good electron transfer kinetics [69-72]. Carbon-based sensors include glassy carbon electrodes [73], carbon fibers [74], pyrolytic graphite [74] and graphene [68].

Activated carbons (ACs) have a large specific surface area around 1000−2000 $m^2\ g^{-1}$. Considering the fast reversible electrostatic process owing to the utilization of high specific surface area AC gate electrodes, the charge required to dedope/dope the channel would be in a relatively narrow electrode potential excursion. As a result, AC gates can be used as quasi-

reference electrodes, which simplify the OECT structure and facilitates the characterization of OECTs by cyclic voltammetry. At the same time, employing an AC electrode ensures that undesired Faradaic (redox) processes at the interface between the electrolyte and the electrode will be limited. Cicoira et al. studied the effects of the gate electrode on the behavior of OECTs [75]. They employed an AC gate combined with a PEDOT:PSS channel. High specific capacitance of the AC gate electrodes leads to higher drain-source current modulation in OECTs compared to PEDOT:PSS gate electrodes of comparable geometric area (Figure 2.13).

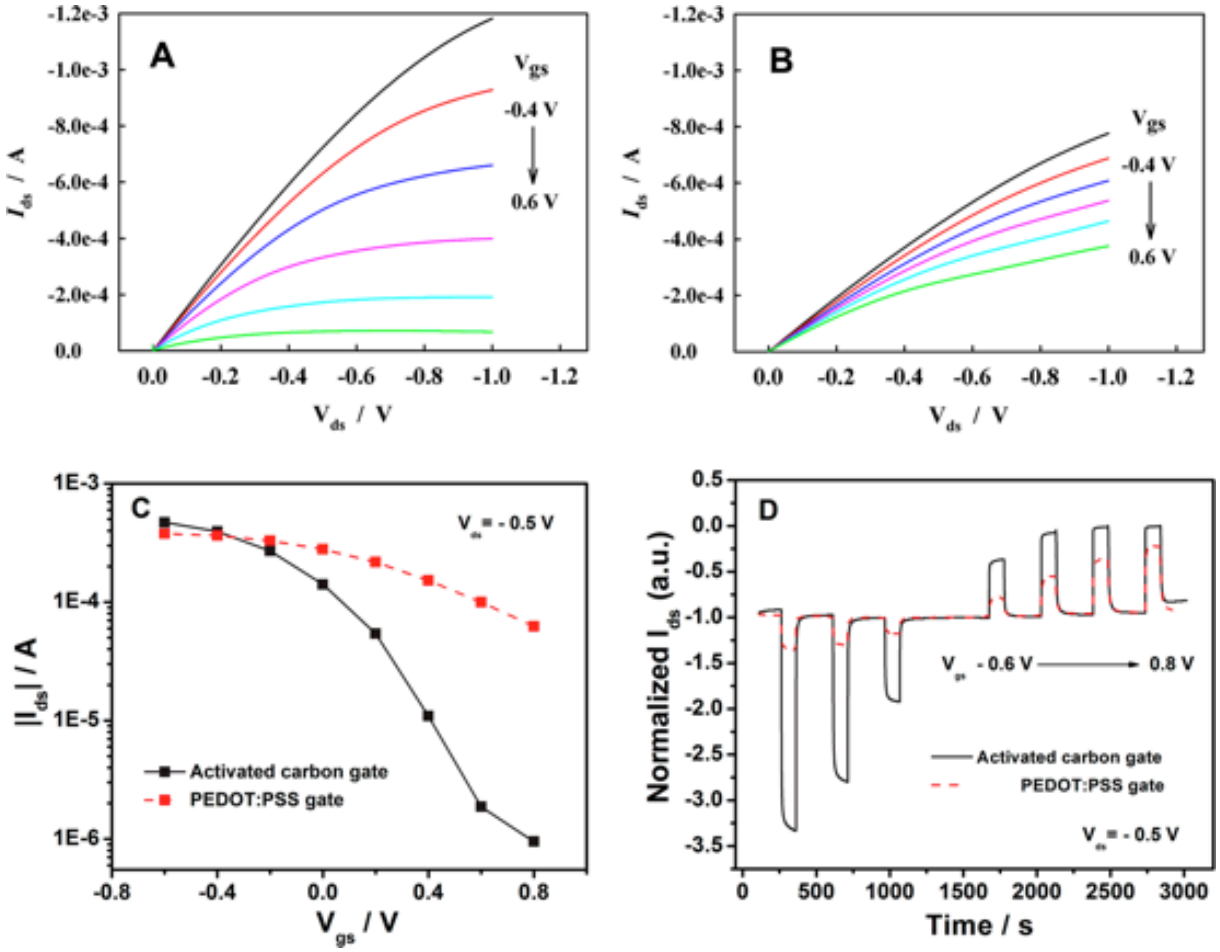

Figure 2. 11. Characteristics of PEDOT:PSS-based OECTs using AC and PEDOT:PSS gate electrodes, employing an aqueous solution of NaCl (0.01 M) as the electrolyte. Typical output characteristics obtained with an AC (A) or a PEDOT:PSS gate electrode (B). The V_d scan rate is 5 mV s^{-1} and V_g is varied from −0.4 to +0.6 V in steps of 0.2 V. Transfer characteristics (C) of PEDOT:PSS OECTs using an AC (black line) and a PEDOT:PSS gate electrode (red line) at V_d =

−0.5 V and −0.6 $V \leq V_g \leq 0.8$ V. Transient (I_d vs time) responses (D) normalized with respect to the current at $V_g = 0$ V of OECTs using AC (black solid line) and PEDOT:PSS (red dashed line) gate electrodes at $V_d = -0.5$ V. From left to right, V_g is pulsed from 0 to −0.6, −0.4, −0.2, +0.2, +0.4, +0.6 and +0.8 V with a pulse duration of 100 s [75]. Reprinted with permission. Copyright © 2015, American Chemical Society.

Cyclic voltammetry studies were carried out with a PEDOT:PSS working electrode (WE) and AC as both reference electrode (RE) and counter electrode (CE). The high double-layer capacitance and absence of Faradaic processes show that the potential of the channel is solely determined by V_g. The intrinsic quasi-reference characteristics of AC provide an opportunity to monitor the potential of the channel of an OECT without an additional reference electrode (Figure 2.14).

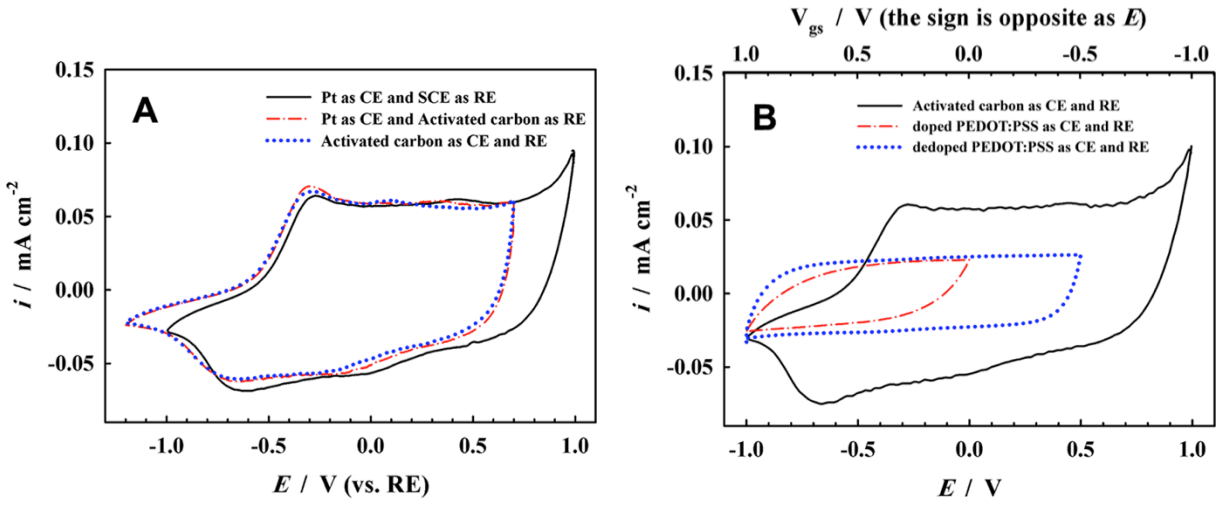

Figure 2. 12. Cyclic voltammograms of various electrochemical cells where the electrolyte is a 0.01 M aqueous solution of NaCl, a doped (pristine) PEDOT:PSS film acts as the working electrode (WE) and different counter electrodes (CE) and reference electrodes (RE) are compared. (A) Three-electrode configuration with a Pt wire CE and a saturated calomel electrode (SCE) RE (black solid line), three-electrode configuration with a Pt wire CE and an AC electrode RE (red dashed curve) and two-electrode configuration with an AC electrode acting as CE and RE (blue dotted curve). (B) Two-electrode configuration with an AC electrode (black solid curve) or a doped (pristine) PEDOT:PSS film (red dashed curve) or a dedoped PEDOT:PSS (blue dotted curve) acting simultaneously as CE and RE. The CV scan rate is 50 mV s^{-1}. The top x-axis

indicates the corresponding V_g in OECTs [75]. Reprinted with permission. Copyright © 2015, American Chemical Society.

Biocompatible gate materials have been widely investigated due to the rapid development of OECTs and their potential for biological applications. As a representation of a non-traditional gate electrode, skin is an interesting candidate for an OECT used as an electrocardiographic (ECG) sensor. Traditional ECG sensors utilize Ag/AgCl to establish a Faradaic contact with the skin [76]. Biscarini et al. demonstrated transparent transistor devices fabricated on a degradable PLGA substrate and utilized the skin as the gate electrode and to transport the heart beating that served as "V_g" [77]. To reduce the skin's impedance, electroconductive gel was used between the skin and the PEDOT:PSS channel. The skin behaves as the gate, and its potential changes with respect to a ground contact. The change of the gate potential modulates the drain current (Figure 2.15a). The OECT recorded the heartbeat with amplitude of 100 nA, whereas the traditional potentiometric recorder monitored spikes of 500 µV (Figure 2.15 b and c).

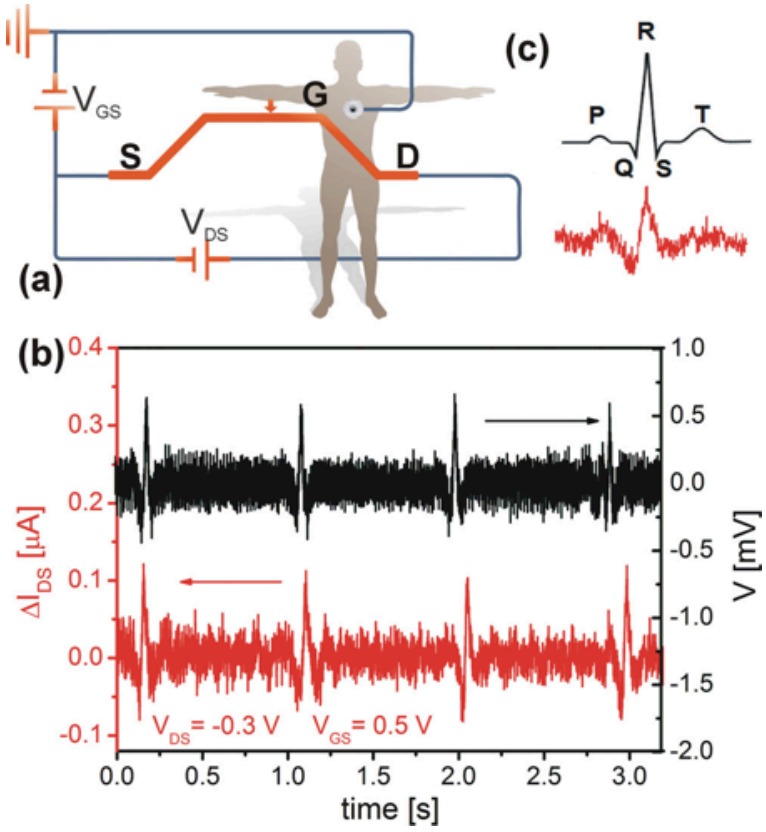

Figure 2. 13. ECG recording with a bioresorbable OECT operated in direct contact with the skin. (a) Wiring diagram of the experiment. (b) Measured drain current trace (red) as obtained during ECG recording (V_g = 0.5 V, V_d = −0.3 V) and comparison with a normal potentiometric recording with standard disposable leads (black). (c) Enlarged transistor ECG trace of a single cardiac cycle and comparison to a schematic textbook example [77]. Reprinted with permission. Copyright © 2014 WILEY‐VCH Verlag GmbH & Co. KGaA, Weinheim.

2.2.4 Substrate

The substrate is one of the most important components for organic electronics, due to the fact that organic electronics are not free-standing except in some special conditions [78-82]. With the development of organic bioelectronics, various substrates have been employed to meet the needs of implantation [83], drug delivery [84], artificial skin [85], sensing [86] or monitoring behavior of cells [87] in vivo or in vitro environments. The most interesting substrates studied in this thesis are OECTs with flexible and degradable substrates.

2.2.4.1 Flexible substrates

The current generation of flexible electronics is highly motivated by the quest for devices that are disposable, low-cost and energy efficient, as a route to cheap and environmentally friendly tools. Substrates such as plastics, papers and metal foils are nowadays widely investigated for applications in flexible electronics [88-90].

Films of the polyester polyethylene terephthalate (PET) are among the most interesting candidates as plastic substrates, because they are lightweight, reasonably stable chemically and thermally, smooth, able to yield thin layers suitable for roll-to-roll processing and show adequate adhesion to organic thin films [91].

Several authors have reported about devices on flexible substrates. A label-free DNA sensor that integrates a flexible PET substrate has been investigated [92]. The OECT was patterned by photolithography. The ssDNA probes was immobilized on the surface of the Au gate electrode, and a poly(dimethylsiloxane) (PDMS) microfluidic well was fixed on top of the patterned PEDOT:PSS channel for the electrolyte (Figure 2.16a). The device can be bent to both sides very

easily (Figure 2.16b). The transfer characteristics show that the device performance is consistent before and after bending (Figure 2.16c). The transient curves show that I_d arrives at stable values in several seconds with different gate voltages (Figure 2.16d). Further investigation revealed that the maximum strain is about 5% by bending, which will not affect the conductance of the PEDOT:PSS film. Thus, the OECT performance is stable with bending in both sides.

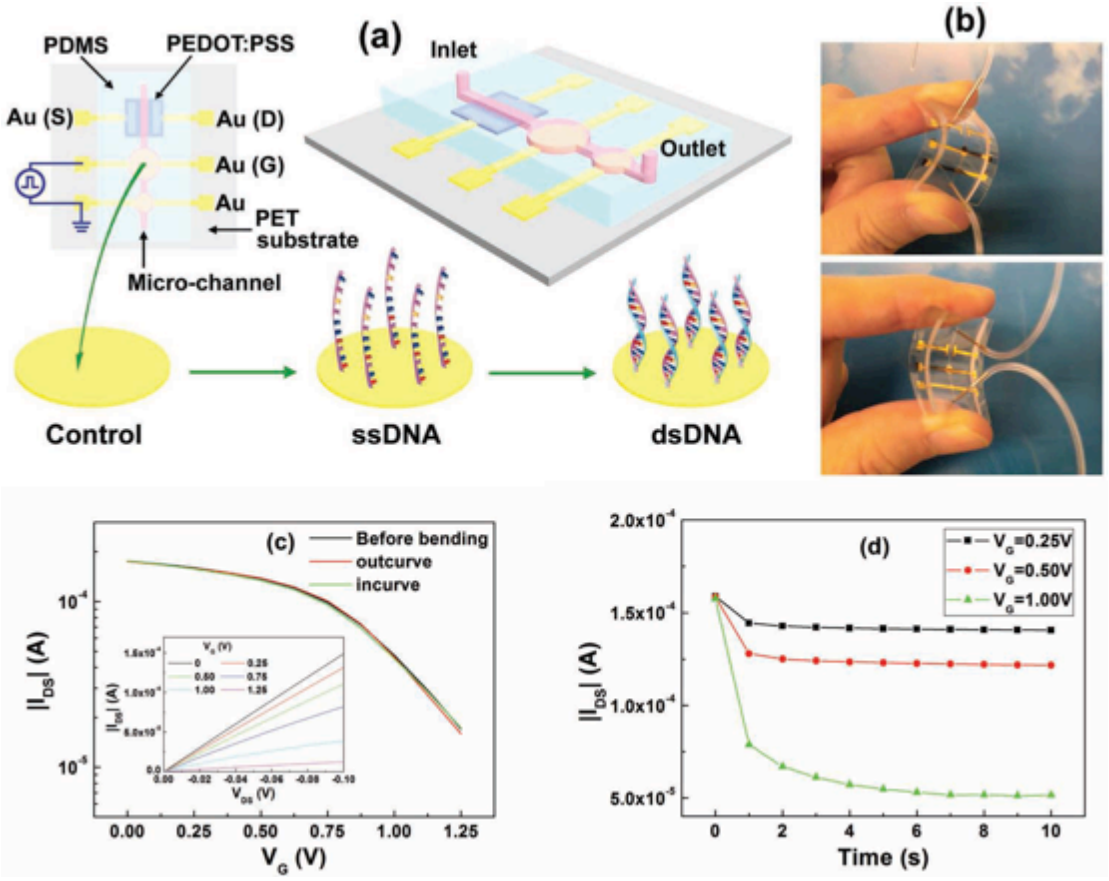

Figure 2. 14. (a) Schematic diagram of an OECT integrated in a flexible microfluidic system, which is characterized before and after the modification and the hybridization of DNA on the surface of Au gate electrode. (b) Photographs of a device bent to both sides. (c) Transfer characteristics (I_d vs. V_g) and output characteristics (I_d vs. V_g) of an OECT measured in different bending states. The microfluidic channel is filled with PBS solution. (d) Time-dependent channel current of an OECT measured after applying different gate voltages. $V_d = -0.1$ V [92]. Reprinted with permission. Copyright © 2011 WILEY‐VCH Verlag GmbH & Co. KGaA, Weinheim.

Malliaras et al. reported OECTs with high transconductance based on parylene C substrates [93]. Transconductance is the main transistor parameter that governs signal amplification, which describes the ability of transistors to convert a change in the gate voltage ΔV_g to a modulation in the drain current ΔI_d ($g_m = \Delta I_d/\Delta V_g$). As shown in Figure 2.17, the OECT can be peeled off its glass substrate and can be used after being crumpled/un-crumpled. There are no major differences in performance between the crumpled and uncrumpled OECTs.

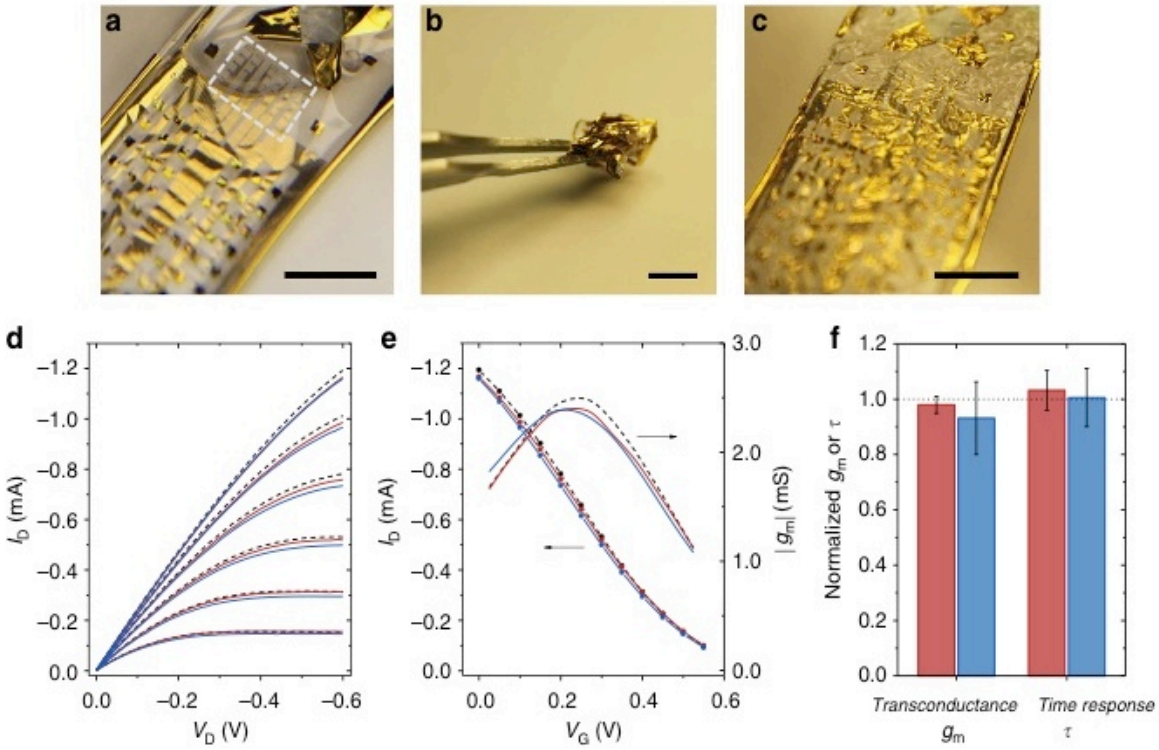

Figure 2. 15. Resistance of OECTs to mechanical deformation. (a) An array of devices removed from the sacrificial glass substrate (active area shown as boxed region). (b) The array aggressively crumpled. (c) The crumpled array converted back to a flat sheet. Scale bar = 1 cm. (d) Output characteristics and (e) transfer characteristics for the same device as-prepared (black), after peeling (red) and after crumpling (blue). (f) Transconductance and time response for devices after peeling (red) and after crumpling (blue), normalized to the performance of each device as prepared. Error bars represent standard deviation of normalized values for N = 16 devices, on three different substrates [93].

2.2.4.2 Degradable substrates

Biodegradable, biocompatible and bioresorbable substrates and electronic materials are attractive for use in organic bioelectronics designed for in vivo applications [94]. “Green” OFETs, composed of natural organic semiconductors and dielectrics combined with biodegradable substrates have been reported [86, 95-99]. Such substrates include paper [89, 100, 101], silk [95, 102-104], leather [105], cellulose-based polymers [106], gelatin [107] and shellac [108].

Synthetic polyesters PLGA are typical materials used for temporary implants [109-110]. They are bioresorbable, hence are transient objects in the body, which is ideal for implants since this minimize the systemic reaction to foreign bodies. The most successful degradable electronic sensors have been recently developed by Rogers et al. [86].

The construction of a millimeter-size biodegradable device involves the use of a ~70 μm-thick nanoporous silicon supporting substrate or ~70 μm-thick magnesium foil, with a membrane of 30 μm PLGA on top (Figure 2.18a and c) transfer printed on the supporting substrate with a microtip-patterned PDMS stamp. In order to have the largest deflection-induced strain, a silicon nanomembrane in a serpentine geometry serves as a piezoresistive element (Figure 2.18b). The silicon nanomembrane is designed to sit on the surface of the membrane near one of the edges of the cavity, because the maximum strain occurs at the midpoint of the left (and right) edge of the trench with any applied pressure (Figure 2.18d). The device can be used as a pressure sensor (Figure 2.18e), motion sensor (Figure 2.18f), temperature sensor (Figure. 2.18g), flow sensor (Figure 2.18h), thermal conductivity/diffusivity sensor (Figure 2.18i) and pH sensor (Figure 2.18j). The sensor degraded after 15 h in buffer solution at pH 12 and room temperature (Figure 2.18k).

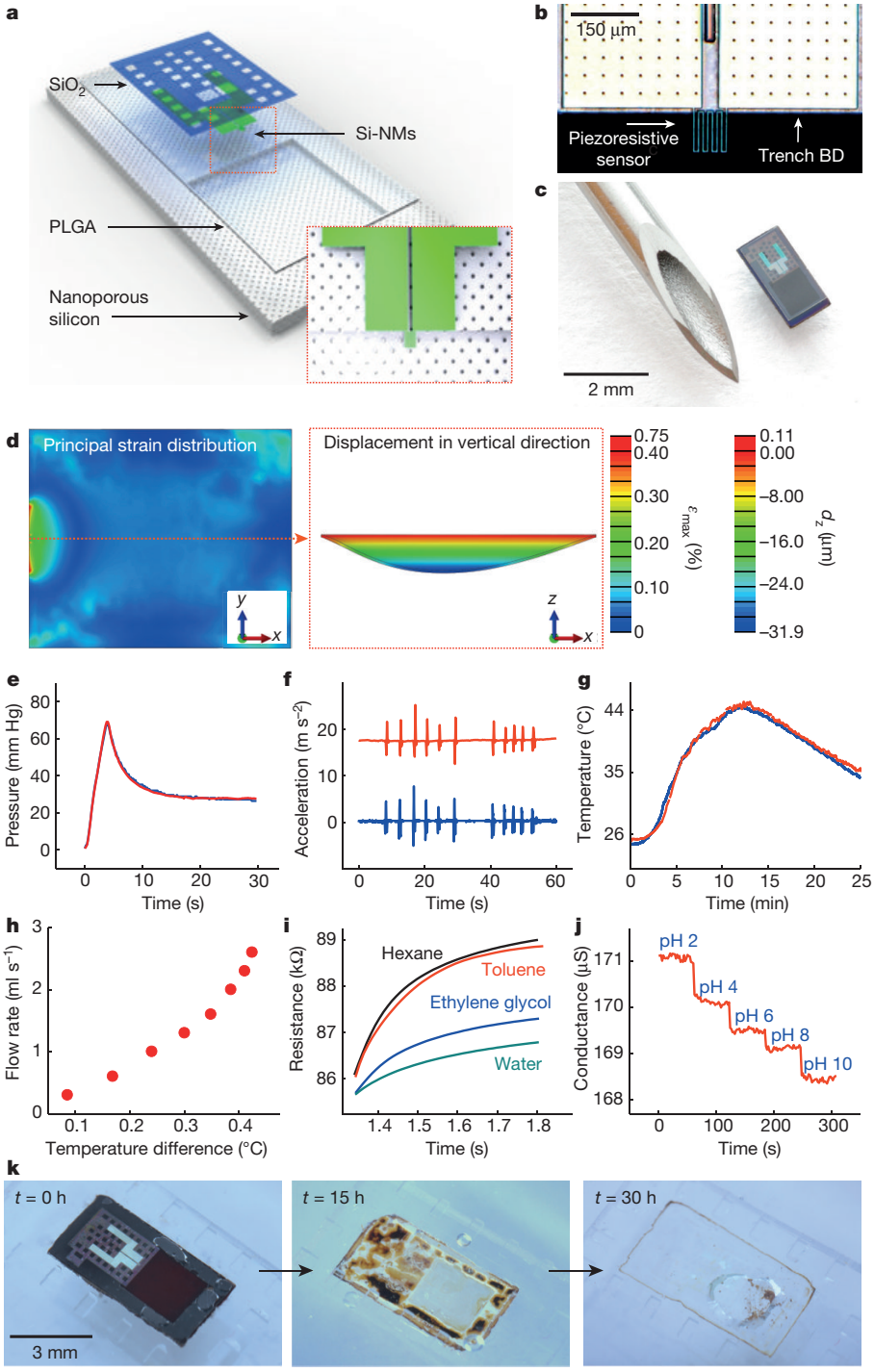

Figure 2. 16. Bioresorbable, silicon-based mechanical/physical/chemical sensors for biomedical applications. (a) Schematic illustration of a biodegradable pressure sensor. The inset shows the location of the silicon nanomembrane (Si-NM) strain gauge. (b) Optical micrograph of the strain-gauge region. 'Trench BD' represents the boundary of the trench. (c) Image of a complete device.

The outer diameter of the hypodermic needle is 1 mm. (d) Image on the left shows the distribution of principal strains across the PLGA layer, including the Si-NM strain gauge at the left edge, determined from finite element analysis (FEA) for an external pressure of 50 mm Hg. The image on the right shows the corresponding displacement profile evaluated along the red dotted line in the left panel. ε_{max} and d_Z are the principal strain and vertical displacement, respectively. (e) Responses of a commercial pressure sensor (blue) and a calibrated biodegradable device (red) to time-varying pressure over a range relevant to intracranial monitoring. (f) Response of a similar biodegradable device (red), but configured as an accelerometer, with comparison to a commercial sensor (blue). (g) Comparison of the calibrated response of such a bioresorbable temperature sensor (red) to a commercial device (blue). (h) The difference in temperature measured by two separate Si-NM temperature sensors placed near a Si-NM element for Joule heating, which allows assessment of flow rate. (i) A single serpentine Si-NM used as both a temperature sensor and a heating element allows measurements of thermal conductivity and heat capacity. The graph shows time-dependent changes in temperature upon actuation of Joule heating in devices immersed in different liquids. The coefficients of thermal conductivity (κ, measured through the rate of resistance change) of hexane, toluene, ethylene glycol and water are 0.12, 0.13, 0.26, and 0.60 W $m^{-1}K^{-1}$, respectively. (j) When the Si-NM is exposed to aqueous surroundings, its conductance depends on pH. The graph shows measurements for immersion in solutions with pH values between 2 and 10. (k) Images collected at several stages of accelerated dissolution of a bioresorbable pressure sensor upon insertion into an aqueous buffer solution (pH 12) in a transparent PDMS enclosure at room temperature [86]. Reprinted with permission.

Müller et al. developed the first silk fiber-based electrochemical transistors [111]. The silk fibers were obtained from the silkworm (*Bombyx mori*) and were dyed by water-soluble poly(4-(2,3-dihydrothieno[3,4-*b*]-[1,4]dioxin-2-yl-methoxy)-1-butanesulfonic acid) (PEDOT-S) via electrostatic interactions throughout the bulk. The fibers are arranged in a cross-junction configuration (Figure 2.19b). The gaps between adjacent fibers are filled with the electrolyte, 1-butyl-3-methylimidazolium bis(trifluoromethanesulfonimide) ([bmim][Tf_2N]) mixed with poly(1-vinyl-3-methylimidazolium) bis(trifluoromethanesulfonimide) (poly[ViEtIm][Tf_2N]) (1:1 w/w) (Figure 2.19a).

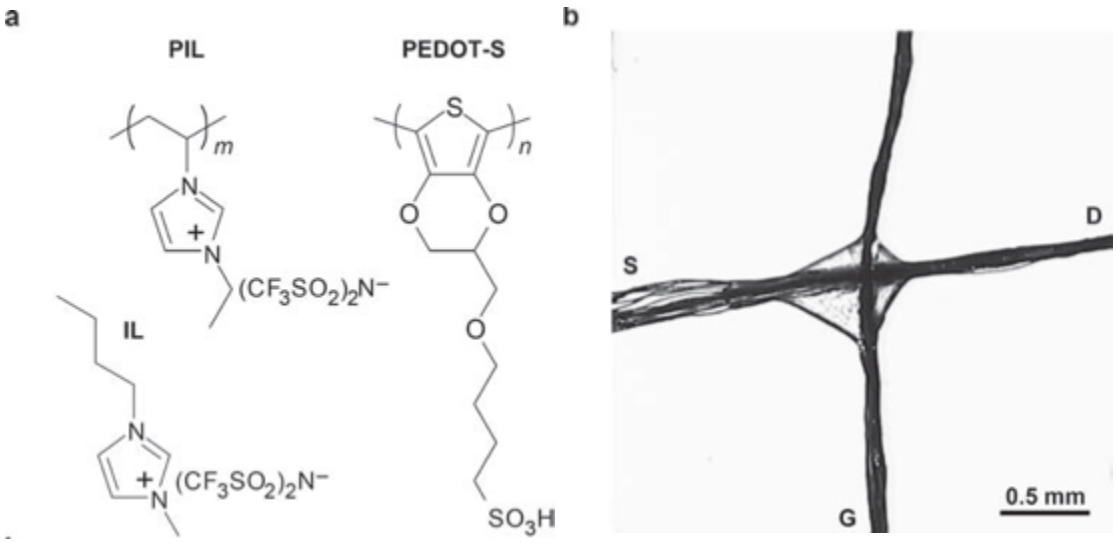

Figure 2. 17. (a) Chemical structure of the imidazolium-based ionic liquid:polymer ionic liquid (IL:PIL) electrolyte mixture [bmim][Tf_2N]:poly[ViEtIm][Tf_2N] and the conjugated polyelectrolyte dye PEDOT-S. (b) Microscopy image of a silk fiber-based ECT device with source (S), drain (D) and gate (G) as indicated. A drop of IL:PIL bridges the gap between the two fibers at the cross-junction. Note that the source-drain fiber has split into monofilaments close to S [111]. Reprinted with permission. Copyright © 2011 WILEY-VCH Verlag GmbH & Co. KGaA, Weinheim.

Shellac, a natural polymer secreted by the insect *Kerria lacca*, which is native to India, Thailand and China, is a biodegradable resin containing polyhydroxy acids, shellolic acid, jalaric acid and aleuritic acid (Figure 2.20) [108]. Shellac has found applications in the past as a coating material for phonograph records and wood, as a binder and encapsulate for pharmaceuticals and food supplements and in other areas, such as in cosmetic products, barrier coatings against gases and moisture for fruits and vegetables, and sacrificial molds for 3D interconnected microchannel networks [112-117].

Shellac can be dissolved in alcoholic solvents and then processed into thin films by simple methods, such as spin coating or drop casting. The films, being robust and smooth, can be used as

substrates for OFETs. The roughness of the shellac surface is around 1 nm for a ~500 μm film. Moreover, the shellac film presents excellent insulating properties and can be used as a high-quality dielectric layer, with a roughness of about 0.4 nm [108].

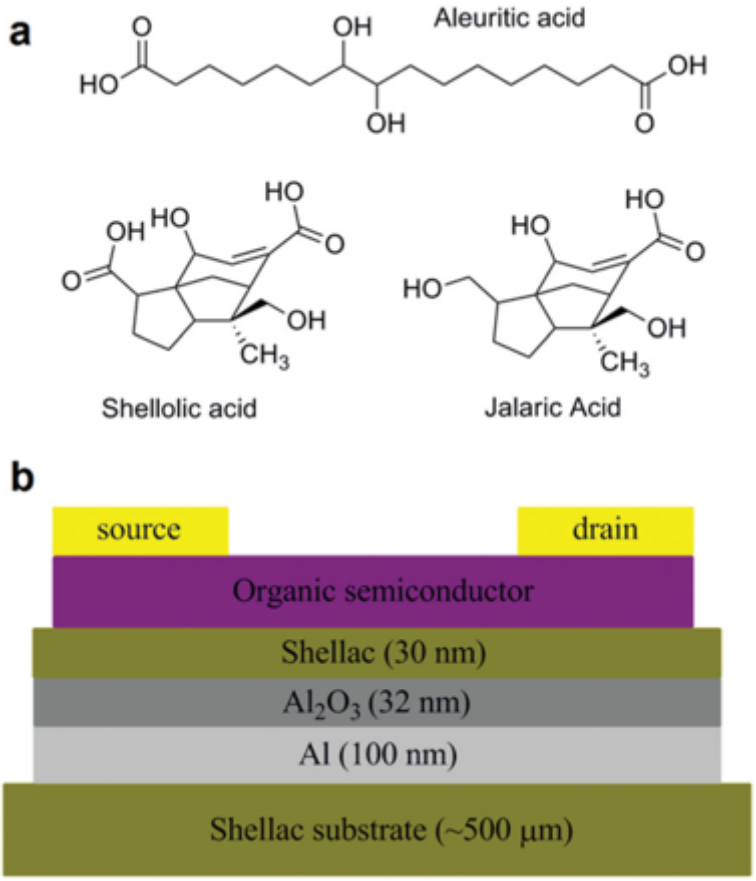

Figure 2. 18. (a) The main chemical components of shellac resin. The constituents can readily undergo polyesterification to produce a cross-linked solid. (b) Schematic of the OFET devices reported in this paper, where shellac functions both as substrate material and dielectric layer [108]. Reprinted with permission. Copyright © 2013, Royal Society of Chemistry.

Paper, composed of compact moist wood cellulose fibers, is a low-cost biodegradable material that is compatible with many chemical and biochemical moieties [89, 118]. Paper can be used as a substrate for biosensors [119], strain sensors [120], energy storage systems [121] and microfluidic devices [122]. The properties and morphology of paper, such as roughness, porosity, impurities, mechanical damping and the type and orientation of fibers, have dominant influences on the performance of the sensors.

Bihar et al. [123] developed OECTs printed on paper substrates, which found applications as alcohol sensors. The ethanol concentration can be detected with breathing onto the device (Fig. 2.21A). Planar OECTs have been utilized with PEDOT:PSS as channel, source (S), drain (D), and gate (G) electrodes. A collagen-based gel was used as the electrolyte, which contains enzyme alcohol dehydrogenase (ADH) and its cofactor nicotinamide adenine dinucleotide (NAD^+) (Fig. 2.21B). The transient curve shows that the I_d decreases with exposing OECT-breathalyzer to ethanol (Fig. 2.21C).

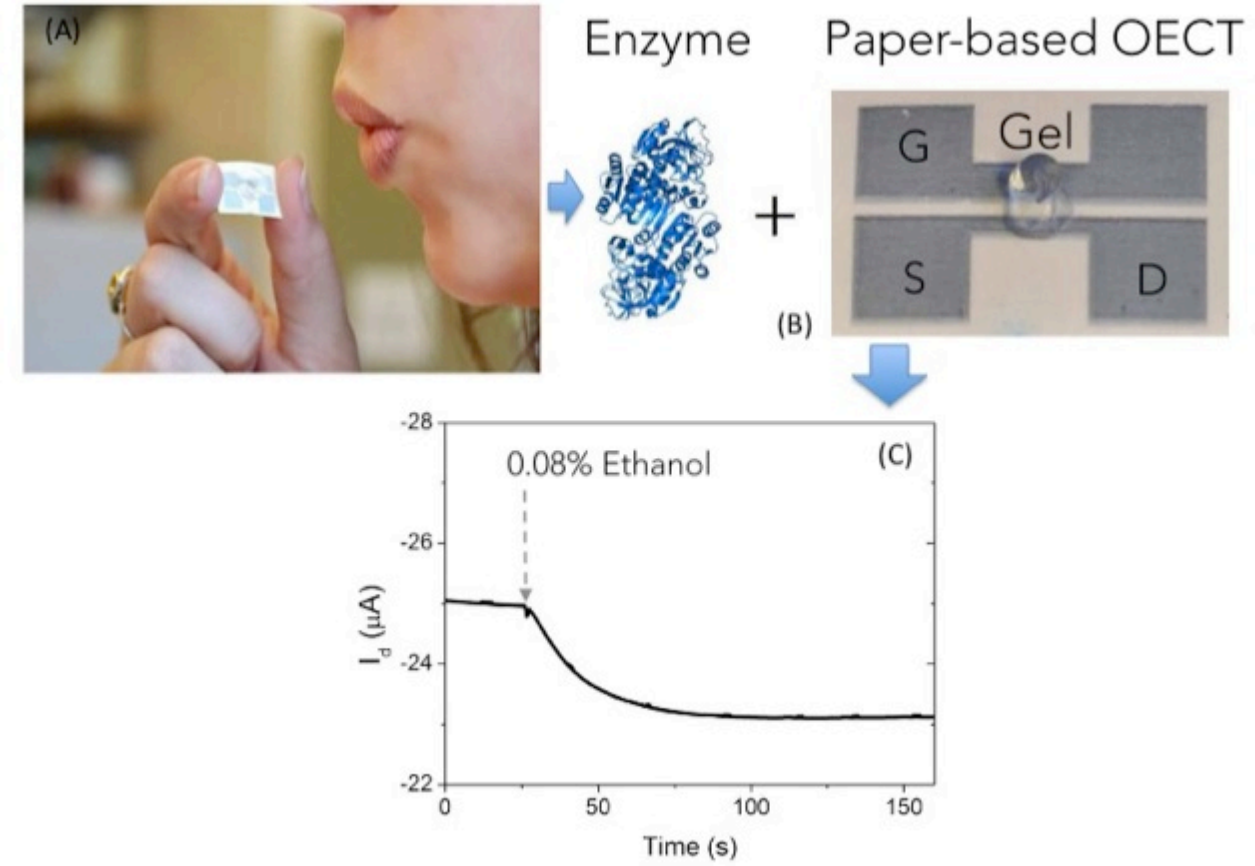

Figure 2. 19. Concept of the OECT-breathalyzer. (A) Simply breathing on the printed PEDOT:PSS OECT allows for alcohol detection. (B) The alcohol dehydrogenase (ADH) enzyme and the OECT are the key components of the sensor. The OECT is printed on paper, and comprises a channel, source (S), drain (D), and gate (G) electrodes made of PEDOT:PSS. The enzyme electrolyte gel is deposited to the OECT bridging the channel and gate. (C) I_d response of the OECT upon exposure to ethanol [123].

CHAPTER 3

ARTICLE 1: Ionic liquid–water mixtures and ion gels as electrolytes for organic electrochemical transistors

This chapter has been published in the Journal of Materials Chemistry C. The supporting information for this article is reprinted in Appendix A of this thesis.

3.1 Authors

Zhihui Yi,[a] Giovanniantonio Natale,[a] Prajwal Kumar,[a] Eduardo Di Mauro,[b] Marie-Claude Heuzey,[a] Francesca Soavi,[c] Iryna I. Perepichka,[d] Sunil K. Varshney,[d] Clara Santato*[b] and Fabio Cicoira*[a]

[a]Department of Chemical Engineering, Polytechnique Montréal, CP 6079, Succursale Centre-Ville, Montréal, Québec H3C 3A7, Canada. E-mail: fabio.cicoira@polymtl.ca

[b] Department of Engineering Physics, Polytechnique Montréal, CP 6079, Succursale Centre-Ville, Montréal, Québec H3C 3A7, Canada. Clara.santato@polymtl.ca

[c]Department of Chemistry "Giacomo Ciamician", Università di Bologna, Via Selmi, 2, 40126, Italy.

[d]Polymer Source, Inc., 124 Avro street, Dorval, Quebec H9P 2X8, Canada.

3.2 Abstract

Organic Electrochemical Transistors (OECTs) are widely investigated for applications in bioelectronics. Ionic liquids (ILs) are, in principle, interesting candidates as gating media in OECTs. Nevertheless, ILs can exhibit excessively high viscosity that prevents their

straightforward application in OECTs. Here we report two processing approaches to apply the highly viscous ionic liquid triisobutyl(methyl)phosphonium tosylate (Cyphos® IL 106) in OECTs based on poly(3,4-ethylenedioxythiophene) polystyrenesulfonate (PEDOT:PSS), namely IL–H_2O binary mixtures and ion gels. The use of Cyphos® IL 106–H_2O binary mixtures and ion gels as gating media determines an increase of the OECT modulation, with respect to the pure ionic liquid. This increase cannot be explained simply by the change of the viscosity and ionic conductivity of the ionic liquid–H_2O mixtures with the increase of the H_2O content. Using high surface area activated carbon gates, ON/OFF ratios as high as 5000 are achieved with Cyphos® IL 106–H_2O mixtures at 5 and 10% H_2O v/v.

3.3 Introduction

Ionic liquids are molten salts at relatively low temperature (typically below 100 °C) that possess high thermal and chemical stability, optical transparency, low volatility, and wide electrochemical stability windows [71,73,74,124]. Owing to these unique properties, ionic liquids have found several technological applications, such as solvents for organic and inorganic synthesis and (bio)catalysis, electrolytes in electrochemical devices, and media for enzyme storage and reactions [33,73,124-129] In particular, phosphonium ionic liquids are interesting for their thermal stability and wide electrochemical stability window [62].

The diverse molecular structures of the anionic and cationic species constituting an ionic liquid can give rise to a variety of interactions, such as electrostatic, van der Waals, and hydrogen bonding. These interactions control the physicochemical properties of ionic liquids, such as ionic conductivity and viscosity [71,73,74,124,130]. The physicochemical properties of ionic liquids can be tailored for specific applications by mixing with a solvent [131].

Electrolyte-gated organic transistors make use of organic materials for the transistor channel and of electrolytes, such as aqueous saline solutions, ionic liquids, and ion gels, as the gating media. These transistors exhibit current modulations of several orders of magnitude upon application of gate voltages as low as 0.5–2 V [21,39,132-135]. On the basis of their operating mechanism, electrolyte-gated transistors can be divided into two groups: electrical double layer transistors and electrochemical transistors. In electrical double layer transistors, current modulation relies on electrostatic doping of the channel at the channel/electrolyte interface. In electrochemical

transistors, the current is modulated by doping/dedoping of the bulk of the organic channel by electrolyte ions. Organic Electrochemical Transistors (OECTs) are investigated in bioelectronics because of their low operating voltage (< 1 V), which is compatible with aqueous media, where biological processes take place [4, 24, 26]. Depending on the targeted application, OECTs can make use of various types of electrolytes, including aqueous or organic solutions, ionic liquids and gels. Among the properties that make electrolytes suitable for OECTs are wide electrochemical stability window, good ionic conductivity and low viscosity.

Here we investigate the use of a highly viscous ionic liquid, i.e. triisobutyl(methyl)phosphonium tosylate (Cyphos® IL 106, inset Figure 3.1a), as electrolyte for OECTs. Cyphos® IL 106 is interesting for bioelectronic applications because of its miscibility with aqueous media, electrochemical stability, ability to act as a reservoir for enzymes and mediators in electrochemical sensors [33, 62]. Furthermore, it is an active and selective solvent for conversion of fructose into hydroxymethylfurfural without any catalyst addition [136, 137]. The interaction between Cyphos® IL 106/H_2O binary mixtures and thin films of the conducting polymer poly(3,4-ethylenedioxythiophene) doped with tosylate has been recently explored [138].

Specifically, we propose two processing approaches to employ Cyphos® IL 106 as electrolyte for OECTs. The first approach consists in using ionic liquid/H_2O binary mixtures. The second consists in incorporating the ionic liquid into an ion gel. With the aim to establish a correlation between the physicochemical properties of the gating media and device characteristics, we studied the viscosity and the ionic conductivity of the electrolytes.

3.4 Results and discussion

The gating properties of Cyphos® IL 106/H_2O binary mixtures were first investigated on planar OECTs employing the conducting polymer poly(3,4-ethylenedioxythiophene) doped with polystyrene sulfonate (PEDOT:PSS) as the transistor channel and the gate electrode (Figure ESI1 in Appendix B). The OECT current modulation, $|(I–I_0)/I_0|$, where I and I_0 are the drain-source currents at $V_g \neq 0$ and at $V_g = 0$, is shown as a function of the gate-source voltage, V_g, for pure Cyphos® IL 106 and for Cyphos® IL 106/H_2O binary mixtures (Figure 3.1a). Mixing Cyphos®

IL 106 with 2% H_2O v/v (*i.e.* 98% Cyphos® IL 106 v/v) leads to a considerable increase of the current modulation with respect to pure Cyphos® IL 106 (*e.g.* from ~0.15 to ~0.25 at $V_g = 0.8$ V). Increasing the H_2O content to 5% v/v further increases the modulation up to ~0.5. Upon further H_2O addition, *i.e.* for 50%, 90%, 95%, and 99% H_2O v/v, the OECT modulation remains substantially unchanged (Figure 3.1a and Figure ESI2). The transfer curves of OECTs using as the gating medium pure Cyphos® IL 106 and Cyphos® IL 106/H_2O mixtures (Figure ESI3) show that the drain-source current (I_d) decreases with the increase of V_g, consistently with the depletion mode of operation of PEDOT:PSS OECTs.

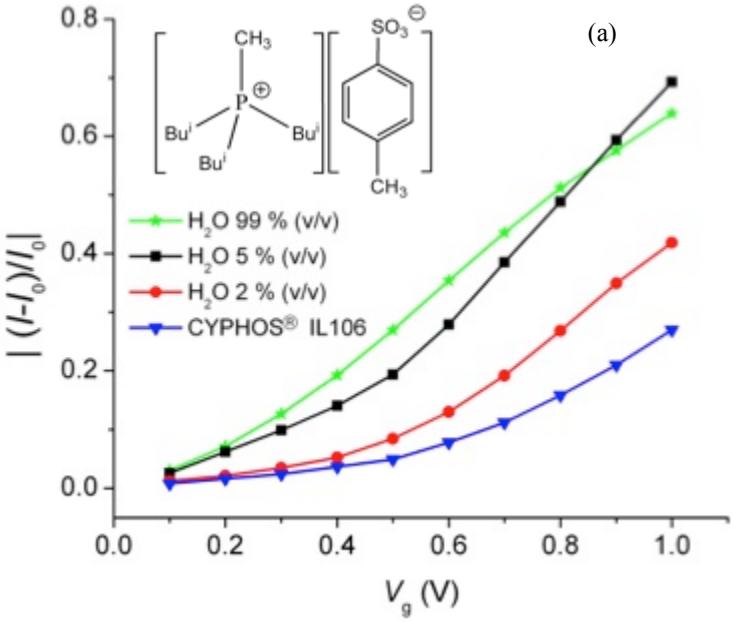

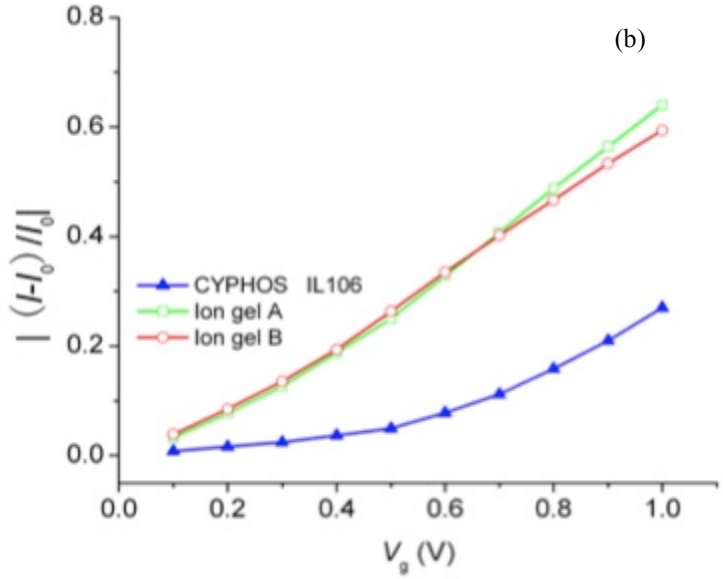

Figure 3. 1. Current modulation $|(I–I_0)/I_0|$ *vs.* V_g for PEDOT:PSS OECTs making use of a PEDOT:PSS gate for: (a) Cyphos® IL 106, and Cyphos® IL 106/H_2O mixtures at 2%, 5%, 99% H_2O v/v and (b) pure Cyphos® IL 106 and ion gels A (SMMAS:Cyphos® IL 106 1:10 g/g) and B (SMMAS:Cyphos® IL 106 1:5 g/g). $V_d = -0.2$ V. Inset (a): Molecular structure of Cyphos® IL 106. The current modulation is obtained from transient measurements (current vs time at different V_g) and it is defined as $|(I–I_0)/I_0|$, where I is the drain-source current at $V_g \neq 0$ V and the I_0 is the current at V_g=0 V taken before each V_g pulse. Lines are guides to the eye.

To gain insight into the improvement of the OECT performance upon H_2O addition to Cyphos® IL 106, we investigated the effect of H_2O on viscosity and ionic conductivity. As shown in Figure 3.2, the Newtonian viscosity (η) decreases dramatically from about 4000 mPa·s, for the pure Cyphos® IL 106, to about 110 mPa·s, for a mixture containing 10% H_2O v/v. For higher H_2O content, the viscosity decreases gradually to a few mPa·s (*e.g.* about 3 mPa·s for 70% H_2O v/v). The presence of complex interactions between H_2O and Cyphos® IL 106 is revealed by Figure 3.2, which shows that the viscosity of our mixtures always lies below the line corresponding to the viscosity of an ideal mixture (the dashed line between the values of the viscosities of the two pure components). The effect of H_2O on the viscosity can be further understood considering the results reported in the inset of Figure 3.2, where the dynamic storage modulus, *G'*, and loss modulus, *G"*, are shown for the pure Cyphos® IL 106 and for Cyphos® IL 106/H_2O mixture with 5% H_2O v/v. The addition of H_2O causes a decrease in the values of both *G'* and *G"*. The lower values of *G'* and *G"* are compatible with a scenario where the interactions between ions with opposite polarity are partially reduced, thus leading to higher ion mobility. *G*' of the pure Cyphos® IL 106 shows a strong deviation from the classic Maxwell behaviour of fluids at low frequencies, while the viscosity is completely Newtonian [139].

The ionic conductivity, as measured by a conductivity meter, increases from a few fractions of mS/cm for pure IL up to ~12 at 70% H_2O v/v, then decreases to ~8 mS/cm at 90%, and ~1.5 mS/cm at 99% H_2O v/v (Table ESI1). Upon addition of molecular solvents to viscous ionic liquids, a significant drop of the viscosity and an increase of the ionic conductivity, followed by a decrease with further addition of solvent, are generally expected [140-144].

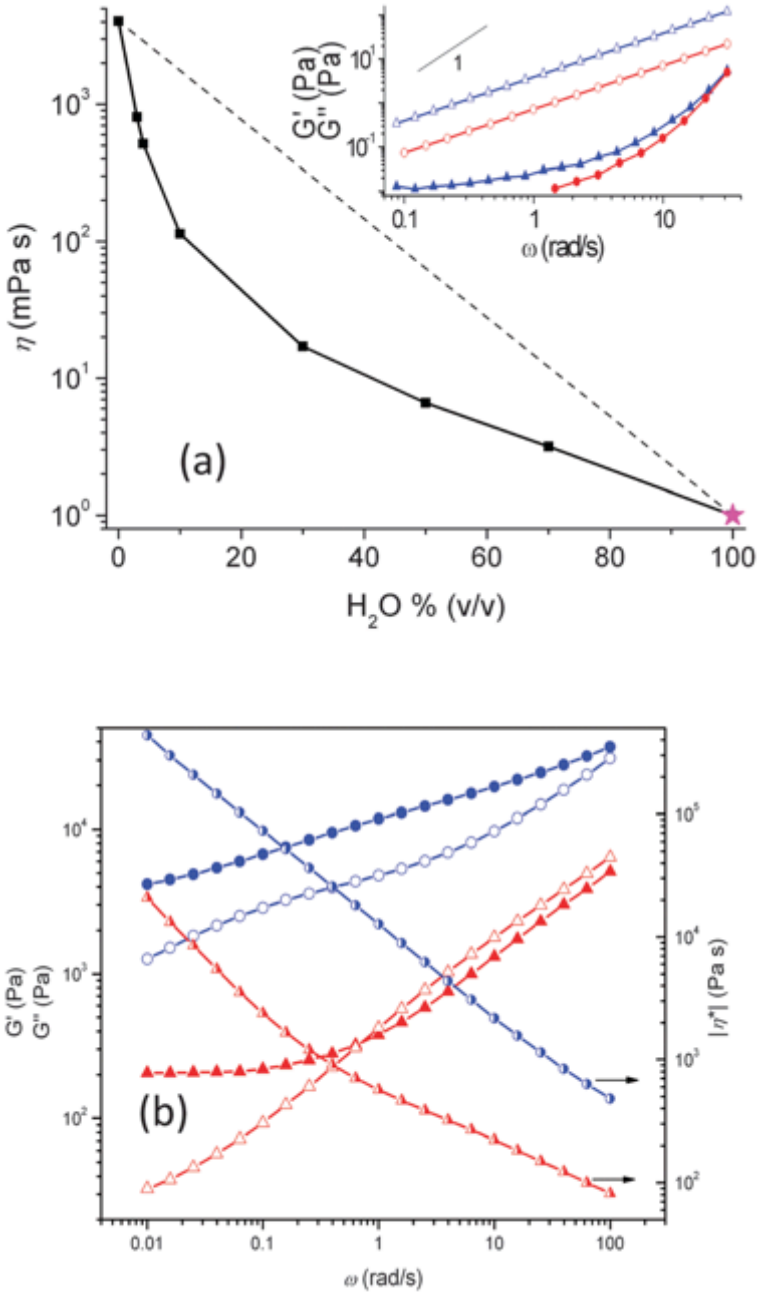

Figure 3. 2. (a) Shear viscosity (η) of pure Cyphos® IL 106, Cyphos® IL 106-H_2O mixtures (2%, 5%, 10%, 30%, 50%, 70% H_2O v/v, filled black squares) and viscosity of pure H_2O (filled star symbol). The dashed line between the values of the viscosities of the two pure components represents the viscosity of an ideal mixture. Inset: Variation of the storage (*G',* solid symbols) and loss (*G",* empty symbols) modulus with the angular frequency for pure Cyphos® IL 106 (blue

triangles) and Cyphos® IL 106/H_2O mixture at 5% H_2O v/v (red circles). The slope 1 is reported as a reference for the classic behavior of G' for a liquid, at low frequency. (b) Storage Modulus (G', solid symbol), loss Modulus (G", empty symbol) and Complex Viscosity η^* (half-filled symbol) of ion gel A (triangle) and ion gel B (circle).

Ion gels have recently found application in bioelectronics, e.g. for sub cutaneous recordings [145] and DNA sensing [146]. We prepared ion gels from Cyphos® IL 106 and the triblock copolymer polystyrene-b-poly(methyl methacrylate)-b-polystyrene (SMMAS, PolymerSource Inc.) at Cyphos® IL 106: SMMAS mass ratios 1:10 (ion gel A) and 1:5 (ion gel B). The OECT modulations obtained with ion gels A and B (corresponding transfer curves shown in Figure ESI 4) are similar and both higher than those observed with analogue OECTs making use of pure Cyphos® IL 106 (Figure 3.1b). At $V_g = 0.8$ V, the modulation is ~0.5 for both ion gels and ~0.15 for pure Cyphos® IL 106. The ionic conductivity measured by electrochemical impedance spectroscopy for ion gel A is $3 \cdot 10^{-2}$ mS/cm whereas for ion gel B it is $7 \cdot 10^{-3}$ mS/cm, in agreement with the higher ionic concentration in ion gel A.

The linear viscoelastic properties of the two ion gels were studied (Figure 3.2b). Ion Gel A presents G' values larger than G'' in all the range of frequencies probed. The slope of G' is $\omega^{0.06}$ confirming the weak frequency dependence. The ion gel B is about two orders of magnitude more viscous than ion gel A (at 0.01 rad/s). This is consistent with the lower content of SMMAS in ion gel A. The storage modulus shows a plateau at low frequencies and it is higher than its complex counterpart. A crossover point is observed at about 0.64 rad/s, where G'' overcomes G'. Despite the high viscosity observed for ion gels, compared to ionic liquid/H_2O mixtures, OECTs with PEDOT:PSS gates show relatively similar values of the modulation.

With the aim to improve the performance of OECTs gated by electrolytes based on Cyphos® IL 106, we used high surface area (1000−2000 $m^2\ g^{-1}$) activated carbon gate electrodes (Figure ESI1) [39,135]. Figure 3.3 shows transfer curves for pure Cyphos® IL 106 and various Cyphos® IL 106/H_2O mixtures. Transfer curves, where the current is reported on a logarithmic scale, are more appropriate than modulation *vs* V_g curves, to display the characteristics of devices with high

ON/OFF ratios. The OECT ON/OFF ratio strongly depends on the water content in the mixtures and increases from ca. 40 (pure Cyphos® IL 106) to ca. 5000 (Cyphos® IL 106/H_2O 10% H_2O v/v). Further increasing the H_2O content leads to a decrease of the ON/OFF ratio yielding to a value close to that found for pure Cyphos® IL 106 for 99% H_2O v/v (inset Figure 3.3 and Table ESI2). The transfer curves of the mixture at 99% H_2O v/v and pure Cyphos® IL 106 overlap. For the sake of comparison, transfer characteristics were measured for 0.1 M NaCl and ionic liquid/H_2O mixture at H_2O 70% (v/v): in the latter case higher values of the ON/OFF ratio are observed (Figure ESI5). The highest values of the ON/OFF ratio are not observed in correspondence to the lowest viscosity (Figure 3.2a) neither to the highest ionic conductivity. The variation of the ON/OFF ratio with the H_2O content suggests that contributions other than the viscosity and the ionic conductivity of the gating medium have to be considered to completely understand the doping/dedoping process of PEDOT:PSS channels exposed to electrolytes based on Cyphos® IL 106.

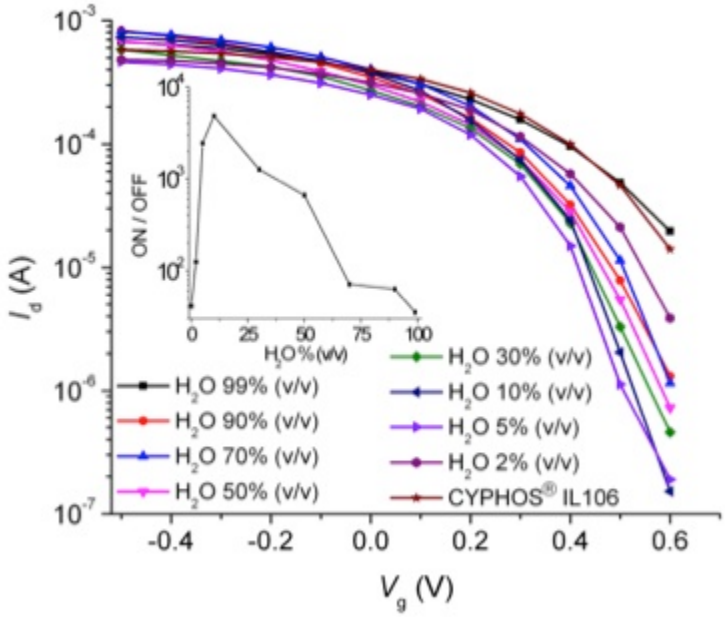

Figure 3. 3. Transfer characteristics of PEDOT:PSS OECTs making use of activated carbon as the gate electrode and different Cyphos® IL106/H_2O mixtures as the gating media. V_d = −0.5 V. Inset: ON/OFF ratio for different Cyphos® IL 106/H_2O mixtures.

3.5 Conclusions

In conclusion, we identified two processing approaches to use the highly viscous, hydrophilic, phosphonium-based ionic liquid Cyphos® IL 106 as the electrolyte in OECTs. The transistor modulation improves from about 0.15 for pure Cyphos® IL 106 to about 0.5 for a binary mixture 5% H_2O v/v. Similar modulations were obtained for ion gels based on the same ionic liquid, when using PEDOT:PSS gates.

Furthermore, by making use of high surface area activated carbon gates, ON/OFF ratios as high as 5000 were reached in OECTs making use of binary mixtures at 10% H_2O v/v. Experiments with activated carbon gates point to the weak dependence of the OECT performance on ionic conductivity and viscosity of the electrolyte, for values >1 mS/cm and <500 mPa s, respectively, at least within the time scale of our experiments. Time resolved experiments, at different gate pulse duration, are expected to improve the understanding of the role played by the physicochemical properties of the gating media on the rate of the doping /undoping process, thus helping to develop high performance OECTs. Our work suggests that the microstructure of the electrolyte (e.g. ion association) might also play a role in the doping/dedoping process in OECTs to be applied in bioelectronics.

3.6 Experimental

Device fabrication and characterization

An aqueous suspension of poly(3,4-ethylenedioxythiophene):poly(styrenesulfonate), PEDOT:PSS (Clevios^{TM} PH1000, Heraeus Electronic Materials), was mixed with ethylene glycol (EG, Sigma Aldrich) 25 % v/v and with a 0.5 % v/v of the surfactant dodecyl benzene sulfonic acid (DBSA, Sigma Aldrich), in order to enhance film electrical conductivity and improve film processability [147,148]. Transistor gate electrodes (only in case of using PEDOT:PSS gate electrode) and channels with a width (W) of 2 mm and a length (L) of 8 mm were patterned on glass slides using a technique described elsewhere [142]. The Clevios^{TM} PH1000/EG/DBSA mixture was spun onto the substrate at 500 RPM for 9 s followed by 1500 RPM for 40 s. The films were then dried on a hot plate at 140 ºC for 60 min. The resulting film thickness was about 200 nm. A glass cloning cylinder (VWR), attached to the glass slide with polydimethylsiloxane (Dow Corning Sylgard 184), was used to confine the electrolyte solution upon the channel and

the gate electrode of the transistor, the channel being defined by the overlapping of the electrolyte with the organic polymer.

OECT electrical characterization was performed using an Agilent B2902A two-channel source/measure unit, controlled by a LabView software. The gate pulse duration ranged between 50-200 s.

The activated carbon gate electrodes were prepared using carbon paper (Spectracorp 2050, 10 mils) coated with an ink of activated carbon (PICACHEM BP9, 28 mg mL^{-1}) and Nafion binder (2.4 mg mL^{-1}) in isopropanol solvent. Drop casting of the carbon ink was followed by thermal treatment at 60 ^{o}C for 24 h to remove the solvent. We used carbon paper stripes 1 cm × 0.4 cm sized.

Electrolyte preparation and characterization

Cyphos® IL 106 (CAS No.: 344774-05-6, product status: developmental), donated by Cytec Industries Inc. (Canada), was mixed with Milli-Q water using a Vortex mixer (VWR). Ion gels based on Cyphos® IL 106 and the triblock copolymer polystyrene-b-poly(methyl methacrylate)-b-polystyrene (SMMAS, Polymer Source Inc.) were prepared in a nitrogen-purged glove box [149]. Cyphos® IL 106 and SMMAS were co-dissolved in ethyl acetate (Et_2O). SMMAS/Cyphos® IL 106/Et_2O mass ratios of 1:10:10 (ion gel A) and 1:5:10 (ion gel B) were used. The mixture was stirred for 2 hrs at room temperature.

For OECT fabrication and characterization, 100 μL ion gel precursor were transferred into the glass tube well, which was fixed on an OECT to confine the electrolyte. The device was then cured at 70º C for 24 hrs to evaporate the ethyl acetate solvent.

The ionic conductivity of pure Cyphos® IL and 106 Cyphos® IL 106/H_2O binary mixtures (with H_2O 2%, 5%, 10%, 30%, 50%, 70%, 90% and 99% v/v, respectively) was measured with a Traceable Expanded Range Conductivity Meter at room temperature (22°C). Electrochemical Impedance Spectroscopy (EIS) was used to validate the conductivity meter measurements and to evaluate the ionic conductivity of the ion gels. EIS was carried out with a two-electrode cell with stainless steel electrode plates (electrode geometric area 0.5 cm^2, electrode spacing 0.15 cm), using a BioLogic equipment (Model: VSP300). An ac amplitude of 5 mV was used and data were collected in the range 200 kHz–10 mHz, in open circuit conditions. In order to provide a good

contact between the ion gel and the stainless steel plates we proceeded as follows. The plates were immersed in the ion gel precursor. Afterwards, the baking of the precursor was carried out at 80 °C, in situ, for 36h, followed by a final treatment at 50 °C in a vacuum oven. The conductivity of the pure ionic liquid and of the ionic liquid/H_2O binary mixtures was calculated from the high frequency real impedance (R), which in turn was evaluated by fitting the EIS Nyquist plots (lines parallel to the imaginary axis) to an RQ equivalent circuit in the high frequency region. For the ion gels, the Nyquist spectrum consisted in a semicircle in the high frequency range, followed by a low frequency tail. In this case, the electrolyte resistance was obtained by fitting the plots to the $(RQ)Q$ equivalent circuit and taking the semicircle diameter as the bulk electrolyte resistance. Q are constant phase elements that model the geometric and double-layer capacitance of the cell.

Rheological measurements on the pure ionic liquid and on the ionic liquid/H_2O binary mixtures were performed at 25 °C using a Physica MCR502 (Anton Paar) rheometer equipped with a rough profiled Couette flow geometry in order to improve the signal. The diameters of the cup and the shaft were 18.09 mm and 16.66 mm, respectively. Shear viscosity data were obtained in simple shear flow using shear rate ramps between 0.01 and 100 s^{-1}. The data reported in Figure 3.2a were measured at a shear rate of 1 s^{-1}. The behavior of the different mixtures was essentially Newtonian. Dynamic shear tests were also performed in the linear viscoelastic regime for the pure Cyphos® IL 106 and the Cyphos® IL 106/H_2O mixture at 5% v/v.

For the rheological measurements of the ion gels, a parallel-disk geometry was used. The diameter of the top disk was 2.5 cm. A disposable metal cup (diameter 5.3 cm, depth 0.8 cm) was used as the bottom disk. The ion gel was baked directly on the bottom disk to ensure good adhesion during the rheological characterization, after confinement into a PDMS well (diameter 2.8 cm, height 0.45 cm). To favor the removal of the ethyl acetate, the solution of the precursors was poured in four steps (one every two hours), while the temperature was kept at 70°C. Afterwards, the material was left to bake at 50°C for 48 hours and finally at 70°C, in a vacuum oven, for 12 hours. The rheological measurements were performed only once per ion gel, and, as a consequence, they only provide the order of magnitude of the measured values.

3.7 Acknowledgements

This work is supported by NSERC Discovery grants (F.C. and C.S.) and startup funds from Polytechnique Montréal (F.C.). Z.Y. is grateful to NSERC for financial support through a Vanier Canada Graduate Scholarship and to the Schlumberger Foundation through the Faculty for the Future Fellowship program. F.S. acknowledges financial support by Università di Bologna (Researcher Mobility Program, Italian-Canadian cooperation agreement). We are grateful to Cytec Canada for the donation of the ionic liquid. This work is supported by CMC Microsystems through the programs MNT financial assistance and CMC Solutions.

CHAPTER 4

ARTICLE 2: Flexible conducting polymer transistors with supercapacitor function

This chapter has been submitted to Journal of Polymer Science Part B: Polymer Physics. The supporting information for this article is reprinted in Appendix B of this thesis.

4.1 Authors

Zhihui Yi,[1] Luca Bettini,[2] Gaia Tomasello,[1] Prajwal Kumar,[1] Paolo Piseri,[2] Irina Valitova,[1] Paolo Milani,[2] Francesca Soavi,[3] Fabio Cicoira[1]

[1] Department of Chemical Engineering, Polytechnique Montréal, CP 6079, Succursale Centre-Ville, Montréal, Québec H3C 3A7, Canada.

[2] CIMaINa and Department of Physics, Università degli Studi di Milano, Via Celoria 16, 20133, Milano, Italy

[3] Department of Chemistry "Giacomo Ciamician", Alma Mater Studiorum - Università di Bologna, Via Selmi 2, 40126, Bologna, Italy.

E-mail: Fabio.cicoira@polymtl.ca

4.2 Abstract

Planar organic electrochemical transistors (OECTs) using PEDOT:PSS as the channel material and nanostructured carbon as the gate electrode material and poly(sodium 4-styrenesulfonate (PSSNa) gel as the electrolyte were fabricated on flexible polyethylene terephthalate (Mylar®)

substrates. Nanostructured carbon was deposited at room-temperature by supersonic cluster beam deposition (SCBD). Interestingly, the OECT acts as a hybrid supercapacitor (to give a device that we indicate as *transcap*). The energy storage ability of transcaps has been studied with two cell configurations: one featuring PEDOT:PSS as the positive electrode and nanostructured carbon as the negative electrode and another configuration with reversed electrode polarity. Potentiostatic charge/discharge studies show that both supercapacitors show good performance in terms of voltage retention. In particular, when PEDOT:PSS is used as the positive electrode. Galvanostatic charge-discharge characteristics show typical symmetric triangular shape, indicating a nearly ideal capacitive behaviour with a high columbic efficiency (close to 100%).

4.3 Introduction

Electrolyte gated transistors are widely investigated for applications in bioelectronics as well as flexible and printed electronics, because of their low operating voltage and ease of process [132, 133, 149, 150]. Several electrolyte-gated transistors have been reported so far, based on organic and inorganic materials, such as organic semiconductors [23, 24, 151-153], conducting polymers [27, 75, 154], metal oxides [28, 29, 155-157] and carbon nanomaterials [30, 31, 158-160]. In particular, organic electrochemical transistors (OECTs) based on the conducting polymer poly(3,4-ethylenedioxythiophene) (PEDOT) doped with poly(styrenesulfonate)(PSS) (PEDOT:PSS) are playing a major role in novel bioelectronics applications, such as neural electrodes and biosensors [34, 38, 39, 40, 41, 157, 161, 162].

The performance of PEDOT:PSS OECTs in terms of current modulation, mechanical and environmental stability strongly depends on several factors, such as the formulation used for the channel material [163], the thickness of the channel [164], the gate electrode material [75], the device geometry [165]. We have recently investigated the role of the gate electrode materials, the electrolytes and the conductivity enhancers on the performance of PEDOT:PSS OECTs [163] on rigid and flexible substrates [166]. In particular, we have demonstrated that high current modulations are achieved using high surface area activated carbon gate electrodes, regardless of the channel materials [135, 75, 163, 164, 167]. In our previous works activated carbon gates have been either immersed in the electrolyte (in the case of aqueous electrolytes) [75, 163, 164] or

casted onto membranes or separators soaked with electrolytes (in case of ionic liquid electrolytes) [155]. The configuration with an external gate electrode, however, results in a device architecture that is not easily integrated into flexible circuits or textiles, for which a planar device architecture is more suitable. A method to deposit and pattern planar activated carbon from carbonized sucrose films have been proposed [168]. However, this process involves temperatures as high as 900°C, which are not compatible with plastic substrates. Therefore, the fabrication of planar and flexible OECTs making use of high specific area carbon gate electrodes represents a major challenge.

Recently, nanostructured carbon (nsC) deposited by supersonic cluster beam deposition (SCBD) has been proposed as promising electrode material for electrochemical energy storage devices [169]. SCBD consists in the room temperature deposition, under high vacuum, of nanoparticles accelerated in a free jet expansion to form a beam in the molecular regime [170]. Characterized by low kinetic energy at impact (upon particle deposition), it produces a random stacking of nanoparticles leading to nanostructured materials with high surface-to-volume ratio. Carbon films deposited by SCBD are characterized by a substantial dominance of sp^2 hybridization, a very low-density (ca. 0.5 g cm^{-3}) [171] and a high specific surface area (ca. 700 $m^2 g^{-1}$) [172] that results in high double layer capacitance both in aqueous and ionic liquid electrolytes [171, 173, 174]. Compared to more traditional physical vapor deposition methods, fabrication of nsC electrodes by SCBD presents several advantages, such as (i) low deposition temperature, which makes it compatible with thermolabile flexible and stretchable polymeric substrates, (ii) high deposition rate, (iii) access to a wide range of thicknesses (from a few nanometers to a few micrometers), (iv) compatibility with standard microfabrication techniques and (v) avoidance of binders and post deposition treatments (e.g. carbon activation) [169, 170, 173, 174].

In this work, we report on planar and flexible PEDOT:PSS OECTs using nanostructured carbon gate electrodes, fabricated at room temperature by SCBD, on plastic substrates. The same architecture was used to demonstrate flexible and planar devices integrating the OECT and the supercapacitor functions. This device, besides showing high specific capacitance and high power density, allows to modulate the OECT current for short times, even in absence of an applied voltage.

4.4 Experimental

Materials and equipment

Mylar® polyethylene terephthalate (PET) sheets were purchased from Dupont. The poly(3,4-ethylenedioxythiophene):poly(styrenesulfonate) PEDOT:PSS aqueous suspension (Clevios PH1000) was purchased from Heraeus Electronic Materials GmbH (Leverkusen, Germany). Ethylene glycol, D-sorbitol (99%), dodecylbenzenesulfonic acid (DBSA, ≥95%) and poly(sodium 4-styrenesulfonate) (PSSNa, M_w ~70,000) were obtained from Sigma-Aldrich. Glycerol (≥99.5%) was purchased from Caledon Laboratories Ltd (Georgetown, ON). The fluorinated photoresist kit (photoresist OSCoR 4000, developer 103 and stripper 700) for orthogonal patterning was obtained from Orthogonal Inc. (Rochester, NY, USA).

Device fabrication

Planar OECTs using PEDOT:PSS channels and nanostructured carbon (nsC) gate electrodes were fabricated on flexible biaxially-oriented polyethylene terephthalate (Mylar®) substrates. Mylar® is among the most interesting candidates for flexible electronics, since it combines lightweight, reasonable chemical and thermal stability, low thickness suitable for roll-to-roll processing with a good adhesion for organic films.

Patterning of the Au electrodes and the PEDOT:PSS channel was achieved by a procedure illustrated in Figure 4.1 (a-k) and detailed in the Supporting Information. The Au source and drain contacts of the OECTs were patterned by conventional photolithography and the PEDOT:PSS channel by orthogonal lithography and reactive ion etching (RIE) using a Karl Suss MA6/BA6 mask aligner and an ENI OEM-6 RIE apparatus. A clean glass slide was covered with PDMS; afterwards, a Mylar® sheet was attached to the PDMS to ensure rigidity during the photolithography process (a-b). After patterning the metal contacts (c-f), a PEDOT:PSS suspension was spin coated on the substrate (g). After drying, the PEDOT:PSS film was coated with a layer of fluorinated photoresist (h), which was then exposed and developed (i). The unprotected PEDOT:PSS film was etched by O_2 plasma (j). The orthogonal photoresist was then removed with a fluorinated stripper (k) and the Mylar® was peeled off from the glass substrate (l). A picture of an array of OECTs on Mylar® is shown in Figure 4.1m.

We employed two different device geometries: one featuring a micron-scale OECT channel (channel width, W = 80 μm, channel length L = 5 μm) and another one using a larger scale OECT channel (W = 0.2 cm and L = 0.8 cm). The active surface areas of PEDOT:PSS and nsC exposed to the electrolyte were 400 μm^2 and 4 mm^2 for the former geometry and 0.16 cm^2 and 0.2 cm^2 for the latter. The larger OECT geometry was used for supercapacitor tests.

Nanostructured carbon films (area 1 cm^2, thickness 750 nm) were deposited by SCBD at room temperature on flexible Mylar® sheets, previously coated by a thin platinum film (200 nm thickness), required to ensure an electrical contact with the measuring probes. Carbon nanoparticles were deposited on top of the Pt coated Mylar® in high vacuum (~10^{-5} mbar) by a SCBD apparatus equipped with a pulsed microplasma cluster source (MPCS) [170, 175]. In the reaction cavity of the PMCS a A-graphite rod was sputtered by a plasma confined by exploiting the pressure gradient produced by a jet of inert gas (He) impinging on its surface. Sputtered C atoms thermalize within the He and condense to form clusters. The mixture of clusters and inert gas leaves then the microplasma cluster source by expanding through a nozzle, thus forming a seeded supersonic beam of aerodynamically accelerated nanoparticles that are finally collected on the substrate to form a carbon film [170, 176]. nsC films to be used as gate electrodes were cut into stripes (1 mm × 4 mm), which were pasted, using PDMS, parallel to the PEDOT:PSS channel with a distance of 1 mm, in planar configuration.

As the electrolyte, we used a gel consisting of a mixture of PSSNa, D-sorbitol, glycerol and deionized water in a mass ratio of 4:1:1:4, that has been already used in PEDOT:PSS OECTs [69]. The gel electrolyte was drop cast on top of the planar OECT channel and gate electrode and left to dry at room temperature overnight.

Characterization of materials and devices

The film thickness was measured with a Dektak 150 profilometer. Scanning electron microscopy (SEM) was performed with a JEOL FEG-SEM, JSM 7600F.

Transistor characterization and electrical measurements were carried out with a two channels source/measure precision unit (Agilent B2902A), controlled by a Labview software. Electrochemical measurements were performed with a VSP-300 electrochemical workstation (BioLogic Instruments).

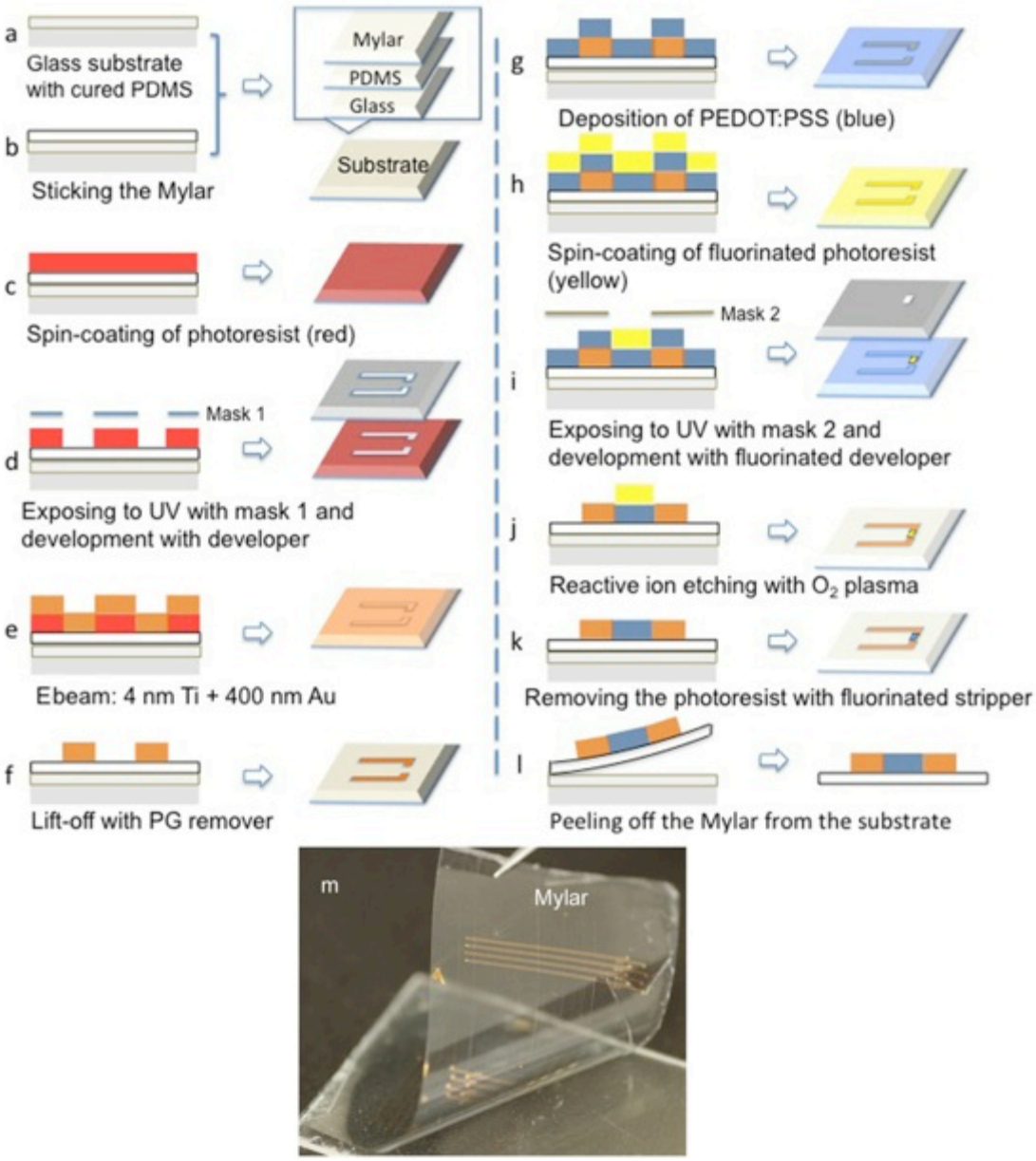

Figure 4. 1. A schematic representation of the process used to fabricate a patterned PEDOT:PSS OECT/supercapacitor utilizing conventional (a-f) and orthogonal photolithography (g-k). Devices patterned on Mylar® can be peeled off from the PDMS-glass support for later use (l-m).

4.5 Results and discussions

The transfer curves of a micron-sized planar OECT using a nsC gate and PSSNa-based electrolyte show the typical behavior of a PEDOT:PSS OECT working in depletion mode (Figure

4.2). The drain-source current (I_d) decreases, in absolute terms, with the increase of the gate voltage (V_g). The *ON*/*OFF* ratio of the device is about 60, which demonstrates that nsC fabricated by SCBD is very promising as gate material for OECTs.

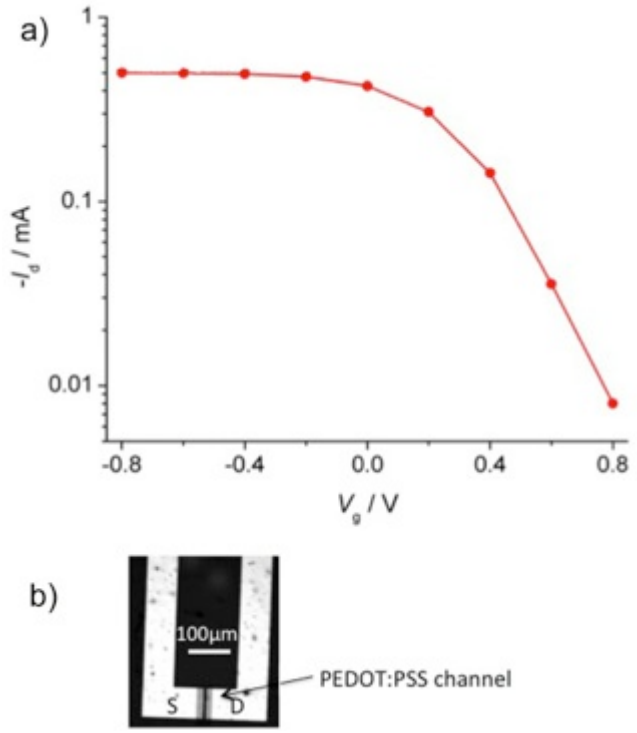

Figure 4. 2. Transfer curves of micron-sized (L= 5 µm, W= 80 µm) OECTs making use of a PSSNa-based gel electrolyte. V_d = -0.5 V (a). SEM image of the microscale device (b). S: source. D: drain.

We have recently demonstrated that electrolyte-gated transistors based on organic polymers can be also exploited for energy storage purposes into a novel device structure named *transcap* (transistor-capacitor) [154]. This device exploits the high pseudocapacitance and capacitance displayed by organic conducting polymers and high surface area carbons at the interface with an electrolyte. Specifically, transcaps combine charge transport and charge storage features to yield a low-energy cost device that can drive/power additional elements [75, 154]. We fabricated transcaps on rigid substrates and employing the organic semiconductor poly[2-methoxy-5-(20-

ethylhexyloxy)-1,4-phenyl-ene vinylene (MEH PPV) as the channel material, the ionic liquid 1-Ethyl-3-methylimidazolium bis(trifluoromethylsulfonyl)imide (EMIM TFSI) as the electrolyte and activated carbon on carbon paper as the gate, in a stacked configuration [154]. Here, we extend the transcap concept to a more versatile planar device architecture on a flexible substrate, using PEDOT:PSS as the channel material and nsC deposited by SCBD as the lateral gate.

Our device acts as a hybrid supercapacitor that features one purely capacitive electrode, i.e. nsC, electrostatically charged/discharged, and a pseudocapacitive one, i.e. PEDOT:PSS, charged/discharged by a faradaic process. Transfer curves of the OECTs show that PEDOT:PSS in its initial state ($V_g = 0$ V) can be either dedoped, by application of a positive V_g, or doped, by application of a negative V_g (Figure 4.2). Therefore, two different hybrid supercapacitor configurations are possible: a cell where PEDOT:PSS is the positive electrode and nsC is the negative electrode (type I supercapacitors), and another one with reversed polarity (type II supercapacitors). Therefore, two different hybrid supercapacitor configurations can be considered: type I, where PEDOT:PSS acts as a positive electrode and nsC as the negative one, and type II, where the electrodes polarity is reversed.

To characterize the energy storage ability of the OECT/supercapacitor, potentiostatic charge/discharge experiments were carried out in a two-electrode configuration, on supercapacitors of type I and II. We used potentiostatic experiments because they mimic OECT operation and permit, at the same time, the evaluation of the energy performance of the supercapacitors. During such experiments, V_{cell} corresponds to $-V_g$ for type I devices and to V_g for type II devices. The following procedure was adopted: charging by chronoamperometry at 1 V for 10 s, followed by 10 s rest in open circuit and discharging by chronoamperometry at 0 V for 10 s.

At $V_g = 0$ V, the nsC electrode is unpolarized and it is at the same potential of the PEDOT:PSS channel. During the charge of type I supercapacitors, i.e. when a voltage bias V_{cell} is applied (Figure 4.3a), PEDOT:PSS is doped with the charge ΔQ. Simultaneously, the nsC electrode is negatively polarized and electrostatically stores the same charge ΔQ (with opposite sign). The amount of the stored charge ΔQ is related to the capacitance of the cell. In the charged state, the cell is storing the energy $E = \Delta Q\, V_{cell}$. During subsequent rest, partial self-discharge takes place due to charge redistribution at the electrode/electrolyte interfaces and parasitic side reactions. The

potential of the nsC electrode increases and that of the PEDOT:PSS electrode decreases, such that part of the ΔQ charge previously stored is dissipated (dQ). Then, setting V_{cell} at 0 V causes depolarization of the surface of the nsC electrode and dedoping of the PEDOT:PSS electrode, thus bringing both electrodes to their initial states. In this process the charge (ΔQ-dQ) and the energy $E = V_{cell}\ (\Delta Q\text{-}dQ)$ are delivered. During the charging of type II supercapacitors (Figure 4.3b), the PEDOT:PSS electrode is dedoped by the charge ΔQ, while the nsC electrode is positively polarized and electrostatically stores the same charge ΔQ (with opposite sign). In this process, the energy $E = \Delta Q\ V_{cell}$ is stored. During subsequent rest, the potential of the nsC electrode decreases, the PEDOT:PSS potential increases, and part of the ΔQ charge previously stored is dissipated (dQ). Setting V_{cell} at 0 V, causes the depolarization of the nsC electrode and the re-doping of the PEDOT:PSS electrode, thus bringing both electrodes to their initial states. The charge (ΔQ-dQ) and energy $E = V_{cell}\ (\Delta Q\text{-}dQ)$ are delivered during the process.

Figures 4.3c and 3d show the voltage *vs.* time and current *vs.* time plots for the potentiostatic measurements. For both supercapacitor configurations, the charging step involves ΔQ values of about 67 μC (evaluated by the integration of the current over time) and an energy E of about 67 μJ (i.e. 413 μJ cm^{-2} or 0.11 μWhcm^{-2}). During rest (no current flowing through the cell), the voltage decreases and a partial self-discharge occurred in both cases. However, type I devices show a better voltage retention, i.e. lower self-discharge, after the open circuit step, i.e. 78% and 80% for two repeated sequences with respect to 69% and 57%, for type II devices. The lowest self-discharge of type I supercapacitors can be explained with the presence of the doping anions in the polymer chain and atmospheric oxygen [164]. Both these factors stabilize the highly doped (oxidized) state of PEDOT:PSS. In the case of type II supercapacitors, the reduced state achieved upon charge is not stabilized, therefore the PEDOT:PSS potential tends to increase (and V_{cell} to decrease) after the open circuit step.

During the discharge process, about 80% (type I supercapacitors) and 70% (type II supercapacitors) of the energy used to charge the supercapacitors and hence to modulate the OECT current, is delivered. The result is a highly energy efficient system. Figure 4.3c and 3d show that the devices keep the applied V_{cell} (corresponding, in absolute value, to V_g) over a short period of time, without being connected to a power supply (at rest). This means that over this period the OECT current modulation can be kept without an applied gate bias.

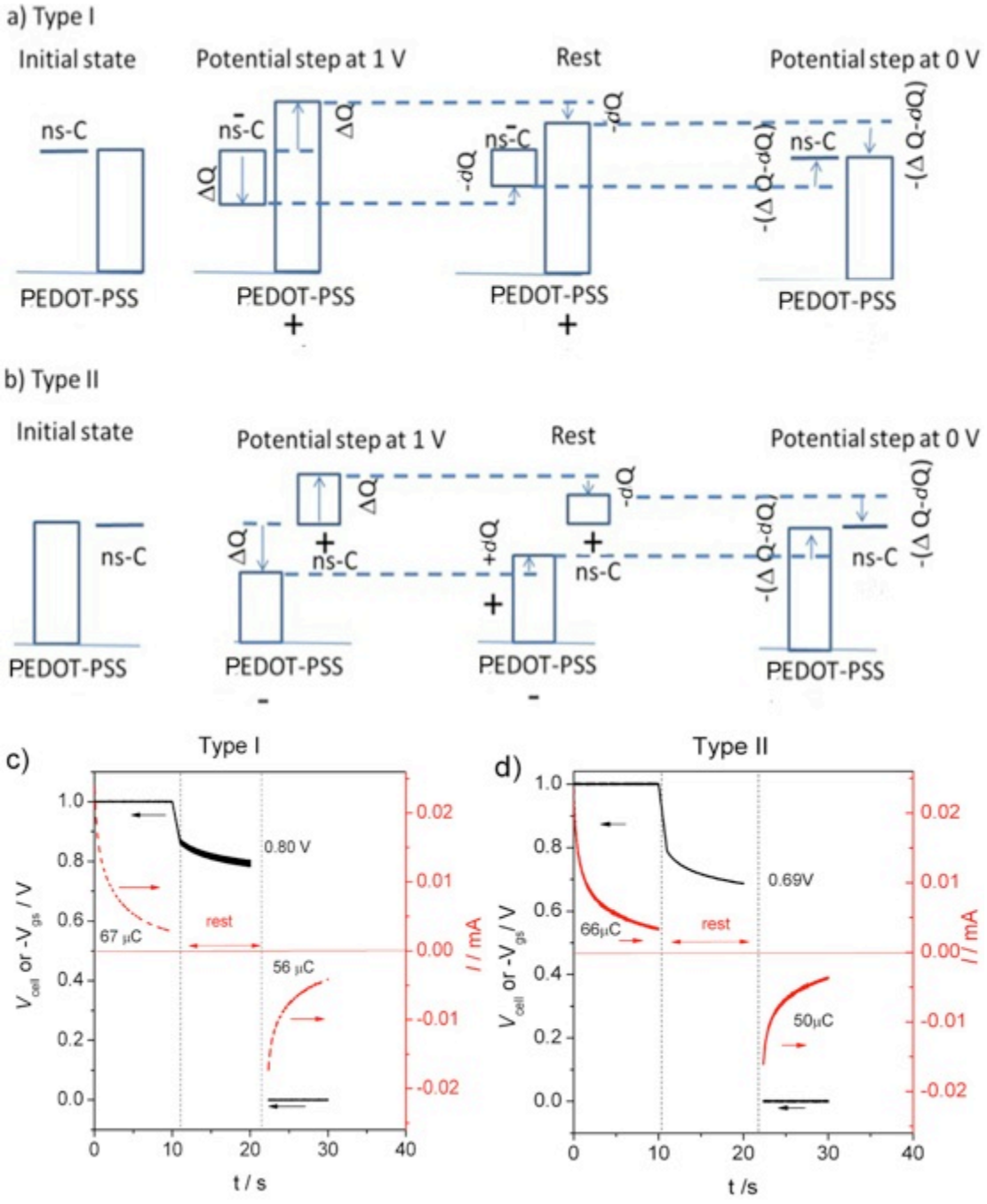

Figure 4. 3. Working principle of hybrid supercapacitors of type I (a) and type II (b). Supercapacitor characteristics of OECTs with PEDOT:PSS positive electrodes and nsC negative electrodes (type I, c), with PEDOT:PSS negative electrodes and nsC positive electrodes (type II, d). In 3d and 3c, voltage (black solid line) and current (red dotted line) vs. time upon potential step at 1 V for 10 s (supercapacitor charge), followed by 10 s rest in open circuit conditions, and potential step at 0 V (supercapacitor discharge).

The electrochemical performance of type I OECTs/supercapacitors (PEDOT:PSS used as positive electrodes and nsC as the negative electrodes) was also studied by galvanostatic charge/discharge experiments carried out at currents (I) of 1, 2.5, 5 and 10 μA. Here, the I is equal to $-I_g$ and the supercapacitor cell voltage V_{cell} (equal to $-V_g$) is up to 1 V. The galvanostatic charge-discharge characteristics exhibit a typical symmetric triangular shape, indicating nearly ideal capacitive behaviour with a high coulombic efficiency, between 98% and 100% (Figure 4.4) [177]. From this two-electrode system, the capacitance (C) for the entire cell, the delivered energy (E) and the power (P) were calculated from equations (1), (2) and (3), respectively. The results are summarized in Table 1. This data well compare with those reported in the literature for PEDOT:PSS based micro-supercapacitors [178].

$$C = \frac{I}{dV_{cell}/dt} \quad (1)$$

$$E = I \int V_{cell}(t)dt \ /3600 \quad (2)$$

$$P = \frac{E}{\Delta t} \quad (3)$$

Table 4.1: Discharge time (t), capacitance (C), delivered energy (E) and power (P) of type I OECTs/supercapacitors at different values of the current (I), normalized to the geometric area and volume (footprint) of the PEDOT:PSS electrode (0.16 cm^2 with a thickness of 470 nm).

I (μA)	t (s)	C (mF cm^{-2})	E (μWh cm^{-2})	P (μW cm^{-2})	C (F cm^{-3})	E (mWh/ cm^{-3})	P (W cm^{-3})
1	143.5	1.08	0.10	2.48	23.0	2.1	0.05
2.5	39.3	0.87	0.06	5.25	18.5	1.2	0.11
5	11.7	0.61	0.03	8.56	13.0	0.6	0.18
10	1.6	0.25	0.005	10.56	5.32	0.1	0.22

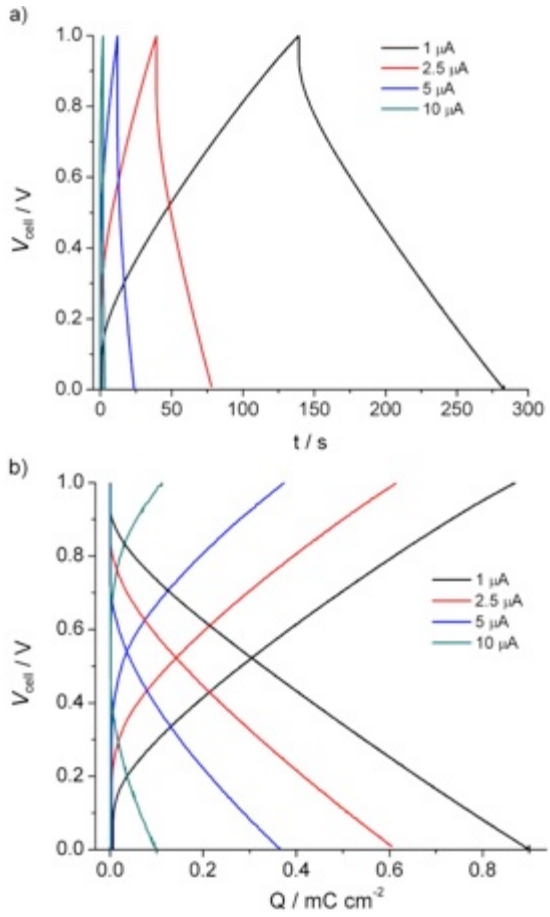

Figure 4. 4. Galvanostatic charge-discharge cycles at different currents from 1 to 10 μA for type I OECTs/supercapacitors (i.e. cells with nsC as negative electrode and PEDOT:PSS as positive electrode). Voltage profiles over a) time and b) cycled capacity (the charge is normalized to PEDOT:PSS footprint area of 0.16 cm^2).

4.6 Conclusions

We have demonstrated that nanostructured carbon (nsC) electrodes, prepared by supersonic cluster beam deposition on flexible Mylar substrates can be used as gate electrodes for planar PEDOT:PSS based organic electrochemical transistors (OECTs), patterned by orthogonal lithography. The electrical characteristics reveal a good current modulation at low voltages.

Moreover, by coupling a lateral nsC electrode to a PEDOT:PSS electrode we were able to exploit

the energy storage properties of OECT devices in planar configuration. The OECTs here reported act as hybrid supercapacitors with efficient charge retention and a satisfying energy storage characteristics.

The integration of transistor and a capacitor provides a very efficient and low–cost energy system, of great interest for autonomous systems for flexible/stretchable electronics and bioelectronics. Furthermore, the charge storage properties of the channel and the gate electrodes of the OECTs permit the operation of the OECT without power supply, for short periods of time.

The concept of a transcap integrating an organic electrochemical transistor and a supercapacitor can be further optimized to achieve faster time responses, decreased self-discharge and optimized electrical and energy storage properties.

4.7 Acknowledgements

This work is supported by NSERC Discovery and FRQNT Nouveau Chercheur grants (F.C.). Z. Y. is grateful to NSERC for financial support through a Vanier Canada Graduate Scholarship and to the Schlumberger Foundation through the Faculty for the Future Fellowship program. F.S. acknowledges financial support by Alma Mater Studiorum Università di Bologna (Researcher Mobility Program, Italian-Canadian cooperation agreement) and the Embassy of Canada in Italy, for a 2015 Canada-Italy Innovation Award.

CHAPTER 5

ARTICLE 3: Water gated organic electrochemical transistors on flexible/degradable shellac substrate

This chapter has been submitted to Journal of Materials Research. The supporting information for this article is reprinted in Appendix C of this thesis.

5.1 Authors

Zhihui Yi, Irina Valitova, Fabio Cicoira

Department of Chemical Engineering, Polytechnique Montréal, CP 6079, Succursale Centre-Ville, Montréal, Québec H3C 3A7, Canada.

E-mail: Fabio.cicoira@polymtl.ca

5.2 Abstract

We developed “green” OECTs, which employ degradable substrates and water as the gating medium. OECTs patterned on PET were transferred onto degradable shellac substrates by heating. To explore the gate effect in presence of water as the gating medium, we employed hydrophobic AC gate electrodes and hydrophilic PEDOT:PSS gate electrodes. OECTs with AC gates present slower current response and higher current modulation than those with PEDOT:PSS gates. The shellac substrate can be degraded in a 1 M KOH solution.

5.3 Introduction

Electrolyte gated transistors are currently the focus of intense research for applications in bioelectronics and large-area electronics, due to their ability to work at low voltage (< 1 V) [21, 39, 132, 149, 150, 151]. The mode of operation of electrolyte gated transistors is mainly governed by electrostatic and/or electrochemical doping/dedoping [20, 25-27]. When channel materials are ion impermeable, the electrostatic doping of the channel at the channel/electrolyte interface induces the modulation of the current. This doping mechanism does not involve the charge transfer or charge transfer occurs only in the electrolyte/channel material interface. A high capacitance (typically higher than $\mu F/cm^2$) is reached due to the formation of an electrical double layer at the electrolyte/channel interface. This high capacitance allows transistors to operate at low voltages [20, 75, 135, 167]. When the channel materials are ion permeable, the ions can migrate into the bulk of the material thus leading to electrochemical doping/dedoping, this phenomenon exploited in organic electrochemical transistors (OECT).

Different biocompatible electrolytes have been used in OTFTs, such as water, aqueous saline solutions, ionic liquids and ion gels [23, 35, 63, 111, 132-135, 179]. Aqueous solutions are the most important electrolyte for biological applications, in spite of some limitations, such as occurrence of electrolysis around 1 V, charge carrier mobility reduction due to water polarization, and trapping of electrons in n-type semiconductors by hydroxyl group. Pure water as the gating medium has attracted a great deal of attention in organic and inorganic transistors since Kergoat introduced the water gated Rubrene and P3HT transistors [179]. Ultra pure water shows an ionic conductivity of 10^{-5} S m^{-1} due to proton transfer and has a minimum ion concentration of solvated protons (H^+) and hydroxyl ions (OH^-) of 10^{-7} M [180]. Grell et al. demonstrated electron transporting in a water-gated transistor, where they avoided electron trapping by passivation of n-type semiconductors with HMDS [181]. Further, the same group used a water gated OTFT as a sensor for water-borne amines [182]. Water-gated phthalocyanine CuPc transistors have been used as transducers tripeptide GSH and GST enzyme interaction [183].

OTFTs can be easily fabricated on flexible and biocompatible polymeric substrates, such as poly(imide) [184], poly(ethylene terepthalate) [185, 186], poly(ether sulfone) [187], cellulose [100, 188] and chitosan [189]. Recent works have shown the possibility of employing these inexpensive biodegradable polymers, and natural insulating materials as substrates and dielectrics

at the same time [108, 189]. The substrate of our choice is natural resin shellac. Shellac is a biodegradable resin of animal origin composed of polyhydroxy acids, primarily aleuritic acid, shellolic acid, and jalaric acid [108]. It is also edible and widely used for many applications in pharmaceutical and food industry [190].

In this work we report on performance of organic thin-film transistor using a PEDOT:PSS in combination with a biodegradable shellac substrate and water as a gating medium. We fabricated devices that consist of nearly entirely biodegradable materials We compared the performance of devices with two different gate electrode materials such as PEDOT:PSS and activated carbon (AC) as well.

5.4 Experimental

Materials and equipment

The Mylar@Polyethylene terephthalate (PET) sheets were purchased from Dupont. The poly(3,4-ethylenedioxythiophene):poly(styrenesulfonate), PEDOT:PSS aqueous suspension (Clevios PH1000) was purchased from Heraeus Electronic Materials GmbH (Leverkusen, Germany). Glycol, D-sorbitol (99%) and dodecylbenzenesulfonic acid (DBSA, ≥95%) were obtained from Sigma-Aldrich. The fluorinated photoresist kit (photoresist OSCoR 4000, developer 103 and stripper 700) for orthogonal patterning was purchased from Orthogonal Inc. (Rochester, NY, USA). A Karl Suss MA6/BA6 mask aligner was used for photolithography. Reactive ion etching was performed with an ENI OEM-6 apparatus. The film thickness was measured with a profilometer (Dektak 150). Transistor characterization and electrical measurements were obtained by a two channels source/measure precision unit Agilent B2902A, controlled by a home-made Labview software. Milli-Q water was obtained from Milli-Q Reference purification system with a resistance of 18.2 MΩ·cm at 25 °C. The conductivity of the Milli-Q water was measured with a Traceable Expanded Range Conductivity Meter.

Device fabrication

Planar OECTs, using a conducting polymer poly(3,4-ethylenedioxythiophene) doped with polystyrene sulfonate (PEDOT:PSS) as the transistor channel, were fabricated on flexible polyethylene terephthalate (PET) substrates followed by transferring onto a shellac substrate.

Patterning of the Au electrodes and the PEDOT:PSS channel was achieved by a procedure shown in Figure 5.1. A clean glass slide was spun coated with PDMS at a spin rate of 500 RPM for 30 s. The PDMS was cured at 80 °C for 20 min (step 1). After cooling down to room temperature, a piece of PET was stuck on top of the PDMS (step 2). A layer of photoresist AZ5214 was spun coated on top of the PET at a rate of 4000 rpm for 30 s, followed by heating at 110 °C for 50 s (step 3). After exposure to a UV light (35 J) through a photomask, the photoresist was developed in an AZ726 developer (step 4). 4 nm titanium was deposited on the substrate followed by 40 nm gold with an Ebeam evaporation method (step 5). The substrate was left in a PG remover to lift-off (step 6). A solution of PEDOT:PSS mixed with ethylene glycol and dodecylbenzenesulfonic acid (DBSA) in a volume ratio of $4:1:10^{-4}$ was spun coated on the substrate. The spun rate is 500 RPM for 9 s followed by1500 RPM for 30 s. Slides were finally baked on a hot plate at 140 °C for 60 min. The thickness of a PEDOT:PSS film is around 150 nm (step 7). A layer of a fluorinated photoresist was spun coated on top of the PEDOT:PSS film, which was then exposed through a photomask and developed with a fluorinated developer 103 (steps 8-9). The unprotected PEDOT:PSS film was etched by O_2 plasma at a flow rate of 10 sccm for 2 min (step 10). The orthogonal photoresist was then removed with a fluorinated stripper 700 (step 11). The OECTs patterned on a PET substrate was peeled off from the glass-PDMS substrate (step 12). The PET was left on a 135 °C hot plate for 10 s, and was drop casted by a shellac/methanol (1g/2mL) solution (step 13). The final OECTs with aspect ratio of L/W = 4 (W = 0.2 cm and L = 0.8 cm) on a shellac substrate can be peeled off from the PET after being heated at 135 °C for 12 h (step 14).

The activated carbon gate electrodes were prepared using carbon paper (Spectracorp 2050, 10 mils) coated with an ink of activated carbon (PICACHEM BP9, 28 mg mL^{-1}) and Nafion binder (2.4 mg mL^{-1}) in isopropanol solvent. Drop casting of the carbon ink was followed by thermal treatment at 60 ^{o}C for 24 h to remove the solvent. We used carbon paper stripes 0.2 cm × 0.8 cm sized, which was placed parallel to the PEDOT:PSS channel with a distance of 1 mm, in planar configuration.

Water has been utilized as the electrolyte and the conductivity is zero measured by a conductivity meter at 25 °C.

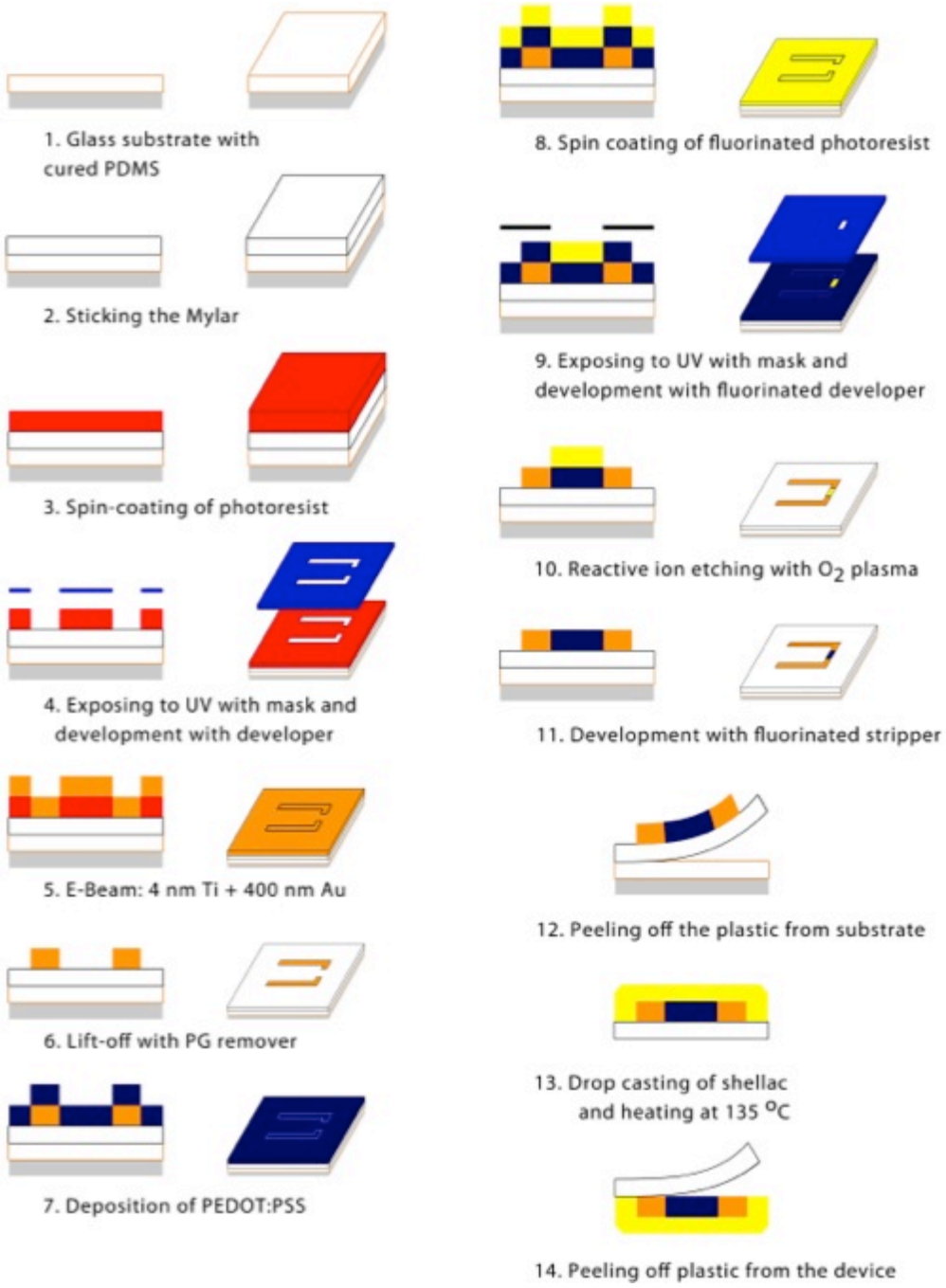

Figure 5. 1. Schematic of the process used to fabricate a patterned PEDOT:PSS OECT/supercapacitor utilizing conventional (1-6) and orthogonal photolithography (7-11). Devices patterned on Mylar® can be peeled off from the PDMS-glass support for later use (12-14).

5.5 Results and discussion

It is noteworthy that films forming from a polymer solution involve two forces, i.e. the forces among polymer molecules (cohesion) and between the film and the substrate (adhesion). It is well known that an increased temperature benefits the adhesion [191]. Herein, the shellac was gelated while the evaporation of ethanol (Fig. S1a). With the increase of temperature, adhesion between the film and the substrate become strong. Devices were finally adhesive on shellac, which can be peeled off from the Mylar® substrate.

To investigate the transfer characteristics of OECTs with a pure water gating medium, two kinds of gate electrodes, i.e. a PEDOT:PSS gate and an activated carbon (AC) gate, have been employed. A schematic cross-section of an OECT gated by pure water is shown in Figure 5.2. The gate electrode was placed parallel with a PEDOT:PSS strip with a double side tape. The PEDOT:PSS strip connected with the gate via carefully drop casted pure water without confinement.

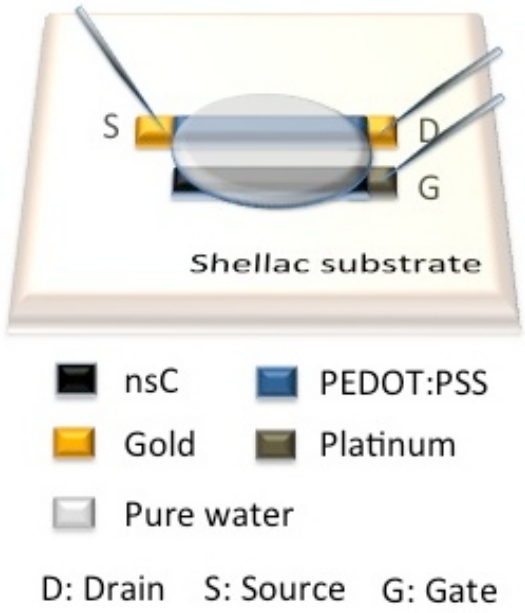

Figure 5. 2. Schematic view of the water-gated OECT.

As shown in Figure 5.3a, the drain-source current (I_d) decreases with the increase of the gate voltage (V_g), as expected for an OECT working in depletion mode. The water gated OECTs exhibits typical OECT characteristics and behave similarly to other electrolyte-gated OECTs.

However, the water gated OECTs present relative low *ON*/*OFF* ratio, which are 5 and 8 for making use of a PEDOT:PSS gate and an AC gate at V_g = 1.2 V and V_d = -1 V, respectively. The OECT current modulation, $|(I–I_0)/I_0|$, where I and I_0 are the drain-source currents at $V_g \neq 0$ and at $V_g = 0$, is shown as a function of the gate-source voltage, V_g. From the current modulation curves shown in Figure 5.3b, the current modulation of an OECT with a AC gate is higher (~0.9) than with a PEDOT:PSS gate (~0.7). The higher *ON*/*OFF* ratio and modulation with an AC gate comparing with a PEDOT:PSS gate of an OECT has been observed from other electrolyte-gated OECTs.

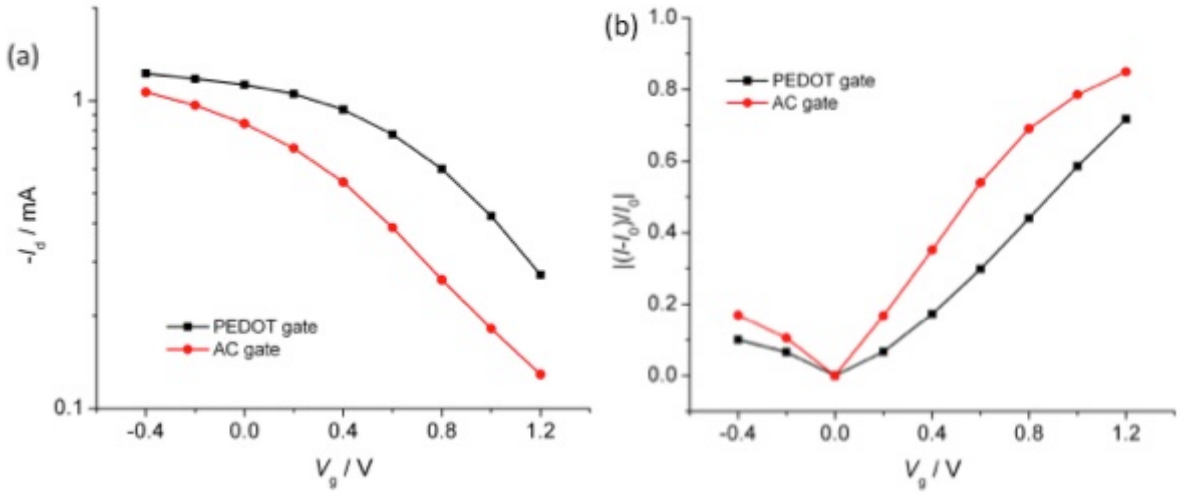

Figure 5. 3. Transfer curves (a) and current modulation (b) of OECTs with AC gate (red solid circle) and PEDOT:PSS gate (black empty square) by making use of Milli-Q water as the gating medium. V_d = -1 V. Lines are guides to the eye.

For further defining the performance of OECTs, we studied the response time, which measures the switching speed of the I_d upon application of a V_g (Figure 5.4). Interestingly, the OECT making use of an AC gate, which exhibits higher *ON*/*OFF* ratio and current modulation, presents slower time response than the OECT employing a PEDOT:PSS gate. By utilizing an exponential fit of the transient curve, time constants of 4.9 s and 1.5 s are obtained for OECTs with the AC gate and PEDOT:PSS gate, respectively. From our previous results, OECTs employing salt-based

aqueous electrolytes, the time response of OECTs making use of AC gate is much faster than the ones with PEDOT:PSS gate [75], which is different from the situation in this context.

Water molecules connect each other through hydrogen bonds as a whole, which benefits transportation of electrons and charge carriers. The hydrophilic PEDOT:PSS supplies opportunities to form hydrogen bonds with water molecules. The possible reason for the faster response of an OECT making use of a PEDOT:PSS gate is that these hydrogen bonds creates channels facilitating the current flow from the gate to the electrolyte. Hence, the formation of the electric double layer at the interface between the gate and the electrolyte is faster in OECTs employing PEDOT:PSS gates.

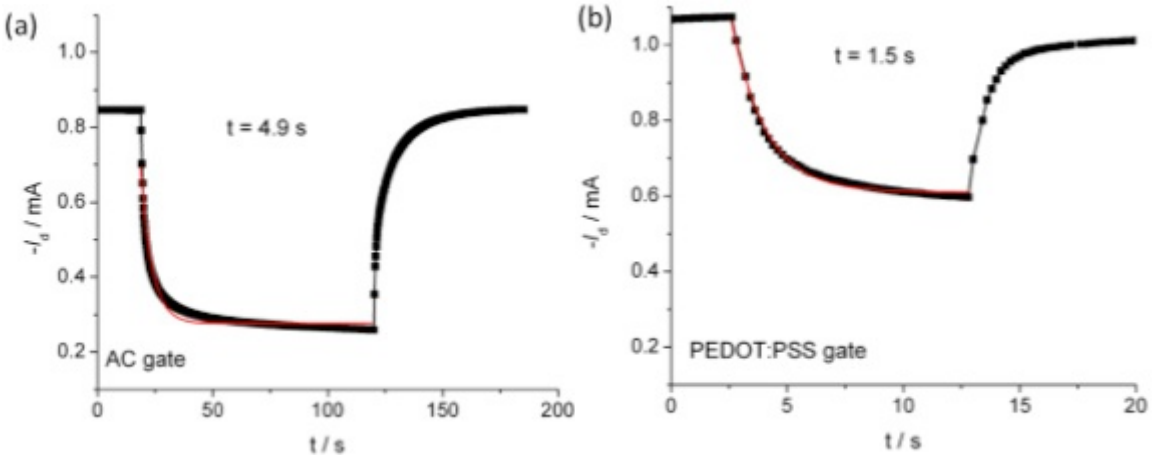

Figure 5. 4. Temporal response of the drain current of OECTs with an AC gate (a) and a PEDOT:PSS gate (b). A pulse of 0.8 V was applied at the gate and the drain-source voltage was -1 V. The red line is an exponential fit with a time constant of 4.9 s for (a) and 1.5 s for (b). The red lines are the simulation results. The black lines are guides to the eye.

The shellac was prepared as a 0.4 mm thick slide. Natural shellac can be dissolved in alcohol, base and most of the molecular solvent. After baking at 135 °C for 12 h, the shellac can be dissolved in 1 M KOH aqueous solution (Figure 5.5). We have also tried DMSO, methanol, acetate acid and ammonia aqueous solution, which can dissolve the natural shellac. However, the annealed shellac can no longer be dissolve in these solutions. This is probably due to the annealing process promote the crosslinking of the shellac.

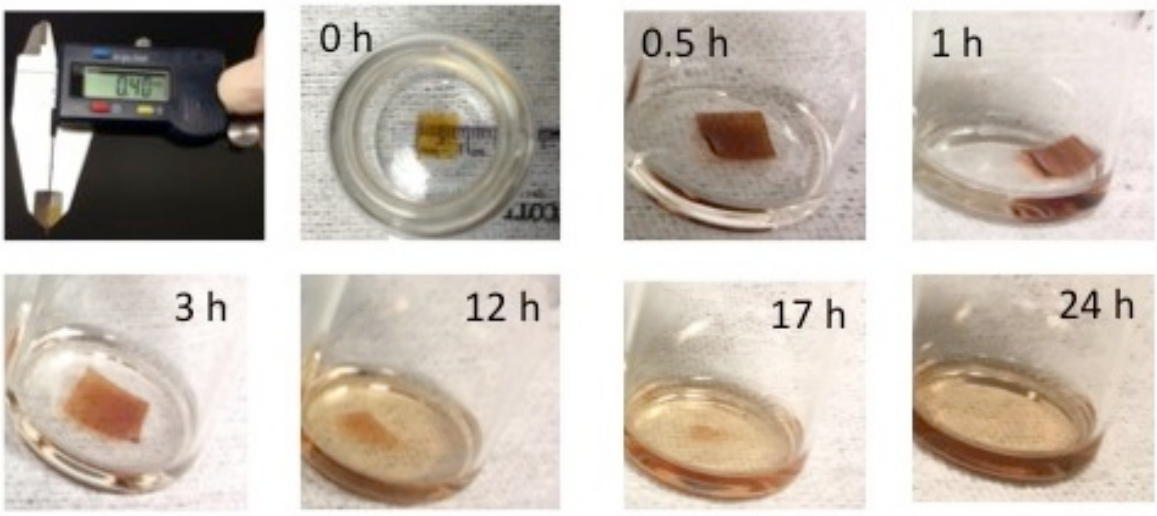

Figure 5. 5. Images collected at several stages of accelerated dissolution of a piece of shellac upon insertion into 1 M KOH solution at room temperature.

5.6 Conclusion

In conclusion, we developed a "Green" OECT, which employs a degradable substrate and water as the gating medium. Poly(3,4-ethylenedioxythiophene) polystyrenesulfonate (PEDOT:PSS) was patterned on a polyethylene terephthalate (PET) substrate followed by being transferred onto a shellac substrate by a "heat and peel-off" method. In order to explore the gate effect in presence of water as the gating medium, hydrophobic gate electrode-activated carbon (AC) and hydrophilic gate electrode-PEDOT:PSS have been investigated. The current modulation of an OECT by making use of an AC gate presents an increase of the OECT modulation, with respect to the OECT employing a PEDOT:PSS gate. The result is consistent with the other electrolyte gated OECTs making use of ion-based electrolytes. Interestingly, further investigation of the response time shows that the OECT with a AC gate responses slower than making use of a PEDOT:PSS gate. The shellac substrate can be degraded in a 1 M KOH solution.

5.7 Acknowledgements

This work is supported by NSERC Discovery grants (F.C.) and startup funds from Polytechnique Montréal (F.C.). Z.Y. is grateful to NSERC for financial support through a Vanier Canada

Graduate Scholarship and to the Schlumberger Foundation through the Faculty for the Future Fellowship program. We are grateful to Cytec Canada for the donation of the ionic liquid. This work is supported by CMC Microsystems through the programs MNT financial assistance and CMC Solutions.

CHAPTER 6 GENERAL DISCUSSION

This chapter describes in details the fabrication methods employed in this thesis, and also results that have not been incorporated in peer-reviewed articles but are believed to be useful for future work.

6.1 OECT fabrication

Patterns of Au electrodes and PEDOT:PSS channels was achieved by a procedure shown in Figure 6.1. Au source and drain contacts of OECTs were patterned by conventional photolithography method. PEDOT:PSS channel were patterned both with Parylene C (Figure 6.1) and orthogonal photoresist (Figure 6.2).

OECTs have been patterned on flexible substrates with the following process. Clean glass slides were spun coated with polydimethylsiloxane (PDMS) (Curing agent:PDMS 1:10 w/w) at a spin rate of 500 RPM for 30 s, and was cured at 80 ºC for 20 min. After cooling down to room temperature, a piece of PET was stuck on top of the PDMS to obtain a 3-layer substrate, which the first layer is glass slide, the second layer is PDMS and the third layer is plastic (Figure 6.1, step 1).

A layer of photoresist AZ5214 was spun coated on top of a clean substrate at a rate of 4000 rpm for 30 s, and was dried at 110 °C for 50 s (step 1-2). The photoresist was exposed to a UV light (35 J) with a photomask, and was developed in AZ726 developer (step 3). 4 nm titanium followed by 40 nm gold was deposited on the substrate with an Ebeam evaporation method (step 4). The substrate was left in a PG remover for lift-off (step 5). In order to pattern the conducting polymer channel, two methods have been employed in this thesis. Method 1: Positive photoresists and Parylene C are involved to pattern the devices. Method 2: Both positive and fluorinated negative photoresists are employed for simplifying and shorten the time of the fabrication process.

Method 1: 1.2 g of Parylene C was thermal evaporated onto the substrate with Au patterns to

obtain a 1.2 um-thick parylene C film (step 6). A layer of photoresist SPR 220.3 (Microchem) was spun coated on the Parylene C (step 7). The photoresist was exposed to a UV light (35J) with a photomask before being developed in an AZ726 developer (step 8). The unprotected Parylene C was etched with O_2 plasma at 150W and a flow rate of 10 sccm min^{-1} for 2 min (step 9). PEDOT:PSS was mixed with ethylene glycol and dodecylbenzenesulfonic acid (DBSA) in a volume ratio of $4:1:10^{-4}$. The mixture was spun coated on the device at 500 RPM for 9 s followed by 1500 RPM for 30 s. The device was left on a 120 °C hot plate for 30 s and was cooled down to room temperature (step 10). The parylene C was peeled off to obtain the patterned channel. Devices were finally baked at 140 °C for 60 min. The thickness of a PEDOT:PSS film is around 150 nm (step 11).

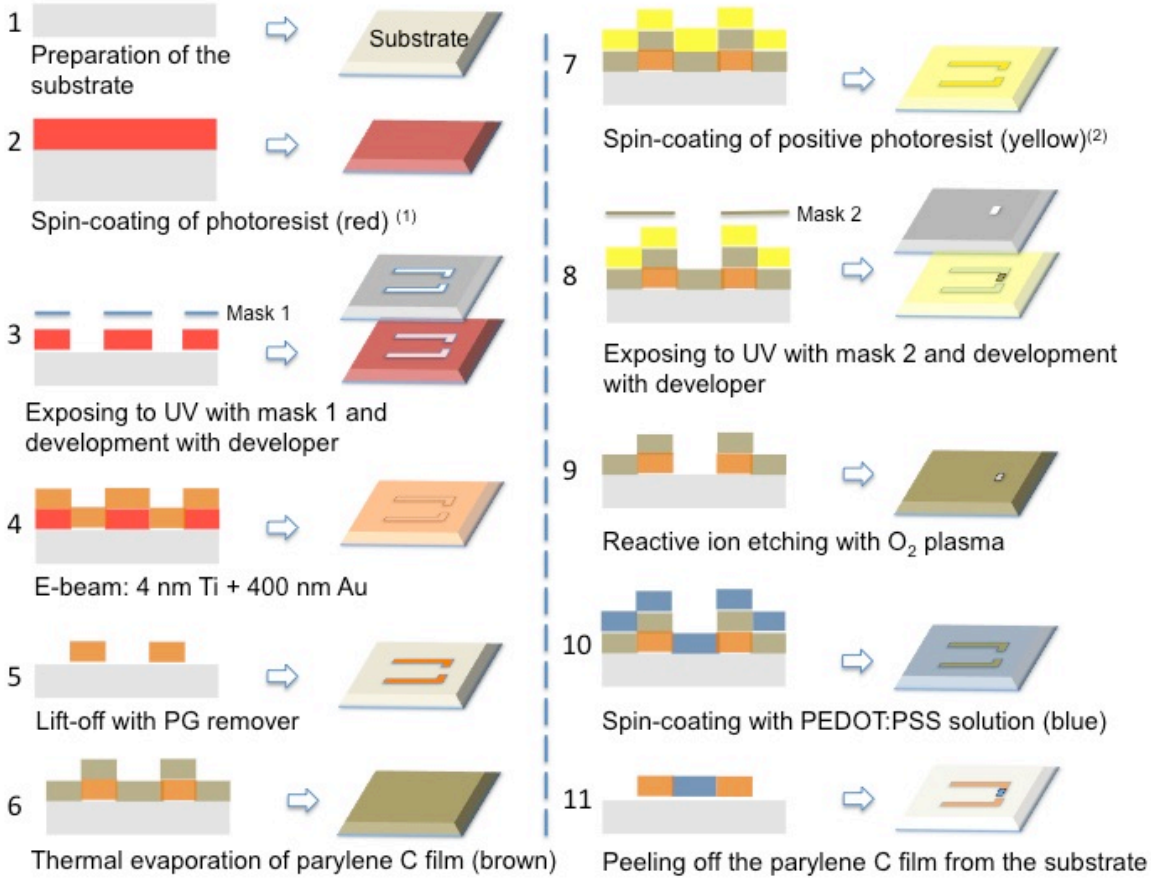

Figure 6. 1. Schematic representation for the process used to fabricate a patterned PEDOT:PSS OECT utilizing a photolithography method with positive photoresist and parylene C. [1] The photoresist is AZ5214. [2] The photoresist is SPR220. 3.

Method 2: The PEDOT:PSS film was prepared on the substrate as described in Figure 6.1 (step 10) (step 6). Orthogonal photoresist was spun coated on top of the PEDOT:PSS film. The photoresist was exposed to UV light through a photomask and was developed with fluorinated developer 103 (steps 7-8). The unprotected PEDOT:PSS film was etched with O_2 plasma for 2 min at a flow rate of 10 sccm min^{-1} (step 9). The orthogonal photoresist was then removed with fluorinated stripper 700 (step 10).

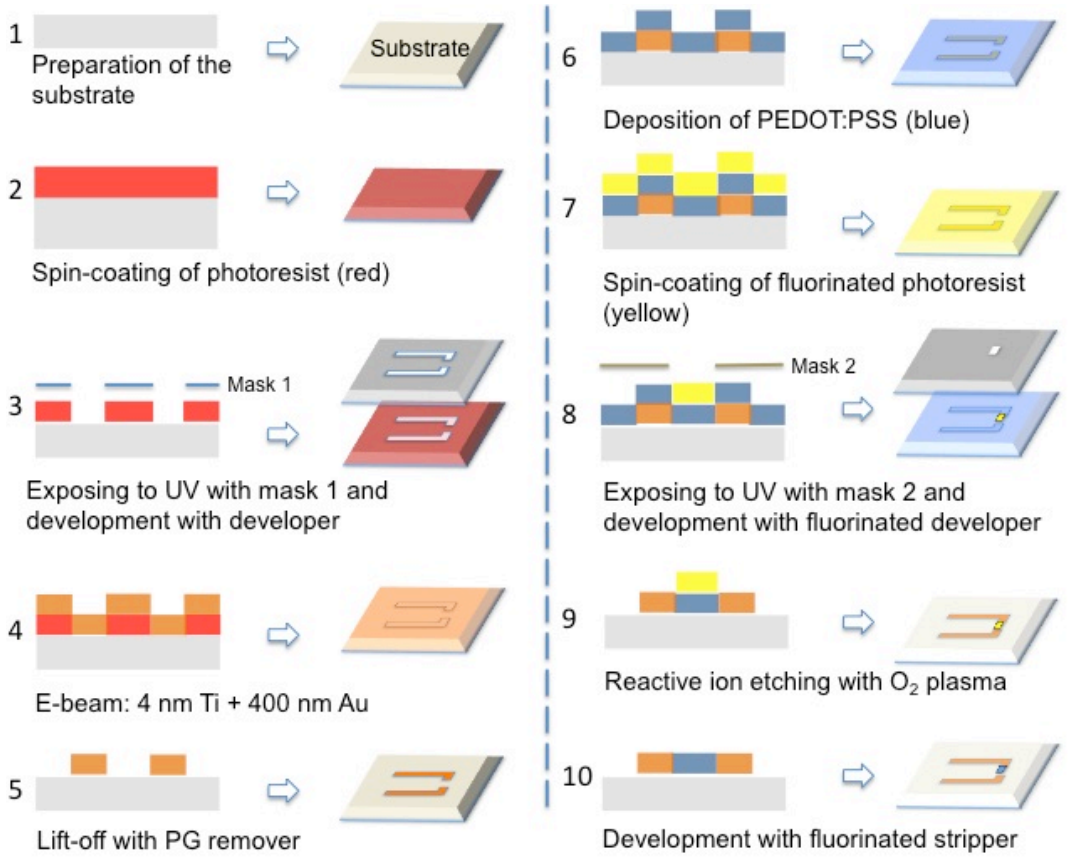

Figure 6. 2. A schematic representation for the process used to fabricate a patterned PEDOT:PSS OECT utilizing photolithography with both conventional and orthogonal (fluorinated) photoresists.

In some cases, glass cloning cylinders (VWR) were attached to confine the electrolyte upon the channel and the gate electrode of the transistor. Channels are defined by the overlapping of the electrolyte with the organic polymer.

6.2 Investigation of OECT processing on OECT performance

6.2.1 Effect of the device geometry

Effects of the device geometry of PEDOT:PSS OECTs were studied with 0.01 M NaCl aqueous electrolyte and PEDOT:PSS gate electrodes. The V_d was kept at -0.2 V, and V_g was in the range of 0 ~ 1 V. As shown in Figure 6.3, different ratios (γ) of areas of channel (A_{ch}) over gate (A_g), i.e. $\gamma = A_{ch} / A_g$, are applied to OECTs with respect to $\gamma > 1$ ($A_{ch} > A_g$), $\gamma < 1$ ($A_{ch} < A_g$) and $\gamma = 1$ ($A_{ch} = A_g$). Higher current modulation was observed in case of $\gamma > 1$ compare to $\gamma = 1$ and $\gamma < 1$. This is attributed to the fact that, in a non-Faradaic regime, the V_{sol} is determined by V_g and A_{ch} / A_g, as described in Figure 2.2 (Chapter 2). In case of an OECT in a $\gamma > 1$ geometry, V_{sol} is smaller than OECTs in geometries of $\gamma = 1$ and $\gamma < 1$. This indicates that minimum voltage drop can be observed near the electrolyte-channel interface, which enables maximum dedoping of the channel. While in a $\gamma < 1$ OECT, maximum voltage drop can be observed at the interface between the gate and the electrolyte, and this non-Faradaic process prohibit the effective dedoping of polymer channel, which is identity to equation (2) in Chapter 2.

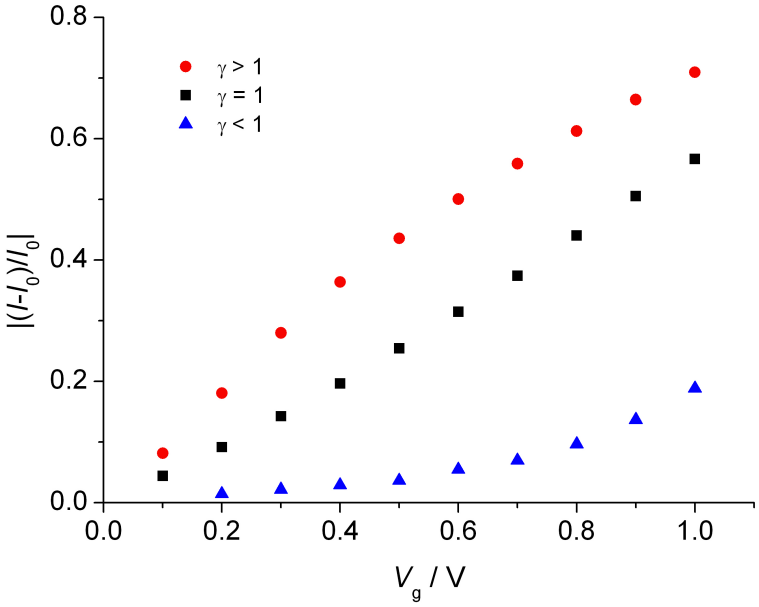

Figure 6. 3. OECT response $|(I-I_0)/I_0|$ as a function of V_g for 10^{-2} M NaCl with $\gamma = 1$, $\gamma < 1$ and $\gamma > 1$. I is the *OFF* current ($V_g \neq 0$) and I_0 is the *ON* current ($V_g = 0$). $V_d = -0.2$ V.

6.2.2 Geometry (α) of the channel

PEDOT:PSS OECTs with three different channel sizes have been investigated in presence of activated carbon (AC) or nanostructured carbon (nsC) gate electrodes and imidazole ionic liquid 1-ethyl-3-methylimidazolium [EMIM] bis(trifluoromethanesulfonyl)imide [TFSI] electrolyte. The channels are (I) W = 80 μm, L = 50 μm (α1 = 1.6); (II) W = 400 μm, L = 50 μm (α2 = 8); and (III) W = 0.2 cm, L = 0.8 cm (α3 = 0.25) (α = W/L). As shown in Figure 6.4 a, OECTs are working under a depletion mechanism with a proof that I_d decreases with the increase of the gate voltage (V_g). Comparing OECTs with channel geometries of type-I, type-II and type-III, which the W/L is in a sequence of α2 > α1 > α3, the I_d increases with the increase of α, i.e. $I_{d,\ type\text{-}II} > I_{d,\ type\text{-}I} > I_{d,\ type\text{-}III}$. The modulation response $|(I\text{-}I_0)/I_0|$ as a function of V_g confirms the depletion working mode of the OECTs (Figure 6.4b). The modulation response of the OECTs show that PEDOT:PSS in its initial state (V_g = 0 V) can be either dedoped, by application of a positive V_g, or doped, by application of a negative V_g. The current modulation of OECTs decreases with the increase of α, i.e. $modulation_{type\text{-}II} < modulation_{type\text{-}I} < modulation_{type\text{-}III}$ while α2 > α1 > α3, which is in an opposite trend comparing to the transfer characteristics.

We further compared two kinds of carbon gate materials with type-I OECT. One is the flexible nanostructured porous carbon that we developed in Chapter 4. The other is the carbon paper with activated carbon ink that employed in Chapter 3. The two carbon materials were cut into 0.2 cm * 0.8 cm and were dipped into the electrolyte with a perpendicular geometry referred to the PEDOT:PSS channel. As shown in Figure 6.4, the transfer characteristics and the current modulation of OECTs employing an AC gate (black squares) and a nsC gate (red circles) are similar.

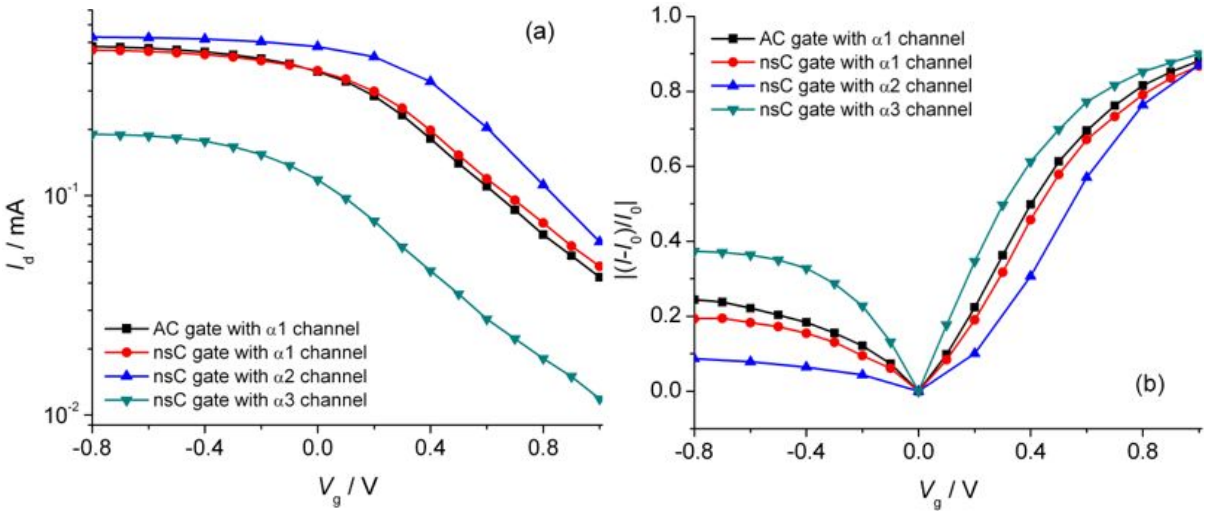

Figure 6. 4. Transfer curves (a) and the OECT response $|(I-I_0)/I_0|$ as a function of V_g (b) for I, II and III-type OECTs with AC gates and nsC gates. V_d = -0.5 V.

6.2.3 Effect of ions of electrolytes

CTAB aqueous solutions at different concentrations were applied to explore the influences of concentrations of CTA^+ on the performance of OECTs (γ = 1) (Figure 6.5). Transfer curves decrease with the increase of V_g (Figure 6.5a), which is consistent with the depletion working mechanism. For the OECT modulation, the maximum modulation was obtained with 10^{-2} M CTAB electrolyte (~0.8), and the minimum value was obtained with 10^{-8} M CTAB electrolyte (~0.5) (Figure 6.5b). The OECT response varies depending on concentrations of CTAB electrolytes. The results are different from the ones discussed in Chapter 2, which the concentrations of CTAB electrolytes have no impact on the OECT modulation when the concentration is below 10^{-4} M ($\gamma > 1$) [24].

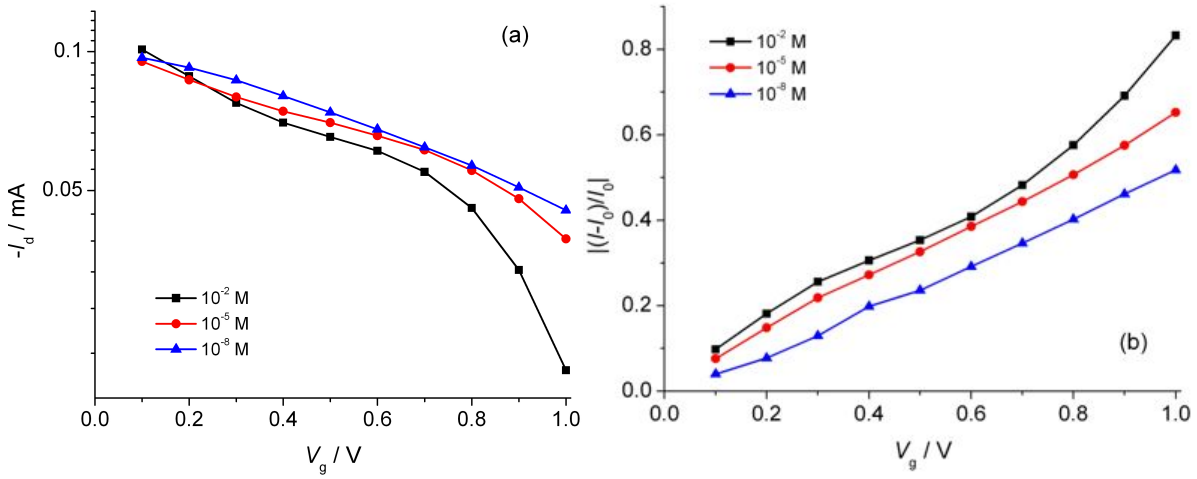

Figure 6. 5. Transfer curves (a) and OECT response $|(I-I_0)/I_0|$ as a function of V_g (b) with CTAB concentrations at 10^{-2}, 10^{-5} and 10^{-8} M. V_d = -0.2 V.

In order to understand the working mechanism of OECTs that works under negative gate voltage, we employed cationic micelle forming CTAB electrolyte and NaCl electrolyte, both of which are 10^{-2} M (Figure 6.6). We adopted OECTs with γ = 10 (channel area = 0.016 cm^2 and gate area = 0.16 cm^2). V_d is equal to -0.2 V and V_g varies from -1 to 0 V. Upon application of negative V_g on PEDOT:PSS OECTs, anions penetrate into the PEDOT:PSS channel and doped the channel. By making use of 10^{-2} M CTAB electrolyte, we observed lower OECT modulation than that with 10^{-2} M NaCl electrolyte. This may be due to the fact that chloride ions (Cl^-) diffuse more effectively into the channel than bromide (Br^-) ions.

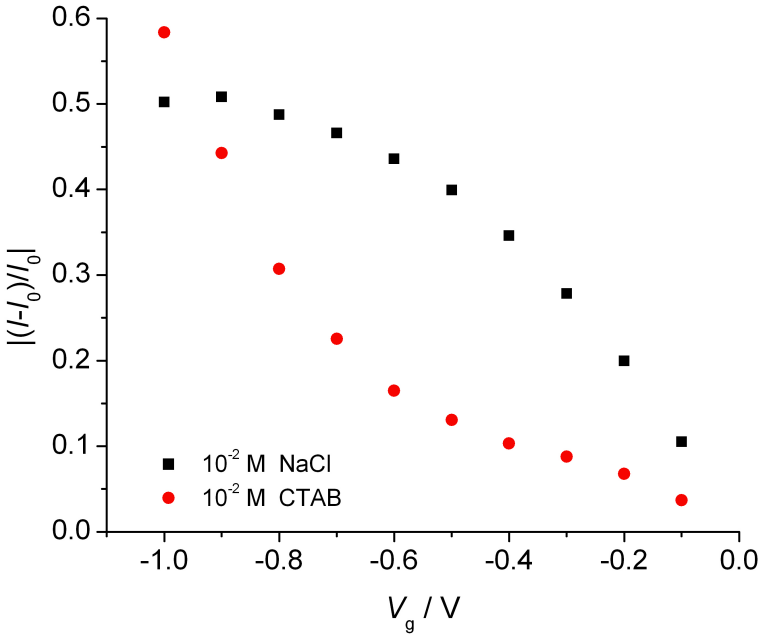

Figure 6. 6. OECT modulation $|(I-I_0)/I_0|$ *vs.* 10^{-2} M NaCl and CTAB with variation of gate voltage in the range of 0.1 to -1 V. V_d = -0.2 V.

Investigation of the influence of ions is further studied by employing more complicated electrolytes, i.e. ionic liquids (ILs) and 0.01 M CTAB micelles with comparison of 0.01 M NaCl aqueous solution. Two phosphornium ionic liquids are used as received, i.e. triisobutyl(methyl)phosphonium tosylate (IL106) and tributyl(methyl)phosphonium methylsulfate (IL108). It is noteworthy that the viscosities of IL106, IL108, 0.01 M CTAB and 0.01M NaCl are 4070 cP, 750 cP, 1cP and 1cP, respectively. At V_g = 1 V, the highest modulation was obtained with a CTAB-OECT (~0.8), which was slightly higher than a NaCl-OECT (~0.6). The OECTs making use of the two pure ILs exhibit similar trends of current modulation, and the current modulation at V_g = 1 V is around 0.3 (Figure 6.7a). From the transfer curves shown in Figure 6.7b, aqueous solution electrolytes based OECTs exhibit higher modulation than IL electrolytes based OECTs. The *ON*/*OFF* ratios of IL106 and IL108 based OECTs are same (~1.4), the 0.01 M NaCl aqueous solution based OECT exhibits slightly higher *ON*/*OFF* ratio with a value of ~3, and the OECT with CTAB electrolyte at a concentration of 0.01 M, with formation of micelles, reaches the highest *ON*/*OFF* ratio (~6).

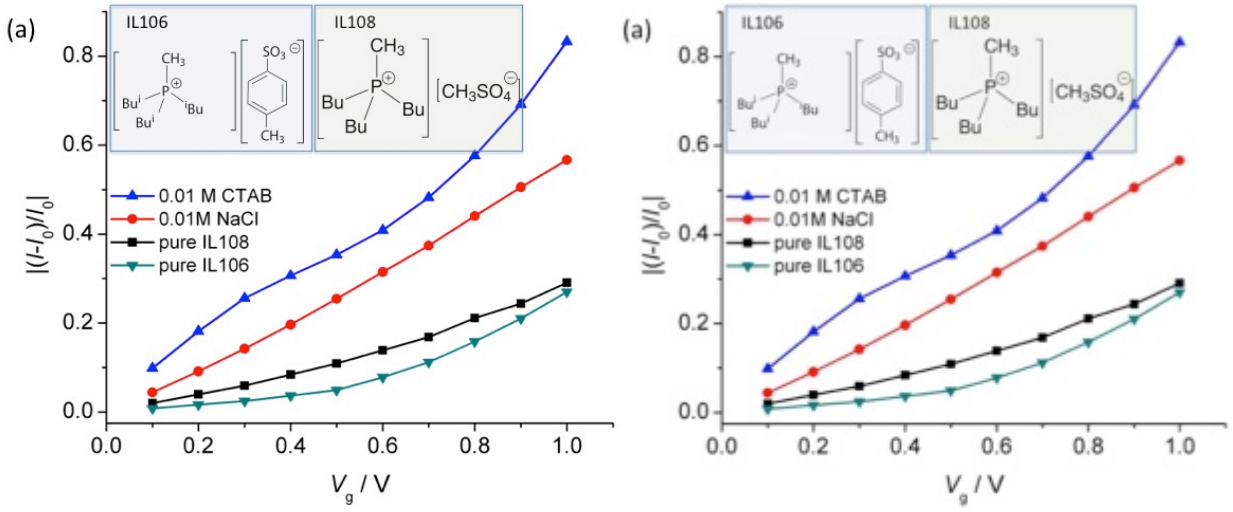

Figure 6. 7. OECT response $|(I-I_0)/I_0|$ as a function of V_g (a) and transfer curves (b) for 0.01 M CTAB, 0.01 M NaCl, pure IL108 and pure IL106. V_d = -0.2 V.

CHAPTER 7 CONCLUSIONS AND RECOMMENDATIONS

OECTs have great potential to be a key technology in the near future. An improved understanding of their working mechanism is expected to advance the state of the art of organic bioelectronics.

In this thesis, we fabricated OECTs on rigid, flexible and degradable substrates patterned with photolithography, which employs conventional photoresists and orthogonal photoresists. We have studied the effects of electrolytes, gates and substrates on the performance of OECTs. With respect to electrolytes, we have investigated the ion species, the chemical structures, as well as concentrations, viscosities and ionic conductivities of electrolytes, and also we have compared liquid and quasi-solid electrolytes (gels). In order to understand the gate effects, we have utilized PEDOT:PSS, carbon paper with activated carbon ink and flexible nanostructured carbon as gate electrodes. We have also studied the geometry effects, including device geometry and channel geometry. In order to investigate the practical in vivo applications, we have fabricated degradable OECTs by a newly developed pattern transfer method.

We identified two processing approaches to use the highly viscous, hydrophilic, phosphonium-based IL 106 as the electrolyte in OECTs. This approach can be considered for utilization of other highly viscous, hydrophilic, phosphonium-based ILs. For ionic liquids or other electrolytes, which are able to permeate into or react with PEDOT:PSS, other factors have to be considered to fully understand the electrochemical doping/dedoping process reacting with the exposed PEDOT:PSS channel, besides the viscosity and the ionic conductivity of the electrolyte. The microstructure of the electrolyte (e.g. ion association) might also play a role in the doping/dedoping process in OECTs.

We have designed planar OECTs including a PEDOT:PSS channel and a planar nanostructured carbon gate deposited by SCBD on flexible Mylar substrates. OECTs with channel lengths as low as 5 μm were patterned by orthogonal lithography. OECTs making use of the PSSNa gel electrolyte exhibit much higher OECT modulations with respect to those making use of aqueous NaCl electrolytes. These OECTs can be used as supercapacitors, leading to a practical example of

transcap. The electrodes of the supercapacitors consist of i) a PEDOT:PSS transistor channel included between source and drain electrodes and ii) the carbon gate. The planar and flexible transcap can be easily cut and paste on different kinds of substrates. By using this OECT as the transcap, we have observed efficient charge retention and satisfying energy storage to keep the ON status of the OECT without power supply.

We developed "green" OECTs, which employ degradable substrates and water as the gating medium. OECTs patterned on PET were transfer patterned onto degradable shellac substrates. In order to explore the gate effect in presence of water as the gating medium, we have employed AC and PEDOT:PSS gate electrodes. Results have indicated that OECTs with AC gates present slower current response and higher current modulation than making use of PEDOT:PSS gates. The shellac substrate can be degraded in a 1 M KOH solution.

We have studied geometry effects on OECT performance by investigating the ratios channel area/gate area (A_{ch}/A_{ch}) and channel width/channel lenght (W/L). As expected, the OECT performance highly depends on device and channel geometry.

In perspective, we propose to investigate patterning methods for degradable OECTs, expected to simplify the fabrication process compared to commonly used patterning methods. It is also important to investigate the degradation conditions/times for the devices, taking into account the intrinsic properties of the materials, such as glass transition temperatures, solubility and reactivity.

Other interesting studies will include i) investigation of OECTs interfaced with phosphonium ionic liquids serving as both electrolytes and dopants, ii) developing electrolytes that can be used for loading drugs or small molecular weight complexes to be delivered by the OECTs and iii) investigation of soft orthogonal photolithography patterning methods for water sensitive materials.

BIBLIOGRAPHY

[1] G. G. Malliaras and R. H. Friend, “An organic electronics primer”, *Phys. Today*, 2005, 58, 53–58.

[2] M. Pope and C. E. Swenberg, “Electronic Processes in Organic Crystals and Polymers” Oxford University Press, NY, 1999.

[3] H. Shirakawa, E. J. Louis, A. G. Macdiarmid, C. K. Chiang and A. J. Heeger, “Synthesis of electrically conducting organic polymers: halogen derivatives of polyacetylene, $(CH)_X$”, *J. Chem. Soc. Chem. Commun*., 1977, 16, 578-580.

[4] P. Lin and F. Yan, “Organic Thin-Film Transistors for Chemical and Biological Sensing”, *Adv. Mater.*, 2012, 24, 34–51.

[5] J. H. Burroughes, D. D. C. Bradley, A. R. Brown, R. N. Marks, K. Mackay, R. H. Friend, P. L. Burns and A. B. Holmes, “Light-emitting diodes based on conjugated polymers”, *Nature*, 1990, 347, 539–541.

[6] R. H. Friend, R. W. Gymer, A. B. Holmes, J. H. Burroughes, R. N. Marks, C. Taliani, D. D. C. Bradley, D. A. Dos Santos, J. L. Brédas, M. Lögdlund and W. R. Salaneck, “Electroluminescence in conjugated polymers”, *Nature*, 1999, 397, 121–128.

[7] E. Bequerel, “Recherches sur les effets de la radiation chimique de la lumière solaire, au moyen des courants électriques”, *C.R. Acad. Sci.*, 1839, 9, 145–149.

[8] M. Grätzel, “Photoelectrochemical cells”, *Nature*, 2001, 414, 338–344.

[9] H. Kallmann and M. Pope, “Photovoltaic effect in organic crystals”, *J. Chem. Phys.*, 1959, 30, 585–586.

[10] J. Nelson, “Polymer: fullerene bulk heterojunction solar cells”, *Mater. Today*, 2011, 14, 462–470.

[11] J. E. Lilienfeld, "Method and apparatus for controlling electric currents", 1930, US 1745175.

[12] R. Coehoorn, H. van Eersel, P. A. Bobbert and R. A. J. Janssen, “Kinetic Monte Carlo Study of the Sensitivity of OLED Efficiency and Lifetime to Materials Parameters”, *Adv. Funct. Mater.*, 2015, 25, 2024–2037.

[13] J. E. Anthony, “Functionalized acenes and heteroacenes for organic electronics”, *Chem. Rev.*, 2006, 106, 5028–5048.

[14] H. Klauk, “Organic thin-film transistors”, *Chem. Soc. Rev.*, 2010, 39, 2643– 2666.

[15] S. Steudel, K. Myny, V. Arkhipov, C. Deibel, S. De Vusser, J. Genoe and P. Heremans, “50MHz rectifier based on an organic diode”, *Nat. Mater.*, 2005, 4, 597–600.

[16] P. Peumans, S. Uchida and S. R. Forrest, “Efficient bulk heterojunction photovoltaic cells using small-molecular-weight organic thin films”, *Nature*, 2003, 425, 158–162.

[17] A. R. Murphy and J. M. J. Fréchet, “Organic semiconducting oligomers for use in thin film transistors”, *Chem. Rev.*, 2007, 107, 1066–1096.

[18] M. Riordan, L. Hoddeson and C. Herring, “The invention of the transistor”, *Rev. Mod. Phys.*, 1999, 71, S336–S345.

[19] R. Völkel, R. A. Street and D. Knipp, “Carrier transport and density of state distributions in pentacene transistors”, *Phys. Rev. B*, 2002, 66, 195336–195344.

[20] S. H. Kim, K. Hong, W. Xie, K. H. Lee, S. Zhang, T. P. Lodge and C. D. Frisbie, “Electrolyte-gated transistors for organic and printed electronics”, *Adv. Mater.*, 2013, 25, 1822–1846.

[21] G. Tarabella, F. M. Mohammadi, N. Coppede, F. Barbero, S. Iannotta, C. Santato and F. Cicoira, “New opportunities for organic electronics and bioelectronics: ions in action”, *Chem. Sci.*, 2013, 4, 1395–1409.

[22] H. Letaw and J. Bardeen, “Electrolytic Analog Transistor”, *J. Appl. Phys*., 1954, 25, 600.

[23] J. Lee, L. G. Kaake, J. H. Cho, X.-Y. Zhu, T. P. Lodge, and C. D. Frisbie, “Ion Gel-Gated Polymer Thin-Film Transistors: Operating Mechanism and Characterization of Gate Dielectric Capacitance, Switching Speed, and Stability”, *J. Phys. Chem. C*, 2009, 113, 8972–8981.

[24] M. J. Panzer and C. D. Frisbie, “Polymer Electrolyte-Gated Organic Field-Effect Transistors: Low-Voltage, High-Current Switches for Organic Electronics and Testbeds for Probing Electrical Transport at High Charge Carrier Density”, *J. Am. Chem. Soc.*, 2007, 129, 6599–6607.

[25] S. Inal, J. Rivnay, P. Leleux, M. Ferro, M. Ramuz, J. C. Brendel, M. M. Schmidt, M. Thelakkat and G. G. Malliaras, “A High Transconductance Accumulation Mode Electrochemical Transistor”, *Adv. Mater.*, 2014, 26, 7450–7455.

[26] S. Inal, J. Rivnay, A. I. Hofmann, I. Uguz, M. Mumtaz, D. Katsigiannopoulos, C. Brochon, E. Cloutet, G. Hadziioannou and G. G. Malliaras, "Organic Electrochemical Transistors Based on PEDOT with Different Anionic Polyelectrolyte Dopants", *J. Polym. Sci., part B: Polym. Phys*., 2016, 54, 147–151.

[27] H. Yoon, J. Jang, "Conducting-Polymer Nanomaterials for High-Performance Sensor Applications: Issues and Challenges", *Adv. Funct. Mater.*, 2009, 19, 1567–1576.

[28] S.-H. Chen, H.-C. Liu, C.-Y. Lee, J.-Y. Gan, H.-W. Zan, J.-C. Hwang, Y.-Y. Cheng, P.-C. Lyu, "High performance electric-double-layer amorphous IGZO thin-film transistors gated with hydrated bovine serum albumin protein", *Org. Electron*., 2015, 24, 200–204.

[29] B. Nasr, D. Wang, R. Kruk, H. Rösner, H. Hahn and S. Dasgupta, "High-Speed, Low-Voltage, and Environmentally Stable Operation of Electrochemically Gated Zinc Oxide Nanowire Field-Effect Transistors", *Adv. Funct. Mater*., 2013, 23, 1750–1758.

[30] E. Penzo, M. Palma, D. A. Chenet, G. Ao, M. Zheng, J. C. Hone and S. J. Wind, "Directed Assembly of Single Wall Carbon Nanotube Field Effect Transistors", *ACS Nano*, 2016, 10, 2975−2981.

[31] H. Yoon and J. Jang, "Conducting-Polymer Nanomaterials for High-Performance Sensor Applications: Issues and Challenges", *Adv. Funct. Mater.* , 2009, 19, 1567–1576.

[32] H. S. White, G. P. Kittlesen and M. S. Wrighton, "Chemical derivatization of an array of three gold microelectrodes with polypyrrole: fabrication of a molecule-based transistor", *J. Am. Chem. Soc.*, 1984, 106, 5375–5377.

[33] X. Strakosas, M. Bongo and R. M. Owens, "The organic electrochemical transistor for biological applications", *J. Appl. Polym. Sci.*, 2015, 132, 41735.

[34] M. Asplund, T. Nyberg and O. Inganäs, "Electroactive polymers for neural interfaces", *Polym. Chem.*, 2010, 1, 1374–1391.

[35] P. Lin, F. Yan, J. Yu, H. L. W. Chan and M. Yang, "The application of organic electrochemical transistors in cell-based biosensors", *Adv. Mater.*, 2010, 22, 3655–3660.

[36] F. Cicoira, M. Sessolo, O. Yaghmazadeh, J. A. DeFranco, S. Y. Yang and G. G. Malliaras, "Influence of device geometry on sensor characteristics of planar organic electrochemical transistors", *Adv. Mater.*, 2010, 22, 1012–1016.

[37] D. A. Bernards, D. J. Macaya, M. Nikolou, J. A. DeFranco, S. Takamatsu and G. G. Malliaras, “Enzymatic sensing with organic electrochemical transistors”, *J. Mater. Chem.*, 2008, 18, 116–120.

[38] S. Y. Yang, F. Cicoira, R. Byrne, F. Benito-Lopez, D. Diamond, R. M. Owens and G. G. Malliaras, “Electrochemical transistors with ionic liquids for enzymatic sensing”, *Chem. Commun.*, 2010, 46, 7972–7974.

[39] H. Tang, F. Yan, P. Lin, J. B. Xu and H. L. W. Chan, “Highly sensitive glucose biosensors based on organic electrochemical transistors using platinum gate electrodes modified with enzyme and nanomaterials”, *Adv. Funct. Mater.*, 2011, 21, 2264–2272.

[40] R.-X. He, M. Zhang, F. Tan, P. H. M. Leung, X.-Z. Zhao, H. L. W. Chan, M. Yang and F. Yan, “Detection of Bacteria with Organic Electrochemical Transistors”, *J. Mater. Chem.*, 2012, 22, 22072–22076.

[41] R. M. Owens and G. G. Malliaras, “Organic electronics at the interface with biology”, *MRS Bull.*, 2010, 35, 449–456.

[42] M. Berggren and A. Richter-Dahlfors, “Organic bioelectronics”, *Adv. Mater.*, 2007, 19, 3201–3213.

[43] A. Richter-Dahlfors, K. Svennersten, K. C. Larsson and M. Berggren, “Organic bioelectronics in nanomedicine”, *Biochim. Biophys. Acta, Gen. Subj.*, 2011, 1810, 276–285.

[44] P. N. Bartlett and Y. Astier, “Microelectrochemical enzyme transistors”, *Chem. Commun.*, 2000, 105–112.

[45] J. M. Leger, “Organic electronics: the ions have it”, *Adv. Mater.*, 2008, 20, 837–841.

[46] O. Larsson, A. Laiho, W. Schmickler, M. Berggren and X. Crispin, “Controlling the dimensionality of charge transport in an organic electrochemical transistor by capacitive coupling”, *Adv. Mater.*, 2011, 23, 4764–4769.

[47] K. Tybrandt, K. C. Larsson, A. Richter-Dahlfors and M. Berggren, “Ion bipolar junction transistors”, *PNAS*, 2010, 107, 9929–9932.

[48] K. Tybrandt, R. Forchheimer and M. Berggren, “Logic gates based on ion transistors”, *Nat. Commun.*, 2012, 3, 871–876.

[49] Z. Yi, G. Natale, P. Kumar, E. Di Mauro, M. Heuzey, F. Soavi, I. I. Perepichka, S. K. Varshney, C. Santato and F. Cicoira, “Ionic liquid–water mixtures and ion gels as electrolytes for organic electrochemical transistors”, *J. Mater. Chem. C*, 2015, 3, 6549–6553.

[50] G. Tarabella, C. Santato, S. Y. Yang, S. Iannotta, G. G. Malliaras and F. Cicoira, "Effect of the gate electrode on the response of organic electrochemical transistors", *Appl. Phys. Lett.*, 2010, 97, 123304.

[51] M. Demelas, E. Scavetta, L. Basiricò, R. Rogani and A. Bonfiglio, "A deeper insight into the operation regime of all-polymeric electrochemical transistors", *Appl. Phys. Lett.*, 2013, 102, 193301.

[52] O. Yaghmazadeh, F. Cicoira, D. A. Bernards, S. Y. Yang, Y. Bonnassieux and G. G. Malliaras, "Optimization of Organic Electrochemical Transistors for Sensor Applications", *J. Polym. Sci. Pol. Phys.*, 2011, 49, 34–39.

[53] D. A. Bernards and G. G. Malliaras, "Steady-State and Transient Behavior of Organic Electrochemical Transistors", *Adv. Funct. Mater.*, 2007, 17, 3538–3544.

[54] D. Khodagholy, M. Gurfinkel, E. Stavrinidou, P. Leleux, T. Herve, S. Sanaur and G. G. Malliaras, "High speed and high density organic electrochemical transistor arrays", *Appl. Phys. Lett*., 2011, 99, 163304.

[55] E. Stavrinidou, P. Leleux, H. Rajaona, D. Khodagholy, J. Rivnay, M. Lindau, S. Sanaur and G. G. Malliaras, "Direct measurement of ion mobility in a conducting polymer", *Adv. Mater.*, 2013, 25, 4488–4493.

[56] G. Tarabella, G. Nanda, M. Villani, N. Coppedè, R. Mosca, G. G. Malliaras, C. Santato, S. Iannotta and F. Cicoira, "Organic electrochemical transistors monitoring micelle formation", *Chem. Sci.*, 2012, 3, 3432–3435.

[57] V. Armel, D. Velayutham, J. Sun, P. C. Howlett, M. Forsyth, D. R. MacFarlane and J. M. Pringle, "Ionic liquids and organic ionic plastic crystals utilizing small phosphonium Cations", *J. Mater. Chem.*, 2011, 21, 7640–7650.

[58] I. S. Martinez and S. Baldelli, "Ionic Liquids: From Knowledge to Application, ed. N. V. Plechkova, R. D. Rogers and K. R. Seddon, *ACS Symposium Series*, 2009, vol. 1030.

[59] M. Armand, F. Endres, D. R. MacFarlane, H. Ohno and B. Scrosati, "Ionic-liquid materials for the electrochemical challenges of the future", *Nat. Mater.*, 2009, 8, 621–629.

[60] D. R. MacFarlane, J. M. Pringle, P. C. Howlett and M. Forsyth, "Ionic liquids and reactions at the electrochemical interface", *Phys. Chem. Chem. Phys.*, 2010, 12, 1659–1669.

[61] M. Galiński, A. Lewandowski and I. Stępniak, "Ionic liquids as electrolytes", *Electrochim. Acta*, 2006, 51, 5567–5580.

[62] K. J. Fraser and D. R. MacFarlane, “Phosphonium-Based Ionic Liquids: An Overview”, *Aust. J. Chem.*, 2009, 62, 309–321.

[63] D. Khodagholy, V. F. Curto, K. J. Fraser, M. Gurfinkel, R. Byrne, D. Diamond, G. G. Malliaras, F. Benito-Lopezb and R. M. Owens, “Organic electrochemical transistor incorporating an ionogel as a solid state electrolyte for lactate sensing”, *J. Mater. Chem.*, 2012, 22, 4440–4443.

[64] C. Liao, M. Zhang, L. Niu, Z. Zheng and F. Yan, “Highly selective and sensitive glucose sensors based on organic electrochemical transistors with graphenemodified gate electrodes”, *J. Mater. Chem. B*, 2013, 1, 3820–3829.

[65] W. Choi, T. An and G. Lim, “Organic electrochemical transistors based on a dielectrophoretically aligned nanowire array”, *Nanoscale Res. Lett.*, 2011, 6, 339.

[66] E. Lahiff, C. Lynam, N. Gilmartin, R. O’Kennedy and D. Diamond, “The increasing importance of carbon nanotubes and nanostructured conducting polymers in biosensors”, *Anal. Bioanal. Chem.*, 2010, 398,1575–1589.

[67] Z. T. Zhu, J. T. Mabeck, C. Zhu, N. C. Cady, C. A. Batt and G. G. Malliaras, “A simple poly(3,4-ethylene dioxythiophene)/poly(styrene sulfonic acid) transistor for glucose sensing at neutral pH”, *Chem. Commun.*, 2004, 1556–1557.

[68] C. Hin Mak, C. Liao, Y. Fu, M. Zhang, C. Y. Tang, Y. H. Tsang, H. L. W. Chan and F. Yan, “Highly-sensitive epinephrine sensors based on organic electrochemical transistors with carbon nanomaterial modified gate electrodes”, *J. Mater. Chem. C*, 2015, 3, 6532–6538.

[69] P. A. Ersman, D. Nilsson, J. Kawahara, G. Gustafsson and M. Berggren, “Fast-switching all-printed organic electrochemical transistors”, *Org. Electron.*, 2013, 14, 1276–1280.

[70] C. Yang, M. E. Denno, P. Pyakurel and B. J. Venton, “Recent trends in carbon nanomaterial-based electrochemical sensors for biomolecules: A review”, *Anal. Chimi. Acta*, 2015, 887, 17–37.

[71] R. L. McCreery, “Advanced Carbon Electrode Materials for Molecular Electrochemistry”, *Chem. Rev.*, 2008, 108, 2646–2687.

[72] C. H. Mak, C. Liao, Y. Fu, M. Zhang, C. Y. Tang, Y. H. Tsang, H. L. W. Chan and F. Yan, “Highly-sensitive epinephrine sensors based on organic electrochemical transistors with carbon nanomaterial modified gate electrodes”, *J. Mater. Chem. C*, 2015, 3, 6532–6538.

[73] S. Ryu, P. Lee, J. B. Chou, R. Xu, R. Zhao, A. John Hart and S. Kim, "Extremely Elastic Wearable Carbon Nanotube Fiber Strain Sensor for Monitoring of Human Motion", *ACS Nano*, 2015, 9, 5929–5936.

[74] M. Lu and R. G. Compton, "Voltammetric pH sensing using carbon electrodes: glassy carbon behaves similarly to EPPG", *Analyst*, 2014, 139, 4599–4605.

[75] H. Tang, P. Kumar, S. Zhang, Z. Yi, G. D. Crescenzo, C. Santato, F. Soavi and F. Cicoira, "Conducting Polymer Transistors Making Use of Activated Carbon Gate Electrodes", *ACS Appl. Mater. Interfaces*, 2015, 7, 969−973.

[76] A. Searle and L. Kirkup, "A direct comparison of wet, dry and insulating bioelectric recording electrodes", *Physiol. Meas.*, 2000, 21, 271–283.

[77] A. Campana, T. Cramer, D. T. Simon, M. Berggren and F. Biscarini, "Electrocardiographic Recording with Conformable Organic Electrochemical Transistor Fabricated on Resorbable Bioscaffold", *Adv. Mater.*, 2014, 26, 3874–3878.

[78] K. Fukuda, T. Sekine, R. Shiwaku, T. Morimoto, D. Kumaki and S. Tokito, "Free-Standing Organic Transistors and Circuits with Sub-Micron Thicknesses", *Sci. Rep.*, 2016, 6, 27450.

[79] A. Bonfiglio, F. Mameli and O. Sanna, "A completely flexible organic transistor obtained by a one-mask photolithographic process", *Appl. Phys. Lett.*, 2003, 82, 3550.

[80] L. Zhang, C. Di, Y. Zhao, Y. Guo, X. Sun, Y. Wen, W. Zhou, X. Zhan, G. Yu and Y. Liu, "Top-Gate Organic Thin-Film Transistors Constructed by a General Lamination Approach", *Adv. Mater.*, 2010, 22, 3537–3541.

[81] H. T. Yi, M. M. Payne, J. E. Anthony and V. Podzorov, "Ultra-flexible solution-processed organic field-effect transistors", *Nat. Commun.*, 2012, 3, 1259

[82] L. Zhang, H. Wang, Y. Zhao, Y. Guo, W. Hu, G. Yu and Y. Liu, "Substrate-Free Ultra-Flexible Organic Field-Effect Transistors and Five-Stage Ring Oscillators", *Adv. Mater.*, 2013, 25, 5455–5460.

[83] A. Jonsson, Z. Song, D. Nilsson, B. A. Meyerson, D. T. Simon, B. Linderoth and M. Berggren, "Therapy using implanted organic bioelectronics", *Sci. Adv.*, 2015, 1, e1500039.

[84] M. R. Abidian, D. Kim and D. C. Martin, "Conducting-Polymer Nanotubes for Controlled Drug Release", *Adv. Mater.*, 2006, 18, 405–409.

[85] H.-H. Chou, A. Nguyen, A. Chortos, J. W. F. To, C. Lu, J. Mei, T. Kurosawa, W.-G. Bae, J.

B.-H. Tok and Z. Bao, "A Chameleon-Inspired Stretchable Electronic Skin with Interactive Color-Changing Controlled by Tactile Sensing", *Nat. Commun.*, 2015, 6, 8011.

[86] S. K. Kang, R. K. Murphy, S. W. Hwang, S. M. Lee, D. V. Harburg, N. A. Krueger, J. Shin, P. Gamble, H. Cheng, S. Yu, Z. Liu, J. G. McCall, M. Stephen, H. Ying, J. Kim, G. Park, R. C. Webb, C. H. Lee, S. Chung, D. S. Wie, A. D. Gujar, B. Vemulapalli, A. H. Kim, K. M. Lee, J. Cheng, Y. Huang, S. H. Lee, P. V. Braun, W. Z. Ray and J. A. Rogers, "Bioresorbable silicon electronic sensors for the brain", *Nature*, 2016, 530, 71–76.

[87] C. Yao, Q. Li, J. Guo, F. Yan and I-M. Hsing, "Rigid and Flexible Organic Electrochemical Transistor Arrays for Monitoring Action Potentials from Electrogenic Cells", *Adv. Healthcare Mater.*, 2015, 4, 528–533.

[88] S. R. Forrest, "The path to ubiquitous and low-cost organic electronic appliances on plastic", *Nature*, 2004, 428, 911–918.

[89] D. Tobjörk and R. Österbacka, "Paper Electronics", *Adv. Mater.*, 2011, 23, 1935–1961.

[90] J. Jang, "Displays develop a new flexibility", *Mater. Today*, 2006, 9, 46–52.

[91] A. J. Bandodkar and J. Wang, "Non-invasive wearable electrochemical sensors: a review", *Trends Biotechnol.*, 2014, 32, 363−371.

[92] P. Lin, X. Luo, I. Hsing and F. Yan, "Organic Electrochemical Transistors Integrated in Flexible Microfluidic Systems and Used for Label-Free DNA Sensing", *Adv. Mater.*, 2011, 23, 4035–4040.

[93] D. Khodagholy, J Rivnay, M. Sessolo, M. Gurfinkel, P. Leleux, L. H. Jimison, E. Stavrinidou, T. Herve, S. Sanaur, R. M. Owens and G. G. Malliaras, "High transconductance organic electrochemical transistors", *Nat. Commun*., 2013, 4, 2133.

[94] M. Irimia-Vladu, "Green" electronics: biodegradable and biocompatible materials and devices for sustainable future", *Chem. Soc. Rev.*, 2014, 43, 588–610

[95] D.-H. Kim, Y.-S. Kim, J. Amsden, B. Panilaitis, D. L. Kaplan, F. G. Omenetto, M. R. Zakin and J. A. Rogers, "Silicon electronics on silk as a path to bioresorbable, implantable devices", *Appl. Phys. Lett.*, 2009, 95, 133701.

[96] L. Miozzo, A. Yassar and G. Horrowitz, "Surface engineering for high performance organic electronic devices: the chemical approach", *J. Mater. Chem.*, 2010, 20, 2513–2538.

[97] M. Irimia-Vladu, P.A.Troshin, M.Reisinger, L.Shmygleva, Y.Kanbur, G. Schwabegger, M. Bodea, R. Schwödiauer, A. Mumyatov, J. W. Fergus, V. F. Razumov, H. Sitter, N. S.

Sariciftci, S. Bauer, “Biocompatible and biodegradable materials for organic field effect transistors”, *Adv. Funct. Mater.*, 2010, 20, 4069–4076.

[98] T. Sekitani, T. Yokota, U. Zschieschang, H. Klauk, S. Bauer, K. Takeuchi, M. Takamiya, T. Sakurai and T. Someya, “Organic nonvolatile memory transistors for flexible sensor arrays”, *Science*, 2009, 326, 1516–1519.

[99] C. J. Bettinger and Z. Bao, “Organic Thin-Film Transistors Fabricated on Resorbable Biomaterial Substrates”, *Adv. Mater.*, 2010, 22, 651–655.

[100] U. Zschieschang, T. Yamamoto, K. Takimiya, H. Kuwabara, M. Ikeda, T. Sekitani, T. Someya and H. Klauk, “Organic Electronics on Banknotes”, *Adv. Mater.*, 2011, 23, 654–658.

[101] A. Hübler, B. Trnovec, T. Zillger, M. Ali, N. Wetzold, M. Mingebach, A. Wagenpfahl, C. Deibel and V. Dyakonov, “Printed Paper Photovoltaic Cells”, *Adv. Energy Mater.*, 2011, 1, 1018–1022.

[102] C.-H. Wang, C.-Y. Hsieh and J.-C. Hwang, “Flexible Organic Thin-Film Transistors with Silk Fibroin as the Gate Dielectric”, *Adv. Mater.*, 2011, 23, 1630–1634.

[103] H. Tao, M. A. Brenckle, M. Yang, J. Zhang, M. Liu, S. M. Siebert, R. D. Averitt, M. S. Mannoor, M. C. McAlpine, J. A. Rogers, D. L. Kaplan and F. G. Omenetto, “Silk-Based Conformal, Adhesive, Edible Food Sensors”, *Adv. Mater.*, 2012, 24, 1067–1072.

[104] D.-H. Kim, J. Viventi, J. J. Amsden, J. Xiao, L. Vigeland, Y.-S. Kim, J. A. Blanco, B. Panilaitis, E. S. Frechette, D. Contreras, D. L. Kaplan, F. G. Omenetto, Y. Huang, K.-C. Hwang, M. R. Zakin, B. Litt and J. A. Rogers, “Dissolvable films of silk fibroin for ultrathin conformal bio-integrated electronics”, *Nat. Mater.*, 2010, 9, 511–517.

[105] D. -H. Kim, Y. -S. Kim, J. Wu, Z. Liu, J. Song, H. -S. Kim, Y. Y. Huang, K. -C. Hwang and J. A. Rogers, “Ultrathin silicon circuits with strain-isolation layers and mesh layouts for high-performance electronics on fabric, vinyl, leather, and paper”, *Adv. Mater.*, 2009, 21, 3703–3707.

[106] M. Irimia-Vladu, N. S. Sariciftci and S. Bauer, “Exotic materials for bio-organic electronics”, *J. Mater. Chem.*, 2011, 21, 1350–1361.

[107] M. Irimia-Vladu, P. A. Troshin, M. Reisinger, G. Schwabegger, M. Ullah, R. Schwoediauer, A. Mumyatov, M. Bodea, J. W. Fergus, V. F. Razumov, H. Sitter, S. Bauer and N. S. Sariciftci, “Environmentally sustainable organic field effect transistors”, *Org. Electron.*, 2010, 11, 1974–1990.

[108] M. Irimia-Vladu, E. D. Głowacki, G. Schwabegger, L. Leonat, H. Zekiye Akpinar, H. Sitter, S. Bauerb and N. S. Sariciftci, "Natural resin shellac as a substrate and a dielectric layer for organic field-effect transistors", *Green Chem.*, 2013, 15, 1473–1476.

[109] D. K. Gilding and A. M. Reed, "Biodegradable polymers for use in surgery—polyglycolic/poly(actic acid) homo- and copolymers: 1", *Polymer*, 1979, 20, 14591–464.

[110] L. Lu, C. A. Garcia and A. G. Mikos, "In vitro degradation of thin poly(DL-lactic-co-glycolic acid) films", *J. Biomed. Mater. Res.*, 1999, 4, 236–244.

[111] C. Müller, M. Hamedi, R. Karlsson, R. Jansson, R. Marcilla, M. Hedhammar, and O. Inganäs, "Woven Electrochemical Transistors on Silk Fibers", *Adv. Mater.*, 2011, 23, 898–901.

[112] Y. Farag and C. S. Leopold, "Investigation of drug release from pellets coated with different shellac types", *Drug Dev. Ind. Pharm.*, 2011, 37, 193–200.

[113] S. Leick, M. Kott, P. Degen, S. Henning and T. Pa, "Mechanical properties of liquid-filled shellac composite capsules", *Phys. Chem. Chem. Phys.*, 2011, 13, 2765–2773.

[114] S. A. Hamad, S. D. Stoyanov and V. N. Paunov, "Triggered cell release from shellac–cell composite microcapsules", *Soft Matter*, 2012, 8, 5069–5077.

[115] D. Phan Thea, F. Debeaufort, D. Luu and A. Voilley, "Moisture barrier, wetting and mechanical properties of shellac/agar or shellac/cassava starch bilayer bio-membrane for food applications", *J. Membr. Sci.*, 2008, 325, 277–283.

[116] R. D. Hagenmaier and P. E. Shaw, "Permeability of shellac coatings to gases and water vapor", *J. Agric. Food Chem.*, 1991, 39, 825–829.

[117] L. M. Bellan, M. Pearsall, D. M. Cropek, and R. Langer, "A 3D Interconnected Microchannel Network Formed in Gelatin by Sacrificial Shellac Microfibers", *Adv. Mater.*, 2012, 24, 5187–5191.

[118] S. K. Mahadeva, K. Walus and B. Stoeber, "Paper as a Platform for Sensing Applications and Other Devices: A Review", *ACS Appl. Mater. Interfaces*, 2015, 7, 8345−8362.

[119] K. A. Mirica, J. G. Weis, J. M. Schnorr, B. Esser and T. M. Swager, "Mechanical Drawing of Gas Sensors on Paper", *Angew. Chem., Int. Ed.*, 2012, 51, 10740−10745.

[120] C. W. Lin, Z. Zhao, J. Kim and J. Huang, "Pencil Drawn Strain Gauges and Chemiresistors on Paper", *Sci. Rep.*, 2014, 4, 3812.

[121] M. Kaempgen, C. K. Chan, J. Ma, Y. Cui and G. Gruner, “Printable Thin Film Supercapacitors Using Single-walled Carbon Nanotubes”, *Nano Lett.*, 2009, 9, 1872−1976.

[122] K. M. Schilling, A. L. Lepore, J. A. Kurian and A. W. Martinez, “Fully Enclosed Microfluidic Paper-based Analytical Devices”, *Anal. Chem.*, 2012, 84, 1579−1585.

[123] E. Bihar, Y. Deng, T. Miyake, M. Saadaoui, G. G. Malliaras and M. Rolandi, “A Disposable paper breathalyzer with an alcohol sensing organic electrochemical transistor”, *Sci. Rep.*, 2016, 6, 27582.

[124] M. Armand, F. Endres, D. R. MacFarlane, H. Ohno and B. Scrosati, "Ionic-liquid materials for the electrochemical challenges of the future" *Nat. Mater.*, 2009, 8, 621–629.

[125] T. L. Greaves and C. J. Drummond, "Protic ionic liquids: properties and applications.", *Chem. Rev.*, 2008, 108, 206−237.

[126] Y. Zhu and F. Chen, “Microwave-assisted preparation of inorganic nanostructures in liquid phase”, *Chem. Rev.*, 2014, 114, 6462−6555.

[127] V. I. Pârvulescu and C. Hardacre, “Catalysis in ionic liquids”, *Chem. Rev.*, 2007, 107, 2615−2665.

[128] F. van Rantwijk and R. A. Sheldon, “Biocatalysis in ionic liquids”, *Chem. Rev.*, 2007, 107, 2757−2785.

[129] M. Moniruzzaman, K. Nakashima, N. Kamiya and M. Goto, “Recent advances of enzymatic reactions in ionic liquids”, *Biochem. Eng. J.*, 2010, 48, 295–314.

[130] K. J. Fraser, E. I. Izgorodina, M. Forsyth, J. L. Scott and D. R. MacFarlane, “Liquids intermediate between “molecular” and “ionic” liquids: Liquid Ion Pairs?”, *Chem. Commun.*, 2007, 3817–3819.

[131] Y. Kohno and H. Ohno, “Ionic liquid/water mixtures: From hostility to conciliation”, *Chem. Commun.*, 2012, 48, 7119–7130.

[132] T. Fujimoto and K. Awaga, “Electric-double-layer field-effect transistors with ionic liquids”, *Phys. Chem. Chem. Phys.*, 2013, 15, 8983–9006.

[133] J. D. Yuen, A. S. Dhoot, E. B. Namdas, N. E. Coates, M. Heeney, I. McCulloch, D. Moses and A. J. Heeger, “Electrochemical Doping in Electrolyte-Gated Polymer Transistors”, *J. Am. Chem. Soc.*, 2007, 129, 14367–14371.

[134] K. H. Lee, S. Zhang, T. P. Lodge and C. D. Frisbie, “Electrical Impedance of Spin-Coatable Ion Gel Films”, *J. Phys. Chem. B*, 2011, 115, 3315–3321.

[135] J. Sayago, F. Soavi, Y. Sivalingam, F. Cicoira and C. Santato, “Low voltage electrolyte-gated organic transistors making use of high surface area activated carbon gate electrodes”, *J. Mater. Chem. C*, 2014, 2, 5690–5694.

[136] W. Liu and J. Holladay, “Catalytic conversion of sugar into hydroxymethylfurfural in ionic liquids”, *Catal. Today*, 2013, 200, 106–116.

[137] L. J. A. Conceiçao, E. Bogel-Łukasikb and R. Bogel-Łukasik, “A new outlook on solubility of carbohydrates and sugar alcohols in ionic liquids”, *RSC Adv.*, 2012, 2, 1846–1855.

[138] V. Armel, J. Rivnay, G. Malliaras and B. Winther-Jensen, “Unexpected interaction between PEDOT and phosphonium ionic liquids”, *J. Am. Chem. Soc.*, 2013, 135, 11309−11313.

[139] N. V. Pogodina, M. Nowak, J. Läuger, C. O. Klein, M. Wilhelm and Ch. Friedrich, “Molecular dynamics of ionic liquids as probed by rheology”, *J. Rheol.*, 2011, 55, 241–256.

[140] B. Yoo, W. Afzal and M. Prausnitz, “Effect of water on the densities and viscosities of some ionic liquids containing a phosphonium cation”, *Z. Phys. Chem.*, 2013, 227, 157−165.

[141] J. Jacquemin, P. Husson, A. A. H. Padua and V. Majer, “Density and viscosity of several pure and water-saturated ionic liquids”, *Green Chem.*, 2006, 8, 172–180.

[142] S. Fendt, S. Padmanabhan, H. W. Blanch and J. M. Prausnitz, “Viscosities of acetate or chloride-based ionic liquids and some of their mixtures with water or other common solvents”, *J. Chem. Eng. Data*, 2011, 56, 31–34.

[143] V. Ruiz, T. Huynh, S. R. Sivakkumar and A. G. Pandolfo, “Ionic liquid–solvent mixtures as supercapacitor electrolytes for extreme temperature operation”, *RSC Adv.*, 2012, 2, 5591–5598.

[144] J. Sayago, X. Meng, E. Bourbeau, F. Quenneville, F. Cicoira, F. Soavi and C. Santato, “Electrolyte-gated polymer thin film transistors making use of ionic liquids and ionic liquid-solvent mixtures”, *J. Appl. Phys.*, 2015, 117, 112809.

[145] P. Leleux, C. Johnson , X. Strakosas , J. Rivnay , T. Hervé, R. M. Owens and G. G. Malliaras, “Ionic Liquid Gel‐Assisted Electrodes for Long‐Term Cutaneous Recordings”, *Adv. Healthcare Mater.*, 2014, 3, 1377–1380.

[146] S. P. White, K. D. Dorfman and C. D. Frisbie, “Label-free DNA sensing platform with low-voltage electrolyte-gated transistors”, *Anal. Chem.*, 2015, 87, 1861−1866.

[147] J. Ouyang, Q. Xu, C.-W. Chu, Y. Yang, G. Li and J. Shinar, "On the mechanism of conductivity enhancement in poly (3, 4-ethylenedioxythiophene): poly (styrene sulfonate) film through solvent treatment", *Polymer*, 2004, 45, 8443–8450

[148] X. Crispin, S. Marciniak, W. Osikowicz, G. Zotti, A. W. D. van der Gon, F. Louwet, M. Fahlman, L. Groenendaal, F. De Schryver and W. R. Salaneck, "Conductivity, morphology, interfacial chemistry, and stability of poly (3, 4‐ethylene dioxythiophene)–poly (styrene sulfonate): A photoelectron spectroscopy study", *J. Polym. Sci., Part B: Polym. Phys.*, 2003, 41, 2561–2583.

[149] J. Rivnay, P. Leleux, M. Ferro, M. Sessolo, A. Williamson, D. A. Koutsouras, D. Khodagholy, M. Ramuz, X. Strakosas, R. M. Owens, C. Benar, J.-M. Badier, C. Bernard, G. G. Malliaras, "High-performance transistors for bioelectronics through tuning of channel thickness", *Sci. Adv.*, 2015;1:e1400251.

[150] H. Du, X. Lin, Z. Xu and D. Chu, "Electric double-layer transistors: a review of recent progress", *J. Mater. Sci.,* 2015, 50, 5641–5673.

[151] F. Zhang, Y. Zang, D. Huang, C. Di, X. Gao, H. Sirringhaus and D. Zhu, "Modulated Thermoelectric Properties of Organic Semiconductors Using Field-Effect Transistors", *Adv. Funct. Mater.*, 2015, 25, 3004–3012.

[152] J. T. Ye, S. Inoue, K. Kobayashi, Y. Kasahara, H. T. Yuan, H. Shimotani and Y. Iwasa, "Liquid-gated interface superconductivity on an atomically flat film", *Nat. Mater.*, 2009, 9, 125–128.

[153] L. Kergoat, B. Piro, M. Berggren, G. Horowitz and M. C. Pham, "Advances in organic transistor-based biosensors: from organic electrochemical transistors to electrolyte-gated organic field-effect transistors", *Anal. Bioanal. Chem.*, 2012, 402,1813–1826.

[154] J. Sayago, U. Shafique, F. Soavi, F. Cicoira and C. Santato, "TransCap: a monolithically integrated supercapacitor and electrolyte-gated transistor", *J. Mater. Chem. C*, 2014, 2, 10273–10276.

[155] S. K. Garlapati, N. Mishra, S. Dehm, R. Hahn, R. Kruk, H. Hahn and S. Dasgupta, "Electrolyte-gated, high mobility inorganic oxide transistors from printed metal halides", *ACS Appl. Mater. Interfaces*, 2013, 5, 11498−11502.

[156] S. Thiemann, S. Sachnov, S. Porscha, P. Wasserscheid and J. Zaumseil, "Ionic Liquids for Electrolyte-Gating of ZnO Field-Effect Transistors", *J. Phys. Chem. C*, 2012, 116, 13536–13544.

[157] H. Shimotani, H. Suzuki, K. Ueno, M. Kawasaki and Y. Iwasa, "Electroresistance Effect in Gold Thin Film Induced by Ionic-Liquid-Gated Electric Double Layer", *Appl. Phys. Lett.*, 2008, 92, 242107.

[158] M. Burghard, H. Klauk and K. Kern, "Carbon-Based Field-Effect Transistors for Nanoelectronics", *Adv. Mater.*, 2009, 21, 2586–2600.

[159] S. Z. Bisri, J. Gao, V. Derenskyi, W. Gomulya, I. Iezhokin, P. Gordiichuk, A. Herrmann and M. A. Loi, "High Performance Ambipolar Field-Effect Transistor of Random Network Carbon Nanotubes", *Adv. Mater.*, 2012, 24, 6147–6152.

[160] S. J. Park, O. S. Kwon, S. H. Lee, H. S. Song, T. H. Park and J. Jang, "Ultrasensitive flexible graphene based field-effect transistor (FET)-type bioelectronic nose", *Nano Lett.*, 2012, 12, 5082−5090.

[161] H. Tang, P. Lin, H. L. W. Chan and F. Yan, "Highly sensitive dopamine biosensors based on organic electrochemical transistors", *Biosens. Bioelectron.*, 2011, 26, 4559–4563.

[162] L. H. Jimison, S. A. Tria, D. Khodagholy, M. Gurfinkel, E. Lanzarini, A. Hama, G. G. Malliaras and R. M. Owens, "Measurement of barrier tissue integrity with an organic electrochemical transistor", *Adv. Mater.*, 2012, 24, 5919–5923.

[163] S. Zhang, P. Kumar, A. S. Nouas, L. Fontaine, H. Tang and F. Cicoira, "Solvent-induced changes in PEDOT: PSS films for organic electrochemical transistors", *APL Mater.*, 2015, 3, 014911.

[164] P. Kumar, Z. Yi, S. Zhang, A. Sekar, F. Soavi and F. Cicoira, "Effect of channel thickness, electrolyte ions, and dissolved oxygen on the performance of organic electrochemical transistors", *Appl. Phys. Lett.*, 2015, 107, 053303.

[165] P. C. Hütter, T. Rothländer, A. Haase, G. Trimmel and B. Stadlober, "Efficiency of the Switching Process in Organic Electrochemical Transistors", *Appl. Phys. Lett.,* 2013, 103, 043308.

[166] S. Zhang, E. Hubis, C. Girard, P. Kumar, J. DeFranco and F. Cicoira, "Water stability and orthogonal patterning of flexible micro-electrochemical transistors on plastic", *J. Mater. Chem. C*, 2016, 4, 1382–1385.

[167] I. Valitova, P. Kumar, X. Meng, F. Soavi, C. Santato and F. Cicoira, "Photolithographically patterned TiO_2 films for electrolyte-gated transistors", *ACS Appl. Mater. Interfaces*, 2016, 8, 14855–14862.

[168] L. Wei, N. Nitta and G. Yushin, "Lithographically Patterned Thin Activated Carbon Films as a New Technology Platform for On-Chip Devices", *ACS Nano*, 2013, 7, 6498–6506.

[169] F. Soavi, L. G. Bettini, P. Piseri, P. Milani, C. Santoro, P. Atanassov and C. Arbizzani, "Miniaturized supercapacitors: key materials and structures towards autonomous and sustainable devices and systems", *J. Power Sources*, 2016 in press. http://dx.doi.org/10.1016/j.jpowsour.2016.04.131.

[170] K. Wegner, P. Piseri, H. Vahedi Tafreshi and P. Milani, "Cluster beam depositon: A tool for nanoscale science and technilogy", *J. Phys. D: Appl. Phys.*, 2006, 39, R439–R470.

[171] L. G. Bettini, G. Bardizza, A. Podestà, P. Milani and P. Piseri, "Electrochemical impedance spectroscopy on nanostructured carbon electrodes grown by supersonic cluster beam deposition", *J. Nanopart. Res.*, 2013, 15, 1429–1439.

[172] C. Lenardi, E. Barborini, V. Briois, L. Lucarelli, P. Piseri and P. Milani, "NEXAFS characterization of nanostructured carbon thin-films exposed to hydrogen", *Diam. Relat. Mater.*, 2001, 10, 1195–1200.

[173] L.G. Bettini, M. Galluzzi, A. Podestà, P. Milani and P. Piseri, "Planar thin film supercapacitor based on cluster-assembled nanostructured carbon and ionic liquid electrolyte", *Carbon*, 2013, 59, 212–220.

[174] L.G. Bettini, P. Piseri, F. De Giorgio, C. Arbizzani, P. Milani and F. Soavi, "Flexible, ionic liquid-based micro-supercapacitor produced by supersonic cluster beam deposition", *Electrochim. Acta*,, 2015, 170, 57–62.

[175] E. Barborini, P. Piseri and P. Milani, "A pulsed microplasma source of high intensity supersonic carbon cluster beams", *J. Phys. D: Appl. Phys.*, 1999, 32, L105–L109.

[176] P. Milani, P. Piseri, E. Barborini, A. Podestà and C. Lenardi, "Cluster beam synthesis of nanostructured thin films", *J. Vac. Sci. Technol. A*, 2001, 19, 2025–2033.

[177] J. Liu, F. Mirri, M. Notarianni, M. Pasquali and N. Motta, "High performance all-carbon thin film supercapacitors", *J. Power Sources*, 2015, 274, 823–830.

[178] L. Nyholm, G. Nyström, A. Mihranyan and M. Strømme, "Toward Flexible Polymer and Paper-Based Energy Storage Devices", *Adv. Mater.,* 2011, 23, 3751–3769.

[179] L. Kergoat, L. Herlogson, D. Braga, B. Piro, M. C. Pham, X. Crispin, M. Berggren and G. Horowitz, "A Water-Gate Organic Field-Effect Transistor", *Adv. Mater.*, 2010, 22, 2565–2569.

[180] T. Cramer, A. Campana, F. Leonardi, S. Casalini, A. Kyndiah, M. Murgia and F. Biscarini, "Water-gated organic field effect transistors – opportunities for biochemical sensing and extracellular signal transduction", *J. Mater. Chem. B*, 2013, 1, 3728–3741.

[181] A. Naim and M. Grell, "Electron transporting water-gated thin film transistors", *Appl. Phys. Lett.*, 2012, 101, 141603.

[182] S. A. Algarni, T. M. Althagafi, A. A. Naim and M. Grell, "A water-gated organic thin film transistor as a sensor for water-borne amines", *Talanta*, 2016, 153, 107–110.

[183] R. F. Oliveira, L. Merces, T. P. Vello and C. C. B. Bufon, "Water-gated phthalocyanine transistors: Operation and transduction of the peptideeenzyme interaction", *Org. Electron.*, 2016, 31, 217–226.

[184] T. Someya, Y. Kato, T. Sekitani, S. Iba, Y. Noguchi, Y. Murase, H. Kawaguchi and T. Sakurai, "Conformable, flexible, large-area networks of pressure and thermal sensors with organic transistor active matrixes", *Proc. Natl. Acad. Sci. USA*, 2005, 102, 12321–12325.

[185] M. E. Roberts, S. C. B. Mannsfeld, R. M. Stoltenberg and Z. Bao, "Flexible, plastic transistor-basd chemical sensors", *Org. Electron.*, 2009, 10, 377–383.

[186] L. Briseno, R. J. Tseng, M. M. Ling, E. H. L. Falcao, Y. Yang, F. Wudl and Z. Bao, "High-Performance Organic Single-Crystal Transistors on Flexible Substrates", *Adv. Mater.*, 2006, 18, 2320–2324.

[187] G. P. Kushto, W. Kim and Z. H. Kafafi, "Flexible organic photovoltaics using conducting polymer electrodes", *Appl. Phys. Lett.*, 2005, 86, 093502.

[188] M. C. Barr, J. A. Rowehl, R. R. Lunt, J. Xu, A. Wang, C. M. Boyce, S. G. Im, V. Bulovic and K. K. Gleason, "Direct monolithic integration of organic photovoltaic circuits on unmodified paper", *Adv. Mater.*, 2011, 23, 3500–3505.

[189] J. Morgado, A. T. Pereira, A. M. Bragança, Q. Ferreira, S. C. M. Fernandes, C. S. R. Freire, A. J. D. Silvestre, C. P. Neto and L. Alcácer, "Self-standing chitosan films as dielectrics in organic thin-film transistors", *eXPRESS Polym. Lett.*, 2013, 7, 960–965.

[190] Report, Contract # FDA-223-78-2100, “Evaluation of the health aspects of shellac and shellac wax as food ingredients”, 1981.

[191] G. S. Banker, “Film Coating Theory and Practice”, *J. Pharm. Sci.*, 1966, 55, 81-89.

APPENDIX A - SUPPORTING INFORMATION FOR ARTICLE 1

Ionic liquid/water mixtures and ion gels as electrolytes for organic electrochemical transistors

Zhihui Yi, Giovanniantonio Natale, Prajwal Kumar, Eduardo Di Mauro, Marie-Claude Heuzey, Francesca Soavi, Iryna I. Perepichka, Sunil K. Varshney, Clara Santato, Fabio Cicoira

Journal of Materials Chemistry C, 2015, 3, 6549-6553.

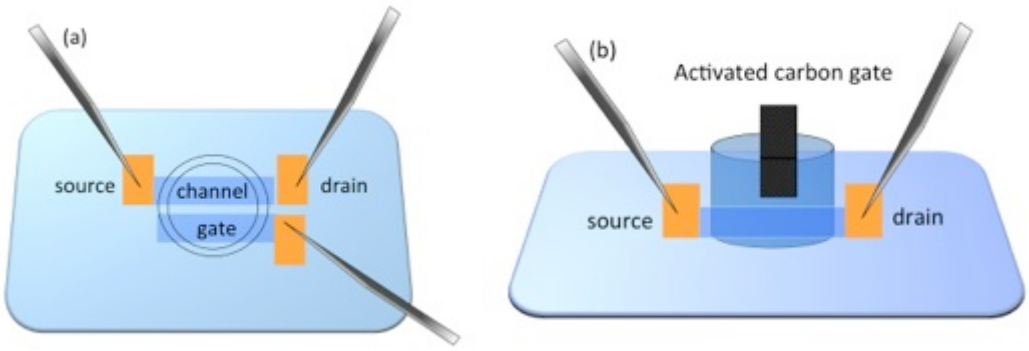

Fig. ESI1 Device structure of the OECTs used in this work. Side view of an OECT employing a planar PEDOT:PSS gate (a). The distance between the parallel PEDOT:PSS stripes (channel and gate electrode) is 2 mm. Top view of an OECT employing an activated carbon gate (b). The gate is immersed into the electrolyte confined within a glass tube (cloning cylinder).

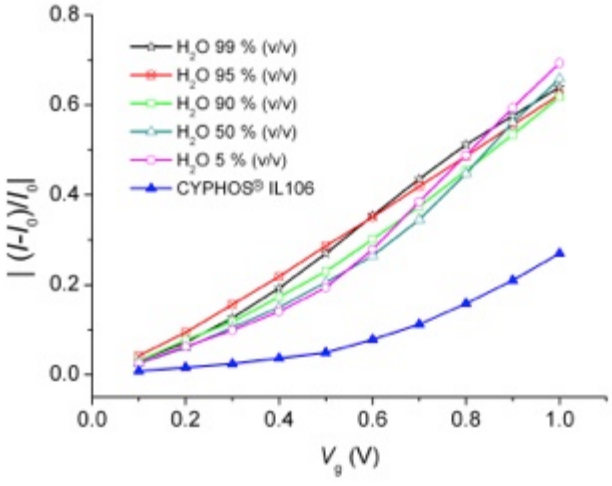

Fig. ESI2: Current modulation $|(I–I_0)/I_0|$ versus V_g for an OECT using as the electrolyte Cyphos® IL 106-H_2O mixtures at different ratios, as specified in the legend. V_d = -0.2 V.

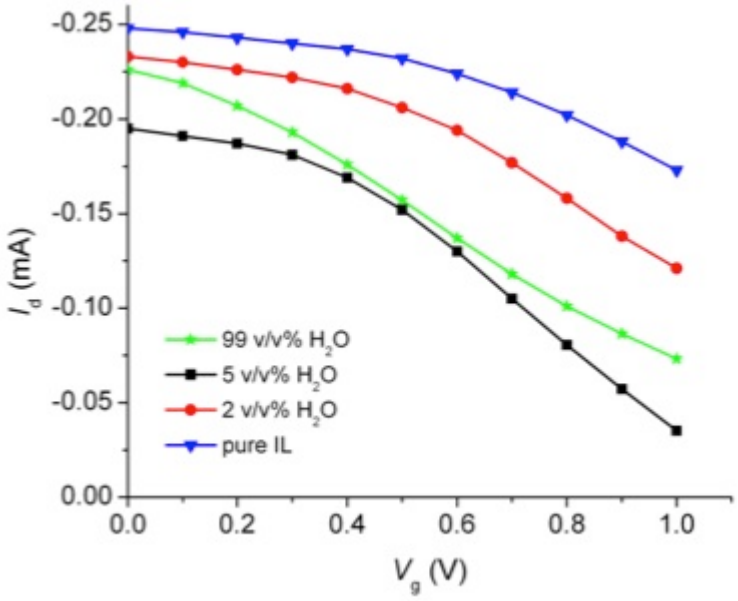

Fig. ESI3: Transfer characteristics of an OECT using as the electrolyte pure Cyphos® IL106 and mixtures of Cyphos® IL106 with H_2O, as specified in the legend. V_d = -0.2 V. See main text for details.

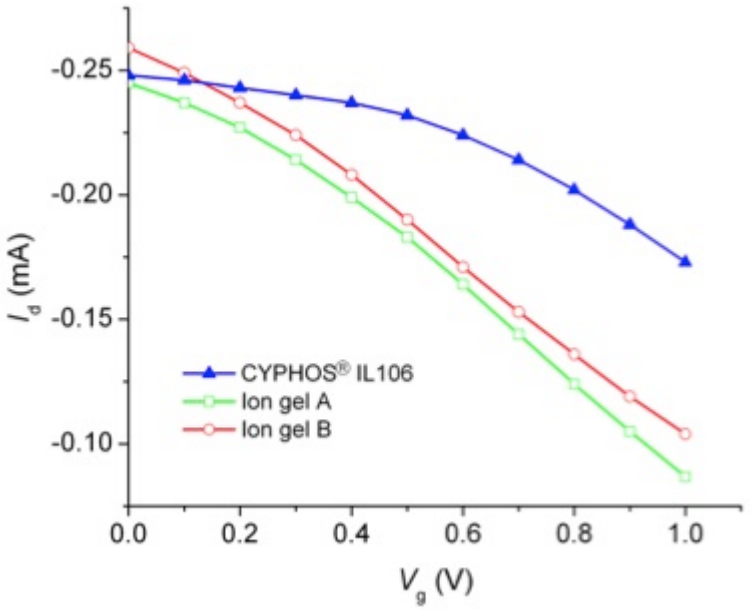

Fig. ESI4: Transfer characteristics of an OECT using as the electrolyte pure Cyphos® IL106, ion gels A and B, as specified in the legend. V_d = –0.2 V. See main text for details.

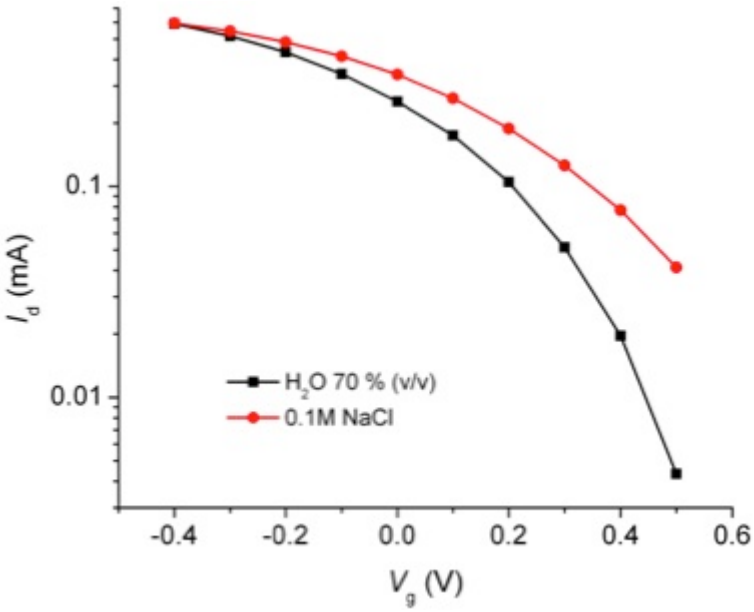

Fig. ESI5: Transfer curves of a PEDOT:PSS OECTs making use of activated carbon as the gate electrode and Cyphos® IL106/H_2O at 70% v/v and 0.1 M NaCl aqueous solution as the gating media. V_d = −0.5 V.

Table ESI1. Ionic conductivity of Cyphos® IL 106/H_2O mixtures at different v/v ratios measured with a conductivity meter. Values for pure Cyphos® IL 106 and Cyphos® IL 106/H_2O mixture at H_2O 99% (v/v) have been validated by Electrochemical Impedance Spectroscopy (EIS). The measurements have been carried out at 22 °C.

H_2O% (v/v)	Ionic conductivity (σ) by conductivity meter (mS/cm)
Pure IL	0.06
2%	0.1
5%	0.3
10%	1
30%	6
50%	10
70%	12
90%	8
99%	1.5

Table ESI2. ON/OFF ratios making use of activated carbon gates and Cyphos® IL 106/H_2O mixtures as electrolytes.

H_2O % (v/v)	ON/OFF ratio
0 (Pure Cyphos® IL 106)	40
2 %	100
5 %	2500
10 %	5000
30 %	1200
50 %	700
70 %	70
90 %	60
99 %	40

APPENDIX B–SUPPORTING INFORMATION FOR ARTICLE 2

Flexible conducting polymer transistors with supercapacitor function

Zhihui Yi, Luca Bettini, Gaia Tomasello, Prajwal Kumar, Paolo Piseri, Irina Valitova, Francesca Soavi, Paolo Milani, Fabio Cicoira

Submitted to *Journal of Polymer Science Part B: Polymer Physics.*

Experimental

Device fabrication and characterization

In this work we employed two different geometries for organic electrochemical transistors: i) channel length (L) = 5 μm and channel width (W) = 80 μm and ii) and W = 2 mm and L = 8 mm (schemes in Figure S1). The former OECTs were patterned on a 0.001 inch-thick Mylar® film (DuPont) with a photolithography process utilizing conventional photolithography for Au patterning and orthogonal photolithography for PEDOT:PSS patterning. [36]. We utilized a polydimethylsiloxane (PDMS) covered glass slide as a supporting substrate for facilitating the photolithography process of the Mylar® film. A mixture of PDMS with curing agent (10:1 w/w) (Sylgard 184, Dow Corning) was spin coated on a clean glass slide with a speed of 500 rpm for 30 s before baking at 70 °C for 20 min. After that, a Mylar® film was stuck on the PDMS and cut to fit the size of the supporting substrate. Mylar® film was cleaned with acetone and isopropanol, followed by a 10 min UV-O_3 treatment. For patterning the electrodes, lift-off resist LOR1A was spin coated on the Mylar® film at 4000 rpm for 30s before baking at 190 °C for 3 min. A layer of AZ5214, which covered the LOR1A, was spin coated at 4000 rpm for 30s and baked at 110 °C for 1 min. After being exposed under a 35 mJ cm^{-2} UV light with a mask, the Mylar® film was developed in the developer AZ726 (MicroChemicals) for 1 min. A 10 s O_2 plasma treatment was applied to further clean the patterned structure. 4 nm Ti followed by 40 nm Au was deposited by electron-beam evaporation on the Mylar® film before lifting off. The Mylar® film was then treated with UV-O_3 for 10 min.

An aqueous suspension of poly(3,4-ethylenedioxythiophene):poly(styrenesulfonate), PEDOT:PSS (Clevios™ PH1000, Heraeus Electronic Materials) was mixed with ethylene glycol (EG, Sigma Aldrich) 25 % v/v and with 0.5 % v/v of the surfactant dodecyl benzene sulfonic acid (DBSA, Sigma Aldrich), in order to enhance film electrical conductivity and improve film processability. The Clevios™ PH1000/EG/DBSA mixture was spin coated onto the Mylar® film for 9 s at 500 rpm followed by 40 s at 1500 rpm before soft baking at 90° C for 2 min. This procedure was repeated 2 times for the PEDOT:PSS film in Figure S1b. The PEDOT:PSS film was then baked at 140° C for 1 h. The film thicknesses were 200 nm for micron-scale devices (Figure S1a) and 470 nm for devices with a larger scale (Figure S1b).

To achieve PEDOT:PSS patterning, the orthogonal photoresist OSCoR 4000 was spun coated onto the Mylar® film at 500 rpm for 40 s, and baked at 85 °C for 2 min. The Mylar® film, which was exposed under 5 mJ cm^{-2} UV light with a second mask, was post-baked 2 min at 85 °C. The unexposed photoresist was eliminated by developing in developer 103 (Orthogonal, Inc.) for 1.5 min, leaving unprotected PEDOT:PSS outside the OECT channel region. A reactive ion etching process, which employed O_2 plasma (150 W, 125 mTorr) at a flow rate of 10 sccm for 1.5 min, was used to remove the unprotected PEDOT:PSS. Finally the exposed photoresist was removed by immersion in orthogonal Stripper (Orthogonal, Inc.) for 1.5 min.

To prepare the electrolyte, poly(sodium 4-styrene sulfonate) (PSSNa, MW ~70,000), D-sorbitol, glycerol and deionized water in a mass ratio of 4:1:1:4 were put into a sealed plastic box. The chemicals were mixed for 10 min at 2000 rpm with a Thinky® mixer. The electrolyte was left in the sealed box overnight before using.

For the micro-scale OECTs, the active surface area of PEDOT:PSS and nsC exposed to the electrolyte were 400 μm^2 and 4 mm^2, respectively (Figure S1a). For the OECT at larger-scale, the active surface area of PEDOT:PSS and nsC exposed to electrolyte were 0.16 cm^2 and 0.2 cm^2 respectively (Figure S1b).

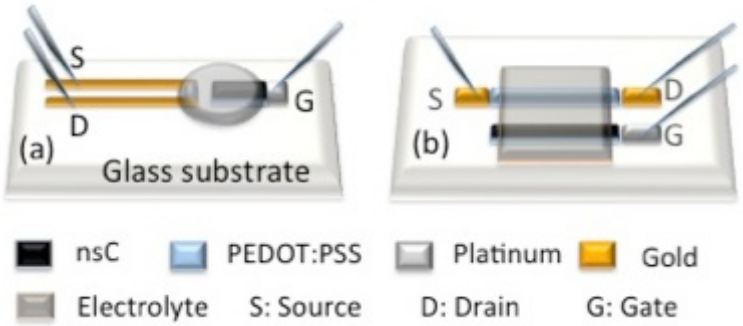

Figure S1. Micron-sized (a) and centimeter-sized (b) OECTs investigated in this work, making use of planar configuration, with electrical contacts.

From: "Journal of Polymer Science-Physics" <em@editorialmanager.com>

Subject: Submission Confirmation for Flexible conducting polymer transistors with supercapacitor function (polb.20160431)

Date: July 24, 2016 at 12:08:51 AM GMT+2

To: "Fabio Cicoira" <fabio.cicoira@polymtl.ca>

Reply-To: "Journal of Polymer Science-Physics" <jpsphys@wiley.com>

Dear Prof. Cicoira,

Your submission entitled "Flexible conducting polymer transistors with supercapacitor function" has been successfully submitted online and is presently being given full consideration in the Journal of Polymer Science, Part B: Polymer Physics. The manuscript number for your submission is polb.20160431.

If you are the corresponding author, you may view your submission by logging in to http://polb.edmgr.com/ by entering your username (FCicoira-366) and password and selecting the "Author Login" option.

This message has also been sent to all named co-authors listed in the submission process to serve as notification of submission.

Thank you for submitting your work to the journal.

Kind regards,

Editorial Office

Journal of Polymer Science, Part B: Polymer Physics

Email: jpsphys@wiley.com

http://www.polymerphysics.org

*****

John Wiley & Sons, Inc.

111 River Street Hoboken, NJ 07030

*****

APPENDIX C – SUPPORTING INFORMATION FOR ARTICLE 3

Water gated organic electrochemical transistors on flexible/degradable shellac substrate

Zhihui Yi, Irina Valitova, Fabio Cicoira

Submitted to *Journal of Materials Research*.

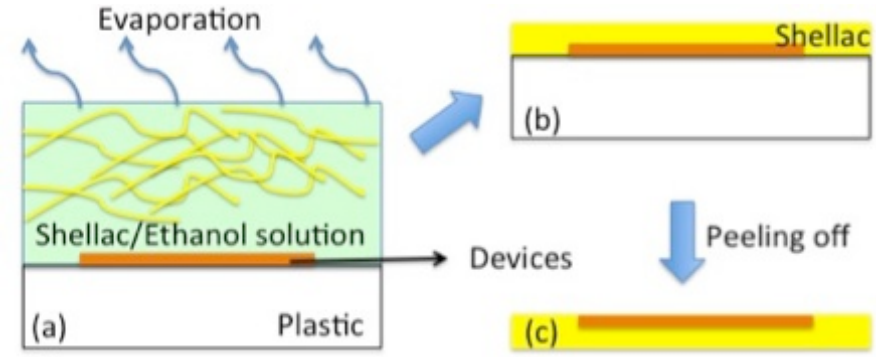

Figure S1. The evaporation of ethanol (a) to produce shellac film (b). Devices stuck on shellac can be peeled off from the plastic substrate (c).

From: Journal of Materials Research <onbehalfof+jmr+mrs.org@manuscriptcentral.com>
Subject: JMR-2016-0746 - Manuscript Submission
Date: August 2, 2016 at 6:00:11 PM GMT-4
To: zhihui.yi@polymtl.ca, irina.valitova@polymtl.ca, fabio.cicoira@polymtl.ca
Reply-To: jmr@mrs.org

Dear Yi, Zhihui; Valitova, Irina; Cicoira, Fabio,

This e-mail is to inform you that the following manuscript for which you are a contributing author has been submitted to Journal of Materials Research:

Manuscript Number: JMR-2016-0746

Manuscript Title: Water gated organic electrochemical transistors on flexible/degradable shellac substrates

Manuscript Authors: Yi, Zhihui; Valitova, Irina; Cicoira, Fabio

Submission of this article to JMR is an acknowledgment that it represents original research (except for review articles) and that it has not been copyrighted, published, or submitted for publication elsewhere.

Occasionally, we find that our communications are not delivered, causing authors to miss important decisions and deadlines regarding their submitted papers. To avoid that problem:

- Please list this email address as an allowable sender ("whitelist") in your institutional email system to ensure that all email notifications are delivered, and not caught in any spam filters.

- Add a personal email address in your User Account in the Primary cc: field.

If you have received this message in error, or if one of your co-authors did not receive this message, please contact us via reply e-mail.

Sincerely,

-Journal of Materials Research Editorial Office

APPENDIX D –LIST OF PUBLICATIONS AT POLYTECHNIQUE MONTREAL NOT INCLUDED IN THE THESIS

H. Tang, P. Kumar, S. Zhang, Z. Yi, G. D. Crescenzo, C. Santato, F. Soavi and F. Cicoira, "Conducting Polymer Transistors Making Use of Activated Carbon Gate Electrodes", *ACS Appl. Mater. Interfaces*, 2015, 7, 969−973.

P. Kumar, Z. Yi, S. Zhang, A. Sekar, F. Soavi, F. Cicoira, "Effect of channel thickness, electrolyte ions, and dissolved oxygen on the performance of organic electrochemical transistors", *Appl. Phys. Lett.*, 2015, 107, 053303.

APPENDIX E –PARTICIPATION IN CONFERENCES AND MEETINGS

Materials Research Society, Spring Meeting, San Francisco, USA, 2014

Materials Research Society, Fall Meeting, Boston, USA, 2014